เดนดริติกพอลิอิเล็กโทรไลต์ฟลูออโรฟอร์ที่มีแกนเป็นเอ็น-แอริลคาร์บาโซล

นายภาคภูมิ อรรถพรพิทักษ์

วิทยานิพนธ์นี้เป็นส่วนหนึ่งของการศึกษาตามหลักสูตรปริญญาวิทยาศาสตรมหาบัณฑิต
สาขาวิชาปิโตรเคมีและวิทยาศาสตร์พอลิเมอร์
คณะวิทยาศาสตร์ จุฬาลงกรณ์มหาวิทยาลัย
ปีการศึกษา 2554

DENDRITIC POLYELECTROLYTE FLUOROPHORES WITH *N*-ARLY CARBAZOLE CORE

Mr. Pharkphoom Auttapornpitak

A Thesis Submitted in Partial Fulfillment of the Requirements

for the Degree of Master of Science Program in Petrochemistry and Polymer Science

Faculty of Science

Chulalongkorn University

Academic Year 2011

Thesis Title	DENDRITIC POLYELECTROLYTE FLUOROPHORES WITH *N*-ARLY CARBAZOLE CORE
By	Mr. Pharkphoom Auttapornpitak
Field of Study	Petrochemistry and Polymer Science
Thesis Advisor	Assistant Professor Paitoon Rashatasakhon, Ph.D.
Thesis Co-advisor	Associate Professor Mongkol Sukwattanasinitt, Ph.D.

Accepted by the Faculty of Science, Chulalongkorn University in Partial Fulfillment of the Requirements for the Master's Degree

…….. Dean of the Faculty of Science

(Professor Supot Hannongbua, Dr.rer.nat.)

THESIS COMMITTEE

……Chairman

(Associate Professor Supawan Tantayanon, Ph.D.)

……Thesis Advisor

(Assistant Professor Paitoon Rashatasakhon, Ph.D.)

……Thesis Co-advisor

(Associate Professor Mongkol Sukwattanasinitt, Ph.D.)

……Examiner

(Associate Professor Voravee Hoven, Ph.D.)

……External Examiner

(Pornpimol Prayongpan, Ph.D.)

ภาคภูมิ อรรถพรพิทักษ์: เดนดริติกพอลิอิเล็กโทรไลต์ฟลูออโรฟอร์ที่มีแกนเป็นเอ็น-แอริลคาร์บาโซล. (DENDRITIC POLYELECTROLYTE FLUOROPHORES WITH *N*-ARYL CARBAZOLE CORE) อ. ที่ปรึกษาวิทยานิพนธ์หลัก: ผศ.ดร.ไพฑูรย์ รัชตะสาคร, อ. ที่ปรึกษาวิทยานิพนธ์ร่วม: รศ.ดร. มงคล สุขวัฒนาสินิทธิ์, 95 หน้า.

ฟลูออโรฟอร์แบบเดนดริเมอร์ชนิดใหม่ได้ถูกออกแบบและสังเคราะห์ โดยใช้แกนกลางเป็นเอ็น-ฟีนิลคาร์บาโซล และมีหมู่รอบนอกเป็นเบนโซเอท ซาลิไซเลท หรือควอเทอร์นารีแอมโมเนียม วิธีการสังเคราะห์ใช้ปฏิกิริยาคู่ควบโซโนกาชิราระหว่างแกนกลาง กับเอไธนิลเบนซีนที่มีหมู่แทนที่ที่แตกต่างกัน และเมื่อทำให้หมู่ปลายกลายเป็นหมู่คาร์บอกซิเลท หรือไตรเมทิลแอมโมเนียมแล้วจะได้ฟลูออโรฟอร์ที่สามารถละลายน้ำได้ และให้ประสิทธิภาพการเรืองแสงที่สูงกว่าฟลูออโรฟอร์ที่มีแกนกลางเป็นไตรฟีนิลเอมีน ซึ่งเป็นผลมาจากการเพิ่มความแข็งเกร็งในโครงสร้างที่ทำให้โมเลกุลในสถานะกระตุ้นเกิดจีโอเมตริกคัลรีเล็กเซชันได้น้อยลง อย่างไรก็ตาม การปรับปรุงประสิทธิภาพการเรืองแสงด้วยวิธีนี้จะเห็นผลชัดเจนในกรณีที่ไม่มีปรากฏการณ์การส่งถ่ายประจุภายในโมเลกุล นอกจากนั้นยังพบว่าสัญญาณการเรืองแสงของฟลูออโรฟอร์ที่มีหมู่ซาลิไซเลทสามารถถูกระงับได้อย่างจำเพาะเจาะจงกับไอออนทองแดง โดยพบว่าความสัมพันธ์ของความเข้มของสัญญาณการเรืองแสงกับความเข้มข้นของไอออนทองแดงไม่เป็นแบบเส้นตรง แต่จะเกิดการระงับสัญญาณได้ในช่วงความเข้มข้นของไอออนทองแดงตั้งแต่ 4 ไมโครโมลาร์ขึ้นไป และในการศึกษาแบบแยกส่วนของฟลูออโรฟอร์ดังกล่าว พบว่าหมู่เอไธนิลซาลิไซเลทที่วงเบนซีนเป็นส่วนที่แสดงผลการระงับสัญญาณด้วยไอออนทองแดง และส่วนอื่นๆของโมเลกุลทำหน้าที่เป็นส่วนขยายสัญญาณการเรืองแสง

สาขาวิชา ปิโตรเคมีและวิทยาศาสตร์พอลิเมอร์ ลายมือชื่อนิสิต .....

ปีการศึกษา 2554 ลายมือชื่อ อ.ที่ปรึกษาวิทยานิพนธ์หลัก .....

ลายมือชื่อ อ.ที่ปรึกษาวิทยานิพนธ์ร่วม .....

5272477123: MAJOR PETROCHEMISTRY AND POLYMER SCIENCE
KEYWORDS: DENDRITIC FLUOROPHORE / FLUORESCENT SWITCHING / NON-LINEAR RELATIONSHIP / COPPER (II) SENSOR

PHARKPHOOM AUTTAPORNPITAK: DENDRITIC POLYELECTROLYTE FLUOROPHORES WITH *N*-ARLY CARBAZOLE CORE. ADVISOR: ASST. PROF. PAITOON RASHATASAKHON, Ph.D., CO-ADVISOR: ASSOC. PROF. MONGKOL SUKWATTASINITT, Ph.D., 95 pp.

Novel dendritric fluorophores are designed and synthesized using *N*-phenyl carbazole as the core and benzoate, salicylate, or quaternaryammonium as the pheripheral groups. The synthesis relies on Sonogashira couplings between the core and ethynyl benzenes with different substituents. Upon conversion of the peripheries into carboxylate or trimethylammonium groups, water-soluble fluorophores with quantum efficiencies greater than their triphenylamine-cored analogs are obtained. This improved quantum yields results from the enhanced structural rigidity, which decreases the geometrical relaxation of the excited molecules. However, this quantum efficiency improvement approach is more apparent in the case where the molecule is lack of the internal charge transfer phenomenon. In addition, it is found that the fluorescent signal of fluorophore with salicylate group can be selectively quenched by copper (II) ion. The non-linear relationship between fluorescent intensity and concentration of copper (II) ion reveals a turn-off fluorescent switching property for the copper (II) ion at 4 micromolar and above. The fractional investigation of this fluorophore indicates that the ethynyl salicylate group attached on the phenyl ring of the core is responsible for fluorogenic response towards copper (II) ion, where as the other parts of molecule function as fluorescent signal amplification units.

Field of Study : Petrochemistry and Polymer Science Student's Signature .....

Academic Year : 2011 Advisor's Signature .....

Co-advisor's Signature .....

ACKNOWLEDGEMENTS

First of all, I would like to express my sincere gratitude to my thesis advisor, Assistant Professor Paitoon Rashatasakhon, Ph.D. and my co-advisor, Associate Professor Mongkol Sukwattanasinitt, Ph.D., for valuable advice, guidance and kindness throughout this research. Sincere thanks are also extended to Associate Professor Supawan Wanichweacharungruang, Ph.D., chairman of thesis committee, Associate Professor Voravee Hoven, Ph.D. and Assistant Professor Pornpimol Prayongpan, Ph.D., attending as the committee members, for their valuable comments and suggestions.

I would like to especially thank Anawat Ajavakom, Ph.D. and Assistant Professor Sumrit Wacharasindhu, Ph.D., in MAPS Group for valuable guidance.

This work was financially supported by the Center for Petroleum, Petrochemicals Advanced Materials Chulalongkorn University and the National Nanotechnology Center (NANOTEC). The research instruments were partially supported by the Thai Government Stimulus Package 2 (TKK2555, SP2). I also thank the National Research University Project (AM 1006A) for the scholarship.

Furthermore, I gratefully thank to my Dr. Nakorn Niamnont, Ms. Waratrip Siripornnoppakhun, Ms. Kunigar Vongnam, Mr. Sakan Sirilaksanapong, for their helpful suggestion and training. Mr. Watcharin, Ms. Sasikarn Ampornpun, Ms. Thichamporn Eaidkong, Ms. Kanoktorn Boonkitpatarakul, Ms. Nattaporn Kimpitak, Mr. Akachai Khumsri, Ms. Daranee Homraruen, Ms. Wanwisa Thongmalai and everyone in MAPS Group for a great friendships and encouragement.

Finally, I would like to specially thank my family for their encouragement and understanding throughout. I would not be able to reach this success without them.

CONTENTS

CHAPTER **Page**

CHAPTER **Page**

LIST OF TABLES

LIST OF FIGURES

LIST OF SCHEMES

LIST OF ABBREVIATIONS

Acetone-d^6	dueterated acetone
calcd	calculated
$CDCl_3$	dueterated chloroform
CH_2Cl_2	methylene chloride
CuI	oopper iodide
d	doublet
DBU	1,8-Diazabicycloundec-7-ene
DMSO	dimethyl sulfoxide
DMSO-*d*6	deuterated dimethyl sulfoxide
EtOAc	ethyl acetate
g	gram (s)
h	hour
H_2SO_4	sulfuric acid
Hz	hertz
J	coupling constant
K_2CO_3	potassium carbonate
KI	potassium iodide
KIO_3	potassium iodate
m	multiplet
MeCN	acetronitrile
MeOH	methanol
mg	milligram (s)
$MgSO_4$	magnesium sulfate
min	minute (s)
mL	milliliter (s)
mmol	millimole
M	molar

M.W.	molecular weight
nm	nanometer (s)
NMR	nuclear magnetic resonance
OLED	organic light-emitting diode
$PdCl_2(PPh_3)_2$	bis(triphenylphosphine)palladium(II) chloride
ppm	parts per million
ppb	parts per billion
rt	room temperature
s	singlet
t	triplet
THF	tetrahydrofuran
TLC	thin layer chromatography
%	percent
δ	chemical shift
$^{\circ}C$	degree of celsius
ε	molar absorptivity
λ	wavelength
Φ	fuorescence quantum yield
μM	micromolar (s)

CHAPTER I

INTRODUCTION

1.1 Fluorescence

Fluorescence spectroscopy has been widely used in analytical chemistry, biochemistry and medical research [1-2] since the detection of emission signals have been estimated to be 10^3 times more sensitive than the detection of absorption signals [3-4]. Fluorescent activity can be schematically illustrated with the classical Jablonski diagram (**Figure 1.1**). When a fluorophore absorbs stimulation energy in a form of light (A), it is usually excited to a higher electronic excited state before rapidly relaxing to the lowest electronic excited state (S_1) which is known an internal conversion (IC) process. Eventually, the molecule will return to ground state (S_0) and release an amount of light energy which is termed fluorescence (F). If the spin state of the initial and final energy levels are different (e.g. $T_1 \rightarrow S_0$), the emission or the loss of energy is called phosphorescence. In the diagram this is depicted by a longer wavelength (lower energy) and therefore shorter length red line (P). Since fluorescent is statistically much more likely than phosphorescence for most molecules, the lifetimes of fluorescent states are very short (10^{-5} to 10^{-8} seconds) and phosphorescence somewhat longer (longer than 10^{-4} seconds).

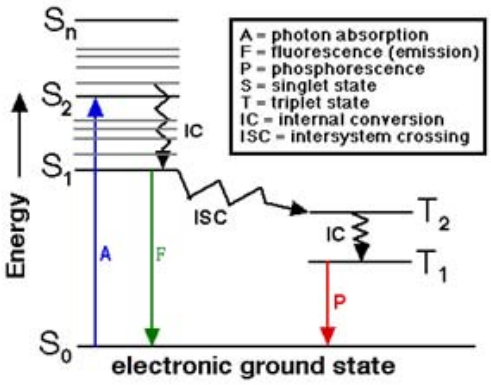

Figure 1.1 Jablonski diagram

In addition, two other non-radiative processes could also happen to the excited fluorophore: intersystem crossing (ISC) and geometrical relaxation (not shown in **Figure 1.1**). Intersystem crossing is a transition between two different spin states whereas geometrical relaxation is the most common radiationless process for most molecules. It occurs very quickly ($<10^{-12}$ seconds) and is enhanced by physical contact of an excited molecule with other particles with which energy, in the form of vibrations and rotations, can be transferred through collisions. Therefore, the decrease of degree of freedom by increasing the molecular rigidity would therefore diminish the geometrical relaxation.

1.2 Structure Fluorescent Compounds

As defined by their structures, there are two groups of fluorescent substances which as 1) small-molecule fluorophores and 2) polymeric fluorophores or conjugated polymers (CPs). Some examples of small-molecule fluorophores are shown in Figure 1.2. The emitting colors of each fluorophores depend on their structures and substituents; for instance blue emission for POPOP and green emission of fluorescein. Small-molecule fluorophores have been extensively studied as part of fluorescent sensors in the past several decades [5-8].

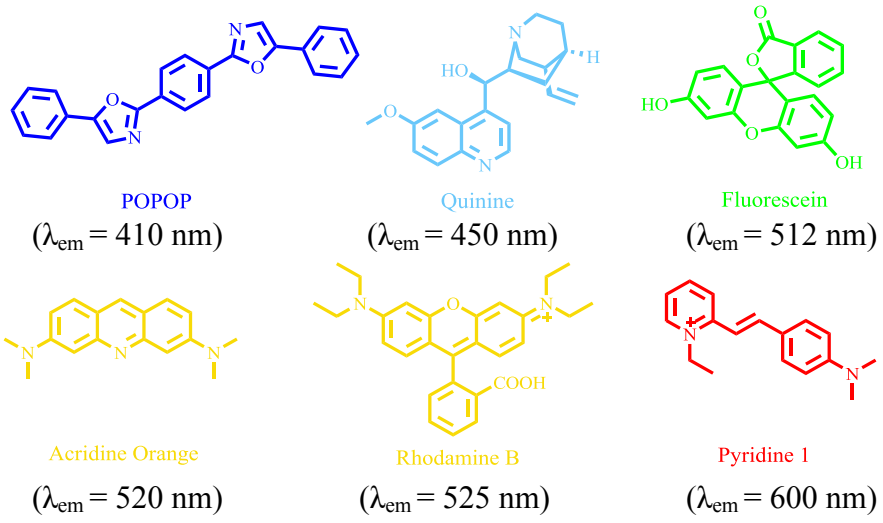

Figure 1.2 Small-molecule fluorescent compounds.

Conjugated polymers (CPs) also constitute a major group of polymeric fluorophores. They have become an important class of materials in a wide variety of applications, including organic light emitting diodes (OLEDs) [9-10], light-emitting electrochemical cells (LECs) [11], field-effect transistors (FETs) [12-14], photovoltaics [15-18], actuators [19], batteries [20-22], plastic lasers [23], and solar cells [24]. Recently, there has been the use of CPs in chemical or biological sensor applications [25, 26]. In particular, the chemical structures of CPs offer several advantages in sensor applications, especially increased sensitivity. In conjugated polymers, each carbon atom along the backbone has sp or sp^2 hybridization. The remaining p orbitals, with one unpaired π electrons each is placed side by side to from π bonds. Since the orbitals of successive carbon atom along the backbone overlap, the π electrons are delocalized along the polymer backbone contributing to the increased sensitivity [27-29]. As shown in **Figure 1.3**, CPs can be constructed from a variety of structural moieties, including poly(*para*-phenylene) (PPP) [30], poly(*para*-phenylene vinylene) (PPV) [4], poly(*para*-phenylene ethynylene) (PPE) [31], polythiophene (PT) [32], polypyrrole (PPy) [33], polyaniline (PANI) [34] and polyfluorene (PF) [35,36].

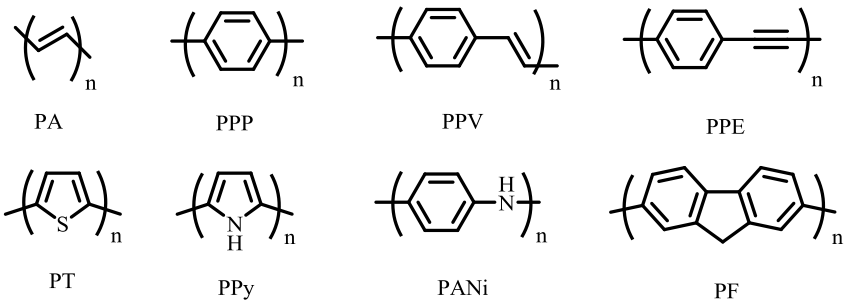

Figure 1.3 Molecular structures of typical CPs.

Conjugated polymers have several advantages over small-molecules for sensing applications due to signal enhancements associated with electronic communication between fluorophores along the polymer backbone. As the shown in **Figure 1.4** [29], when a polymeric sensor detects a specific analyte, the fluorescent signal of the whole

polymeric system will be affected. On the other hand, the use of small-molecule sensor will result in fluorescent signal changes only on fluorophore-analyst complex.

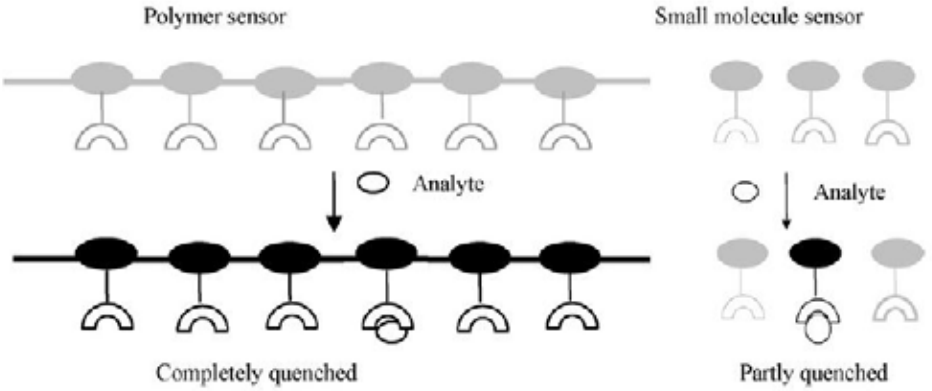

Figure 1.4 This schematic representation demonstrates sensory signal using the conjugated polymer (left) and small-molecule fluorophore (right)

1.3 Fluorescence sensor

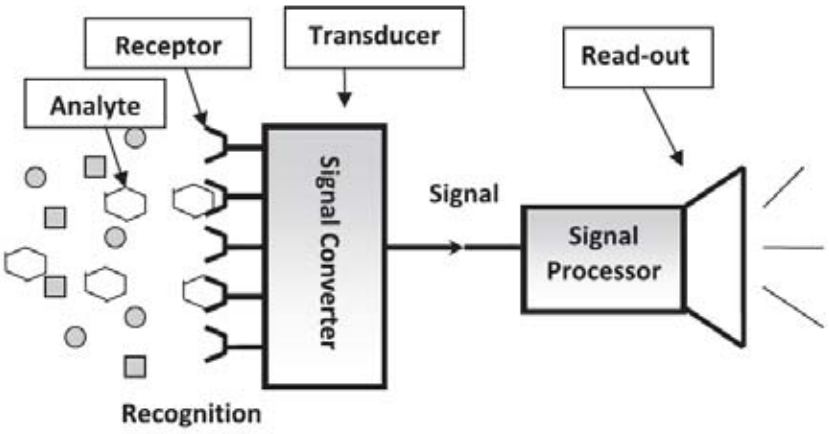

Figure 1.5 Schematic illustration of a chemical sensor.

In general, a sensor generally contains three fundamental components: a receptor a signal transducer and a read-out system (**Figure 1.5**) [29]. The receptor should have the ability to discriminate and bind a specific target substance known as the analyte. A successful and selective receptor-analyte complex formation depends on the size, shape

and binding energy of the receptor and analyte. Signal transduction is the process through which an interaction of receptor with analyte yields a measurable from of energy change and is converted to a signal change that can be read and quantified. The read-out domain is the part responsible for reporting the binding event. Some parameters that define a sensor's performance are selectivity, sensitivity, stability, reproducibility and cost. For a fluorescence sensor, the signal transducers could be fluorophores which are capable of turning chemical or physical changes into fluorescent signals.

1.4 Fluorescent quenching

Fluorescent quenching is important process which affects the fluorescent intensity and/or lifetime of fluorescent signals. At a molecular level, the quenching mechanism can be divided into two modes - dynamic and static quenching mechanisms.

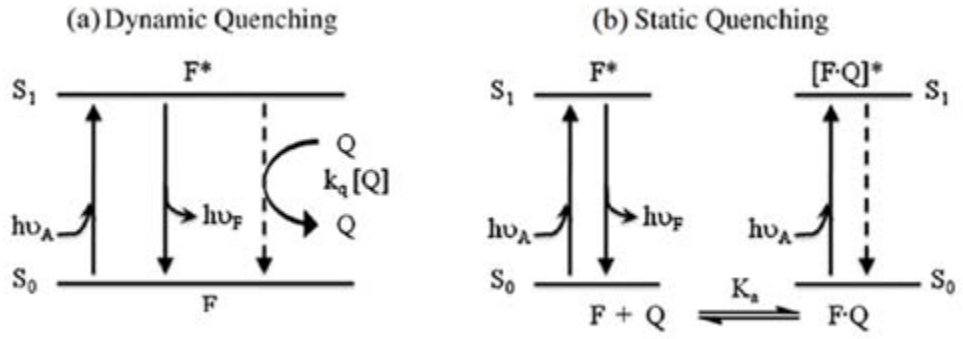

Figure 1.6 Schematic illustrations of fluorescent quenching [8].

Dynamic quenching, also called collisional quenching, depends on the diffusion of the quencher. As shown in **Figure 1.6 (a)**, dynamic quenching occurs when excited fluorophore (**F***) is deactivated upon a diffusive encounter via quencher (**Q**) and relaxes to S_0 without emission of a photon (dash line). **Figure 1.6 (b)** illustrates static quenching which occurs as a result of formation of a stable non-fluorescent complex between fluorophore and quencher in the ground state (**F·Q**). When this complex absorbs light, it immediately returns to the ground state without fluorescent emission. Since complex

formation occurs in the ground state, the efficiency of static quenching is related to the association constant (K_a) for the formation of **F·Q**.

The modes of quenching (dynamic or static) can be distinguished in several ways [4]. The first is fluorescence lifetime dependence on quencher concentration. In dynamic quenching, the presence of an additional deactivation pathway shortens the observed fluorescence lifetime. In contrast, in static quenching, the fluorescence lifetime is independent of the quencher concentration since complexation takes place in the ground state. Uncomplexed fluorophore can be excited and exhibits normal fluorescence behavior with the same lifetime.

Secondly, temperature effects on the quenching efficiency can be carefully examined to distinguish between the two mechanisms. The dynamic quenching efficiency is expected to increase with increasing temperature due to larger diffusion coefficient at higher temperature (**Figure 1.7** (**a**)), while static quenching decreases at higher temperature due to dissociation of weakly bound complexes formed in the quenching process (**Figure 1.7** (**b**)).

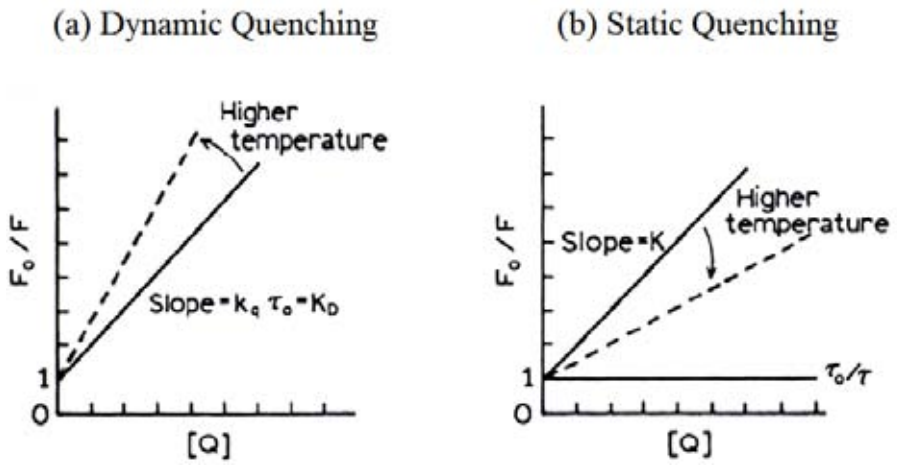

Figure 1.7 Effect of temperature on Dynamic and static quenching.

Thus, a change in the absorption spectra in the presence of quencher can be indicative of a static quenching mechanism. However, it is important to note that both dynamic and static quenching processes operate concurrently in many systems.

1.5 Stern-Volmer equation

The Stern–Volmer (SV) equation which is written in equation **1** is often using to evaluate quenching efficiency of both dynamic and static quenching modes. In this equation, I_0 and I are the fluorescence intensities observed in the absence and presence of quencher, respectively, whereas [Q] is the quencher concentration, and K_{SV} is the SV quenching constant [5].

$$\frac{I_0}{I} = 1 + K_{SV}[Q] \qquad (1)$$

A plot of I_0/I versus $[Q]$ is known as a Stern–Volmer plot, which ideally yields a straight line with a slope equal to K_{SV} for both pure dynamic and static quenching. However, in many instances, the SV plot displays a non-liner, upward curvature, which indicates the fluorophore is quenched by both collision (dynamic) and complex formation (static) with the same quencher. In such circumstances, a modification of original SV equation (equation **2**) should be carried out.

$$\frac{\tau_0}{\tau} = \frac{I_0}{I} = 1 + k_q\tau_0[Q] = 1 + K_D[Q] \qquad (2)$$

This form of the SV equation is second-order in $[Q]$ and it combines the effects of dynamic and static quenching on the fluorescence intensity. The dynamic portion of the observed quenching can be determined by lifetime quenching (τ_0 and τ).

1.6 Literature review on fluorescent sensors

Examples of literatures related to rigidity effect on quantum yield are as follow:

In 2008, Nijegorodov and coworkers [37] studied the effect of molecular rigidity on the optical properties of several polyaromatic hydrocarbons and found that the molecules with more rigidity would exhibit higher quantum yields (Φ_F).

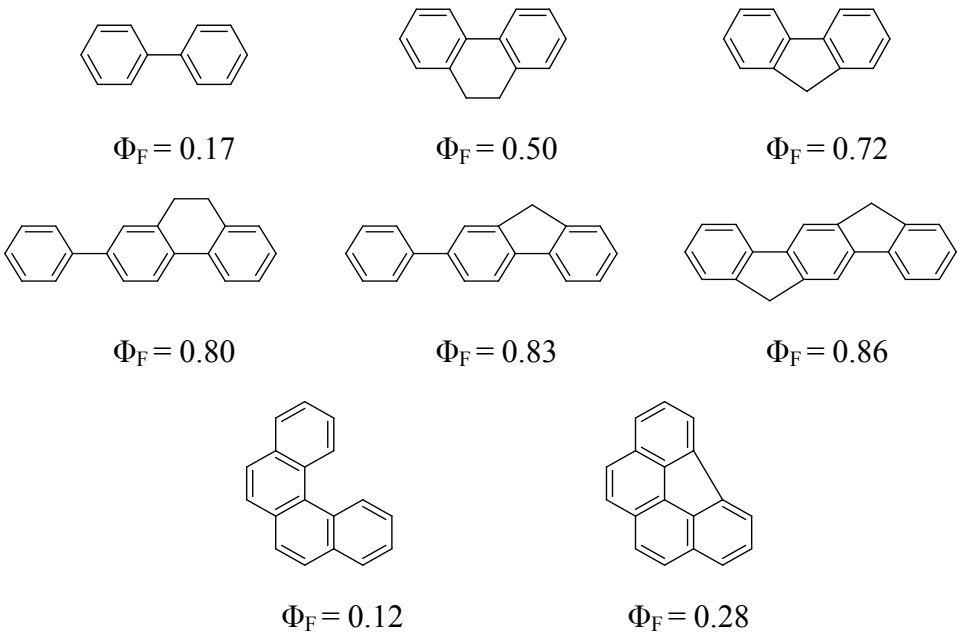

Figure 1.8 The structures of polyaromatic hydrocarbon.

In addition, Brunel, et. al. [38] and a group of Chinese researchers [39] reported the quantum yields of fluorophore **I** (29%) and **II** (91%). These could represent additional examples of the enhancement of quantum efficiency by increasing of molecular rigidity.

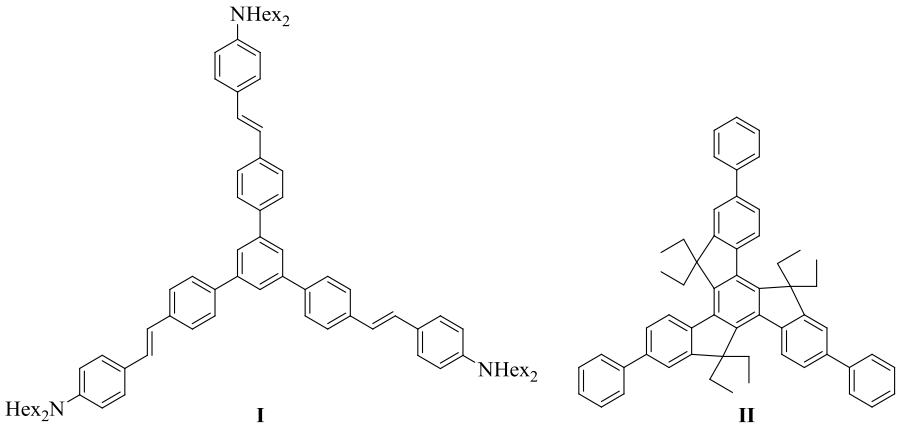

$\Phi_F = 0.29$ $\Phi_F = 0.91$

Figure 1.9 The structures of fluorophores are peripheral of triphenylamine (**I**) and truxene (**II**).

In 2009, Wang and coworkers [40] synthesized derivatives of quinoxaline with carbazole (**III**) and triphenylamine (**IV**) peripheries using a one-step synthetic method. Importantly, they found that the compound with carbazole peripheries (**III**) showed greater quantum yield (60%) than the compound with triphenylamine groups (**IV**). It is a convincing evidence that supports the idea of quantum yield enhancement by increasing the molecular rigidity.

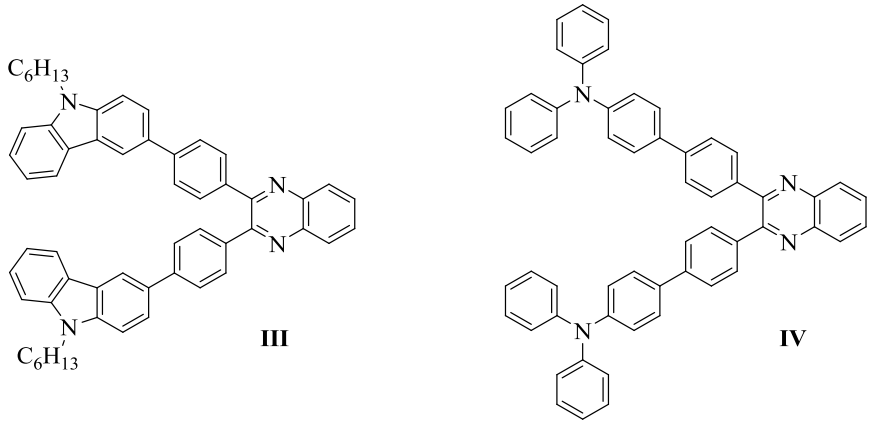

Figure 1.10 The structures derivatives of quinoxaline are peripheral of carbazole (**III**) and triphenylamine (**IV**).

Examples of literatures related to fluorescent sensors are as follow:

In 2006, Kim and Bunz [41] studied the use of poly(phenyleneethynylene) (**V**) and a number of proteins on the detection of metal ions. They found that the combination of **V** and papain resulted in a highly sensitive fluorescent sensor for Hg^{2+}. Addition of Hg^{2+} ion to **V** in the absence of papain, caused a fluorescent quenching with a Stern-Volmer constant (K_{SV}) of 1.3 x 10^4 M^{-1}. In contrast, the quenching efficiency increased to 5.6 x 10^5 M^{-1} in the presence of papain. This signal amplification resulted from the Hg^{2+}-induced agglutination of **V**/papain complex.

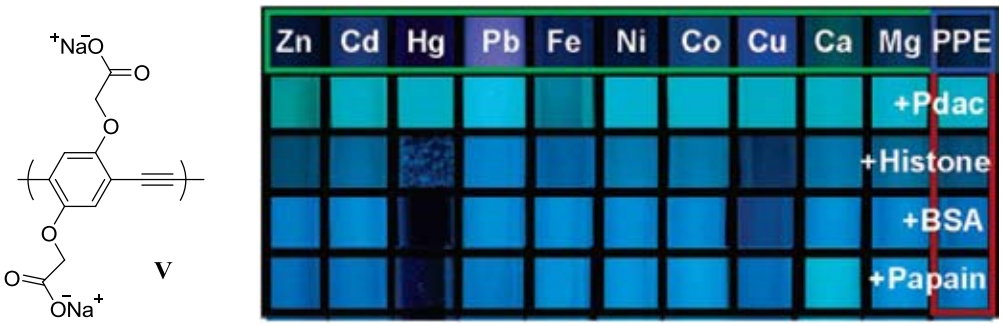

Figure 1.11 The structure of PPE (**V**) (left) and addition of metal ions to PPE (**V**) in the absence and the presence of cofactors (right).

In 2008, Li and coworker [42] developed a sensitive and selective chemosensor for copper (Cu^{2+}). In this study, various metal cations such as Mn^{2+}, Fe^{2+}, Cd^{2+}, Cr^{3+}, Pb^{2+}, Ag^{+}, Zn^{2+}, Fe^{3+}, Ni^{2+}, and Co^{2+} did not significantly alter the fluorescent signal of the imidazole-functionalized polyfluorene (**P1**). However, the fluorescence of **P1** could be selectively and completely quenched by Cu^{2+} ions. The complete and efficient quenching resulted in the detection limit of 0.2 ppm.

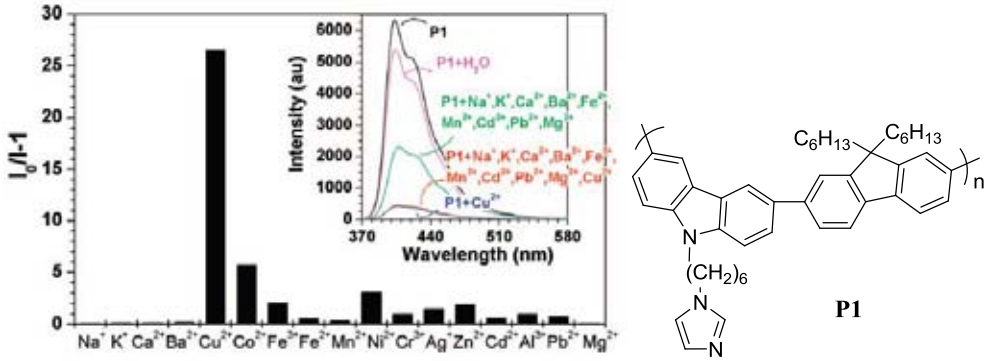

Figure 1.12 Fluorescence emission response profiles and structure of **P1** by Cu^{2+} with and without other metal ions.

In 2009, Kim and coworker [43] synthesized dichlorofluorescein derivatives with two aza-crown ether binding units using Mannich reaction (**Figure 1.13**). The chemosensing behaviors toward transition metal ions were investigated as well. They reported that the 18-crown-6 ether derivative (**1**) exhibited prominent Cu^{2+}-selectivity in abundant metal ions. The compound also displayed 1:1 complex formation with Cu^{2+} ion, with a detection limit of 2.9×10^{-6} M in DMSO and HEPES buffer solution (20 mM, pH 7). The 15-Crown-5 ether (**2**) analogue also revealed selective Cu^{2+} signaling, although with somewhat inferior signaling selectivity.

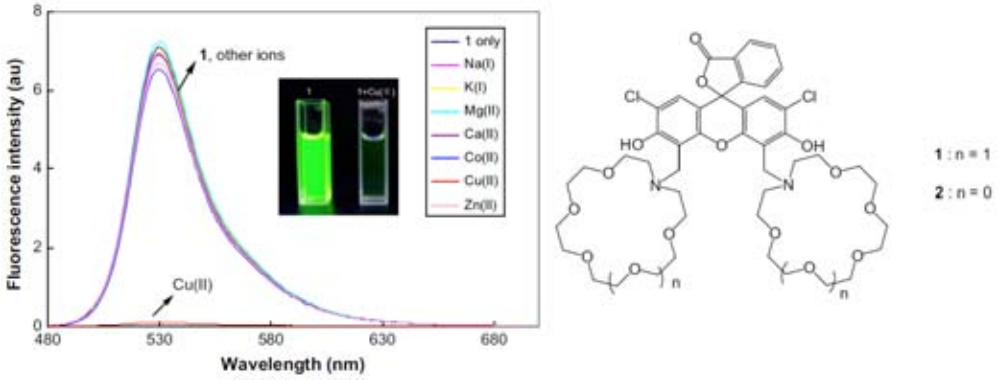

Figure 1.13 Fluorescence spectra of **1** in the presence of 7 metal ions and structure of dichlorofluorescein derivatives.

In 2010, Xu and coworker [44] studied the use of two 4,5-disubstituted-1,8-naphthalimide derivatives **1** and **2** as sensors for Cu^{2+} on the basis of ICT and deprotonation mechanisms. Compound **1** could serve as a ratiometric fluorescent sensor for Cu^{2+} which strongly emitted fluorescent signal at a shorter wavelength upon addition of Cu^{2+}. On the other hand, compound **2** could behave as a naked-eye colorimetric sensor with high selectivity toward the same metal ion. The detection limits for the use of **1** and **2** were estimated to be 1.0×10^{-8} M and 1.0×10^{-9} M, respectively.

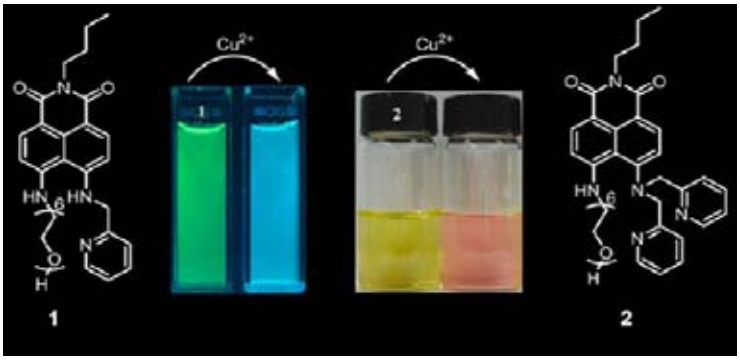

Figure 1.14 Visible emissions and color changes observed from fluorophore of **1** and **2** with the addition of Cu^{2+}.

In 2009, Niamnont and coworker [45] presented the synthesis and sensing properties of water-soluble fluorescent dendritic compound **VI** composed of phenylene-ethynylene repeating units and anionic carboxylate peripheral groups. It was found that the first generation dendrimer **VI** had a low fluorescent quantum yield, but the addition of surfactant (Triton X-100) would improve the quantum yield as well as the selectivity for the detection of Hg^{2+} ions as the Stern-Volmer constant (K_{SV}) was increased from 5,800 to 33,700 M^{-1} .

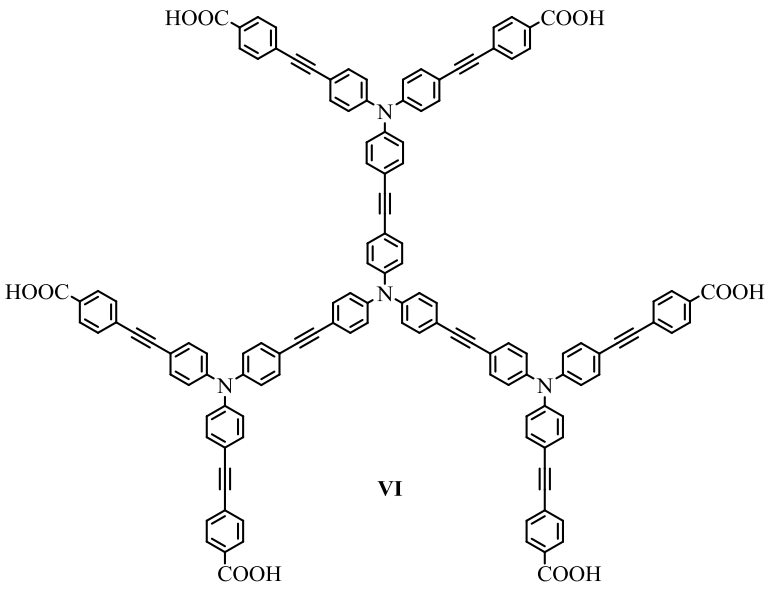

VI

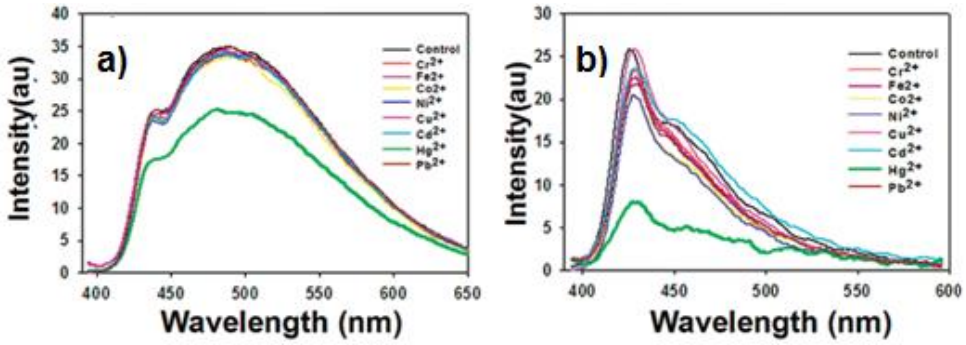

Figure 1.15 Dendritic fluorophore **VI** and its selectivity toward Hg^{2+} ion before (**a**) and after (**b**) the addition of surfactant.

In 2012, Sirilaksanapong and coworker [46] demonstrated the synthesis of three water-soluble fluorophores containing a 1,3,5-triphenylbenzene moiety and one of them showed a selective quenching by Cu^{2+} ion. A comparison of the K_{SV} at different temperatures indicated a static mode of quenching and the detection limit could be improved from 6.49 ppb to 0.19 ppb by the addition of Triton X-100, which is a comparable sensitivity compared to the electrochemical analysis.

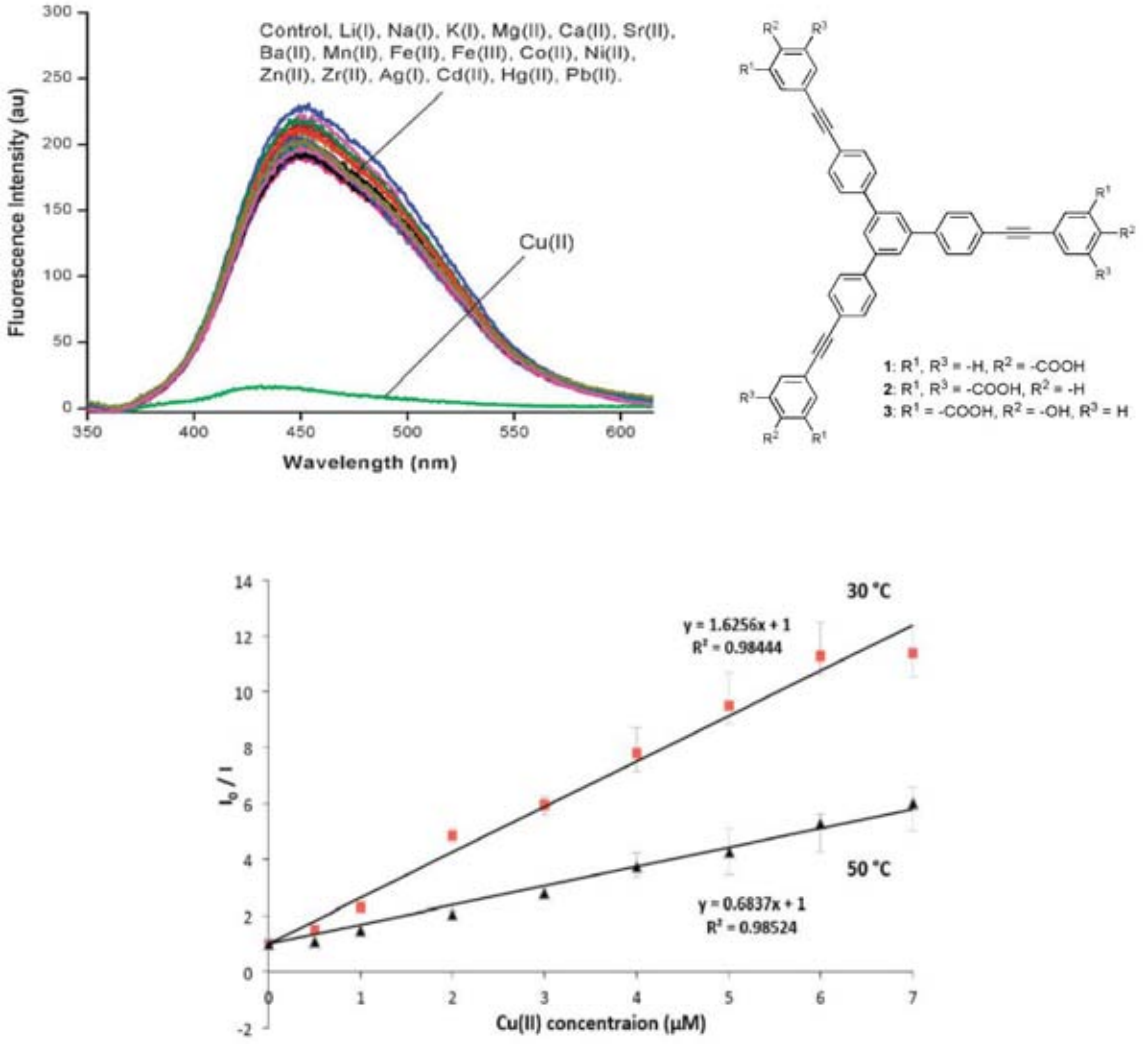

Figure 1.16 Top: Fluorescence spectra of **3** in the presence of various metal ions and structure of three water-soluble fluorophores containing a 1,3,5-triphenylbenzene moiety. Bottom: Stern-Volmer plots for the fluorescence quenching of **3** by Cu^{2+} at 30 and 50 °C.

1.7 Objective of this research

This research involves a synthesis of new water-soluble fluorophores derived from 9-phenyl-9*H*-carbazole. All compounds contain phenyleneethynylene repeating units and anionic carboxylate, anionic salicylate or cationic ammonium peripheral groups (**Figure 1.17**). In addition, structurally related compounds (**5** and **6**) are also synthesized in order to gain additional information on sensing properties of **2**.

For the assessment of rigidity effect on fluorescent efficiency, the study of photophysical properties of these compounds and comparison their quantum yields with those of their structurally related analogs containing triphenylamine core are conducted. The application of these compounds (**1-3**) for metal sensor in aqueous media is also investigated.

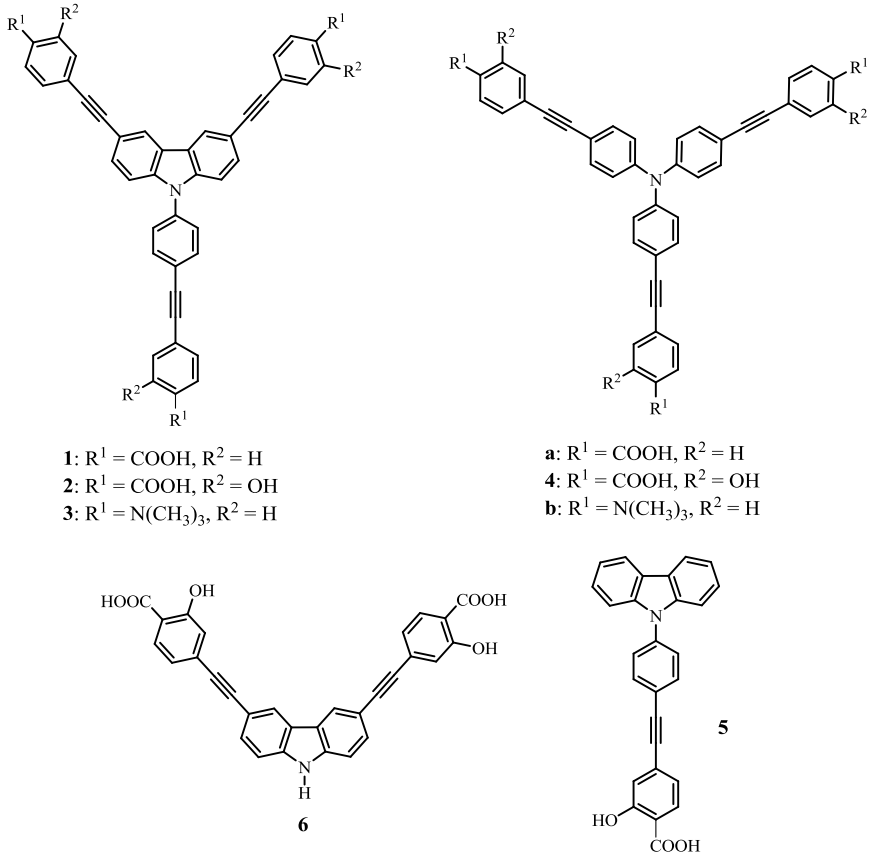

Figure 1.17 The target molecules were synthesized.

CHAPTER II

EXPERIMENTAL

2.1 Chemicals and materials

1,4-Diiodobenzene, carbazole, potassium carbonate, potassium hydroxide, potassium iodide, potassium iodate, sodium thiosulfate, sodium sulfate, copper powder, copper(I)iodide, bis(triphenylphosphine)palladium(II)dichloride ($PdCl_2(PPh_3)_2$), 18-crown-6, iodine, methyl 2-hydroxy-5-iodobenzoate, 1,8-diazabicyclo [5.4.0] undec-7-ene (DBU), methyl iodide, acetic acid and sulfuric acid were purchased from Sigma-Aldrich (USA), Fluka® (Switzerland) and Merck® (Germany). For general reactions, solvents such as dichloromethane (CH_2Cl_2) and acetonitrile (MeCN) were reagent grade. In anhydrous reactions, solvents such as toluene (PhMe), tetrahydrofuran (THF) and dimethylformamine (DMF) were dried and distilled before use according to the standard procedures. All column chromatography were operated using silica gel 60 (70-230 mesh) purchased from Merck®. The stationary phase, thin layer chromatography (TLC) was performed on silica gel plates (Merck F_{245}). Solvents used for extraction and column chromatography such as CH_2Cl_2, hexane, ethyl acetate (EtOAc) and methanol (MeOH) were commercial grade and distilled before use. Diethyl ether (Et_2O) and chloroform ($CHCl_3$) used for extraction were reagent grade. Deionized water and Milli-Q water were used in all experiments unless specified otherwise. The most reactions were carried out under positive pressure of N_2 filled in rubber balloons.

2.2 Analytical instruments

All products were characterized by ^1H NMR and ^{13}C NMR spectra were recorded on Varian Mercury NMR spectrometer (Varian, USA) and Bruker Mercury NMR spectrometer (Bruker, Germany), which executed at 400 MHz and 100 MHz, respectively. NMR spectrometer was acquired from solution in $CDCl_3$, CD_3OD, DMSO-*d6* and acetone-d^6. Mass spectra were performed on a Microflex MALDI-TOF mass

spectrometer (Bruker Daltonics) using doubly recrytallizedα-cyano-4-hydroxy cinnamic acid (CCA) as a matrix. The UV-Visible absorption spectra were recorded on a Varian Cary 50 UV-Vis spectrophotometer (Varian, USA) and fluorescence emission spectra were obtained from a Varian Cary Eclipse spectrofluorometer (Varian, USA) and Perkin Elmer precisely LS 45 Luminescence Spectrometer (Perkin Elmer, UK). The melting points operated on a melting point apparatus (Electrothermal 9100), Fisher Scientific (USA).

2.3 Synthesis procedures

2.3.1 Preparation of 3,6-diiodo-*9H*-carbazole (7)

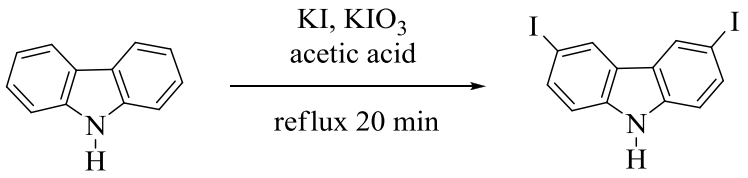

95%

To a stirred solution of carbazole (3.0 g, 17.9 mmol) in acetic acid (30 mL) was added potassium iodide (3.9 g 23.8 mmol), potassium iodate (5.6 g, 26.9 mmol). The reaction mixture was refluxed for 20 minute. The reaction mixture was diluted with water (50 mL) and extracted with EtOAc (2 × 50 mL). The combined organic phase was dried over anhydrous Na_2SO_4, filtered, and concentrated under reduced pressure. The crude product was recrystallized in methanol and water to afford **7** as light brown crystalline solid (7.2 g, 95% yield). ^{1}H NMR (400 MHz, DMSO-*d6*): δ (ppm) 7.33 (d, 2H, *J* = 8.4 Hz), 7.64 (d, 2H, *J* = 8.4 Hz), 8.55 (s, 2H), 11.54 (s, 1H); ^{13}C NMR (100 MHz, DMSO-*d*6): δ (ppm) 138.7, 134.0, 129.1, 123.8, 113.5, 81.8.

2.3.2 Preparation of 9-(4-iodophenyl)-9*H*-carbazole (8)

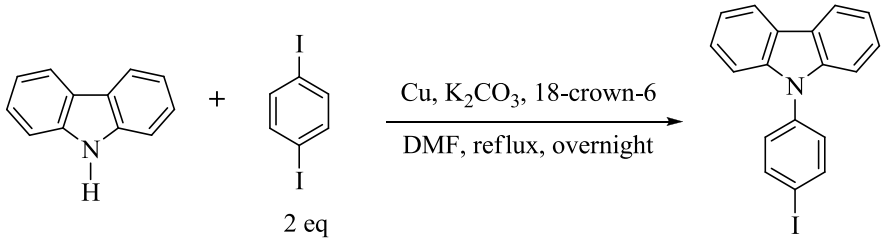

62%

To a solution of carbazole (2.0 g, 11.96 mmol) and 1,4-diiodobenzene (4.0 g, 23.92 mmol) in DMF (60 mL) were added Cu bronze (0.81 g, 12.76 mmol), K_2CO_3 (1.98 g, 14.35 mmol) and 18-crown-6 (0.085 g, 0.32 mmol). The reaction mixture was refluxed for overnight. The reaction mixture was diluted with water (30 mL) and extracted with CH_2Cl_2 (2 × 50 mL). The combined organic phase was dried over anhydrous Na_2SO_4, filtered, and concentrated under reduced pressure. The crude product was purified by column chromatography starting from pure hexane to hexane/CH_2Cl_2 (4/1) as the eluent to afford **8** as white crystalline solid (2.74 g, 62% yield). ^{1}H NMR (400 MHz, $CDCl_3$): δ (ppm) 7.29-7.35 (m, 4H) 7.38-7.45 (m, 4H), 7.93 (d, 2H, *J* = 8.4 Hz), 8.15 (d, 2H, *J* = 7.6 Hz); ^{13}C NMR (100 MHz, $CDCl_3$): δ (ppm) 92.1, 109.6, 120.3, 120.4, 123.6, 126.1, 129.0, 137.6, 139.1, 140.6.

2.3.3 Preparation of 3,6-diiodo-9-(4-iodophenyl)-9*H*-carbazole (9)

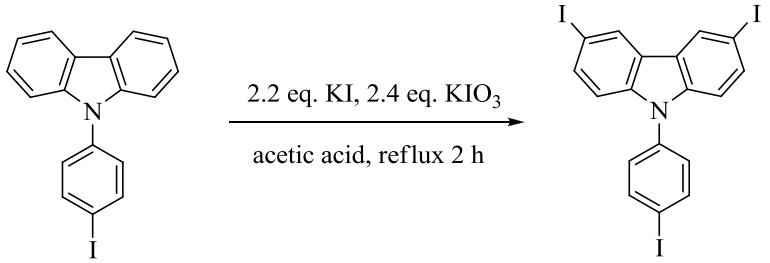

92%

Iodo compound **8** (1.0 g, 2.71 mmol) was dissolved in acetic acid (20 mL) and KI (0.99 g, 5.96 mmol) along with KIO_3 (1.39 g, 6.5mmol) were added. The reaction mixture was refluxed for 2 hour and poured into 100 mL of cooled water. Precipitates

were collected by filtration and re-dissolved in hot $CHCl_3$. The insoluble residue was filtered off and the volatile solvent was evaporated. The crude product was recrystallized in CH_2Cl_2 to afford **9** as white crystalline solid (1.55 g, 92% yield). ^{1}H NMR (400 MHz, $CDCl_3$): δ (ppm) 7.12 (d, 2H, *J* = 8.8 Hz), 7.24 (d, 2H, *J* = 8.4 Hz), 7.67 (d, 2H, *J* = 8.4 Hz), 7.93 (d, 2H, *J* = 8.4 Hz), 8.38 (s, 2H); ^{13}C NMR (100 MHz, $CDCl_3$): δ (ppm) 83.2, 93.0, 111.7, 124.6, 128.7, 129.5, 135.1, 136.5, 139.4, 139.8.

2.3.4 Preparation of methyl 4-iodobenzoate

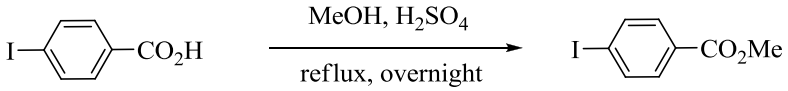

98%

Methyl 4-iodobenzoic acid (10.0 g, 40.32 mmol) was dissolved in MeOH (50 mL) and were added concentration sulfuric acid (2 mL) slowly. The reaction mixture was allowed to reflux overnight. The solvent was evaporated, and the residue was diluted with water (30 mL) and extracted with and CH_2Cl_2 (3 × 50 mL) and was then dried anhydrous Na_2SO_4. The combined filtrate was evaporated as an eluted to afford methyl 4-iodobenzoate as a white crystal (10.35 g, 98%). ^{1}H NMR (400 MHz, $CDCl_3$): δ (ppm) 3.90 (s, 3H), 7.73 (d, 2H, *J* = 8.4 Hz), 7.79 (d, 2H, *J* = 8.4 Hz); ^{13}C NMR (100 MHz, $CDCl_3$): δ (ppm) 52.3, 100.5, 129.5, 131.0, 137.7, 166.5.

2.3.5 Preparation of methyl 4-((trimethylsilyl)ethynyl)benzoate

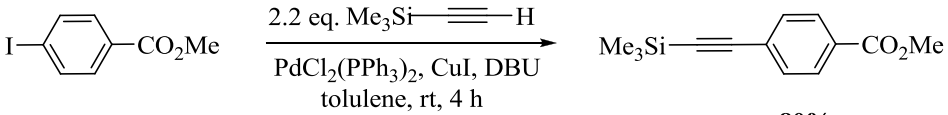

80%

Methyl 4-iodobezoate (4.0 g, 15.27 mmol), CuI (87.6 mg, 0.46 mmol), $PdCl_2(PPh_3)_2$ (322.9 mg, 0.46 mmol) and trimethylsilylacetylene (4.7 mL, 33.6 mmol) in toluene (20 mL) were added DBU (2.5 mL) slowly and the mixture was stirred at room temperature for 4 hour. The reaction mixture was diluted with water (30 mL) and extracted with CH_2Cl_2 (3 × 50 mL). The combined organic phase was dried over

anhydrous Na_2SO_4, filtered, and concentrated under reduced pressure. The crude product was purified by column chromatography starting from pure hexane to hexane/CH_2Cl_2 (2/1) as the eluent to afford methyl 4-((trimethylsilyl)ethynyl)benzoate as a white solid (2.83 g, 80% yield). ^{1}H NMR (400 MHz, $CDCl_3$): δ (ppm) 0.23 (s, 9H), 3.91 (s, 3H), 7.52 (d, 2H, J = 8.0 Hz), 7.97 (d, 2H, J = 8.0 Hz); ^{13}C NMR (100 MHz, $CDCl_3$): δ (ppm) -0.2, 52.0, 97.5, 104.0, 127.5, 129.2, 129.5, 131.6, 166.3.

2.3.6 Preparation of methyl 4-ethynylbenzoate

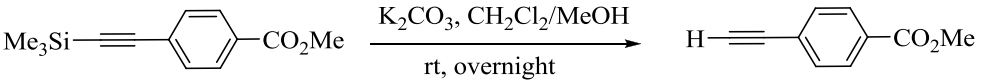

87%

Methyl 4-((trimethylsilyl)ethynyl)benzoate (2.0 g, 8.62mmol) and K_2CO_3 (0.2 g, 1.47 mmol) in CH_2Cl_2 (30 mL) and MeOH (30 mL) was stirred at room temperature for overnight. The reaction mixture was diluted with water (30 mL) and extracted with CH_2Cl_2 (2 × 50 mL). The combined organic phase was dried over anhydrous Na_2SO_4, filtered, and concentrated under reduced pressure. The crude product was purified by column chromatography starting from pure hexane to hexane/CH_2Cl_2 (1/1) as the eluent to afford Methyl 4-ethynylbenzoate as a white solid (1.2 g, 87% yield).^{1}H NMR (400 MHz, $CDCl_3$): δ (ppm) 3.22 (s, 1H), 3.91 (s, 3H), 7.54 (d, 2H, J = 8.4 Hz), 7.98 (d, 2H, J = 8.4 Hz); ^{13}C NMR (100 MHz, $CDCl_3$): δ (ppm) 52.2, 80.0, 82.7, 126.7, 129.4, 130.1, 132.0, 166.3.

2.3.7 Preparation of 4-iodo-*N,N*-dimethylaniline

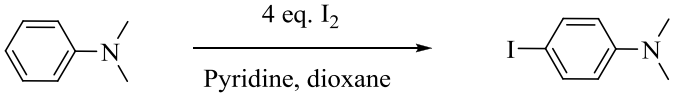

85%

N,N-dimethylaniline (2.0 g, 16.5 mmol) was dissolved in Pyridine (50 mL) and Dioxane (50 mL) was stirred in ice-bath and was added with I_2 (8.0 g, 32 mmol) after 1 hour, removed the ice-bath, then stirred 1 hour at room temperature. The mixture was extracted with CH_2Cl_2 (2 × 50 mL) and the combined organic layer was washed with

$Na_2S_2O_8$ and dried anhydrous Na_2SO_4. The combined filtrate was evaporated and purified by crystallization with MeOH and water 4-iodo-*N,N*-dimethylaniline was obtained as a white crystal (3.49 g, 85% yield). ^{1}H NMR (400 MHz, $CDCl_3$): δ (ppm) 2.92 (s, 6H), 6.49 (d, 2H, *J* = 8.8 Hz), 7.46 (d, 2H, *J* = 9.2); ^{13}C NMR (100 MHz, $CDCl_3$): δ (ppm) 40.5, 114.7, 137.5.

2.3.8 Preparation of *N,N*-dimethyl-4-((trimethylsilyl)ethynyl)aniline

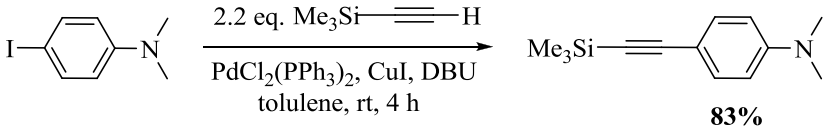

83%

4-iodo-*N,N*-dimethylaniline (2.0 g, 8.1 mmol) CuI (46.3 mg, 0.243 mmol), $PdCl_2(PPh_3)_2$ (170.6 mg, 0.243 mmol) and trimethylsilylacetylene (2.5 mL, 17.82 mmol) in toluene (10 mL) were added DBU (1.5 mL) slowly and the mixture was stirred at room temperature for 4 hour. The reaction mixture was diluted with water (30 mL) and extracted with CH_2Cl_2 (2 × 50 mL). The combined organic phase was dried over anhydrous Na_2SO_4, filtered, and concentrated under reduced pressure. The crude product was purified by column chromatography starting from pure hexane to hexane/EtOAc (4/1) as the eluent to afford *N,N*-dimethyl-4-((trimethylsilyl)ethynyl)aniline as a yellow solid (1.46 g, 83% yield). ^{1}H NMR (400 MHz, $CDCl_3$): δ (ppm) 0.24 (s, 9H), 2.97 (s, 6H), 6.59 (d, 2H, *J* = 8.8 Hz), 7.35 (d, 2H, *J* = 9.2 Hz); ^{13}C NMR (100 MHz, $CDCl_3$): δ (ppm) 0.01, 40.0, 91.0, 106.5, 109.6, 111.4, 133.0, 150.0.

2.3.9 Preparation of 4-ethynyl-*N,N*-dimethylaniline

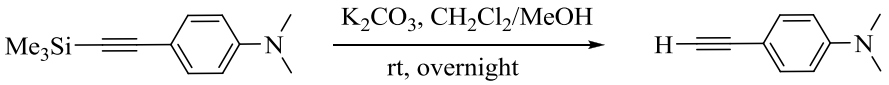

90%

N,N-dimethyl-4-((trimethylsilyl)ethynyl)aniline (1.0 g, 4.61 mmol) and K_2CO_3 (0.11 g, 0.78 mmol) in CH_2Cl_2 (15 mL) and MeOH (15 mL) was stirred at room temperature overnight. The reaction mixture was diluted with water (30 mL) and extracted with CH_2Cl_2 (2 × 30 mL). The combined organic phase was dried over

anhydrous Na_2SO_4, filtered, and concentrated under reduced pressure. The crude product was purified by column chromatography starting from pure hexane to hexane/EtOAc (4/1) as the eluent to afford 4-ethynyl-*N,N*-dimethylaniline as a yellow solid (0.6 g, 90% yield).[1]H NMR (400 MHz, $CDCl_3$): δ (ppm) 2.98 (s, 7H), 6.62 (d, 2H, J = 8.8 Hz), 7.37 (d, 2H, J = 8.8 Hz); [13]C NMR (100 MHz, $CDCl_3$): δ (ppm) 40.0, 75.0, 85.0, 108.6, 111.7, 133.2, 150.4.

2.3.10 Preparation of methyl 2-hydroxy-4-((trimethylsilyl)ethynyl)benzoate

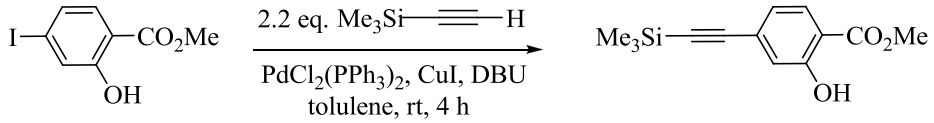

85%

Methyl 2-hydroxy-4-iodobenzoate (1.0 g, 3.6 mmol), CuI (20.6 mg, 0.108 mmol), $PdCl_2(PPh_3)_2$ (75.8 mg, 0.108 mmol) and trimethylsilylacetylene (1.1 mL, 7.92 mmol) in toluene (10 mL) were added DBU (0.6 mL) slowly and the mixture was stirred at room temperature for 4 hour. The reaction mixture was diluted with water (30 mL) and extracted with CH_2Cl_2 (2 × 30 mL). The combined organic phase was dried over anhydrous Na_2SO_4, filtered, and concentrated under reduced pressure. The crude product was purified by column chromatography starting from pure hexane to hexane/EtOAc (4/1) as the eluent to afford methyl 2-hydroxy-4-((trimethylsilyl)ethynyl)benzoate as a yellow solid (0.75 g, 85% yield). [1]H NMR (400 MHz, $CDCl_3$): δ (ppm) 0.24 (s, 9H), 3.92 (s, 3H), 6.93 (d, 1H, J = 8.0 Hz), 7.05 (s, 1H), 7.73 (d, 1H, J = 8.0 Hz) 10.71 (s, 1H); [13]C NMR (100 MHz, $CDCl_3$): δ (ppm) 0.07, 52.6, 98.1, 103.8, 112.4, 120.9, 122.8, 129.8, 130.4, 161.2, 170.2.

2.3.11 Preparation of methyl 4-ethynyl-2-hydroxybenzoate

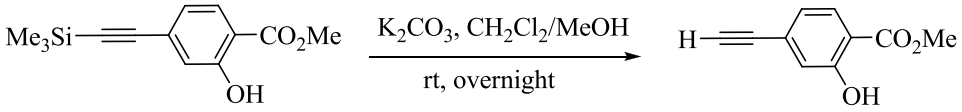

89%

Methyl 2-hydroxy-4-((trimethylsilyl)ethynyl)benzoate (0.8 g, 3.22 mmol) and K_2CO_3 (0.076 g, 0.55 mmol) in CH_2Cl_2 (10 mL) and MeOH (10 mL) was stirred at room temperature overnight. The reaction mixture was diluted with water (30 mL) and extracted with CH_2Cl_2 (2 × 30 mL). The combined organic phase was dried over anhydrous Na_2SO_4, filtered, and concentrated under reduced pressure. The crude product was purified by column chromatography starting from pure hexane to hexane/EtOAc (4/1) as the eluent to afford methyl 4-ethynyl-2-hydroxybenzoate as a yellow solid (0.50 g, 89% yield). ^{1}H NMR (400 MHz, $CDCl_3$): δ (ppm) 3.21 (s, 1H), 3.95 (s, 3H), 6.99 (d, 1H, J = 8.0 Hz), 7.10 (s, 1H), 7.78 (d, 1H, J = 8.4 Hz), 10.76 (s, 1H); ^{13}C NMR (100 MHz, $CDCl_3$): δ (ppm) 52.4, 80.1, 82.5, 112.7, 121.1, 122.8, 129.3, 129.8, 161.2, 170.0.

2.3.12 Preparation of 10

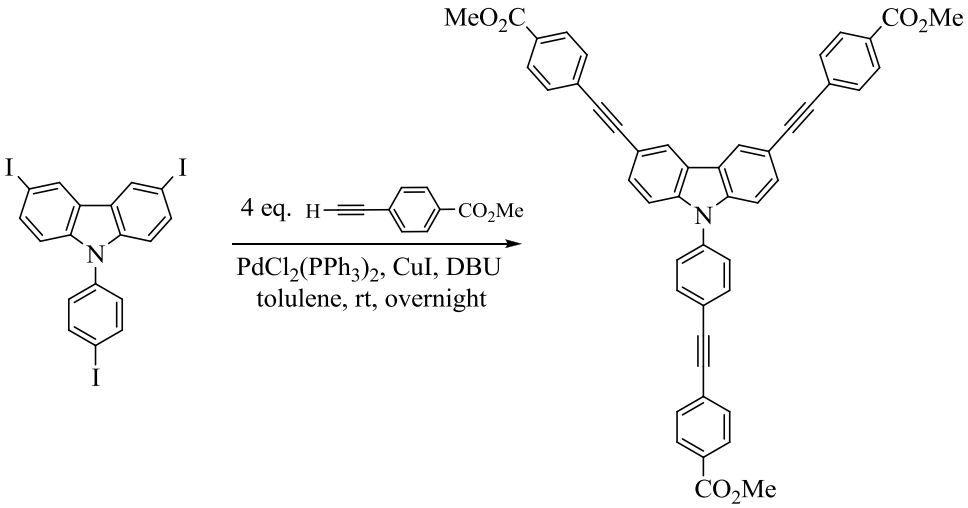

73%

To a mixture of **9** (0.4 g, 0.64 mmol), CuI (12.3 mg, 0.1mmol), $PdCl_2(PPh_3)_2$ (45.2 mg, 0.1mmol) and methyl 4-ethynylbenzoate (0.52 g, 3.22mmol) in toluene (5.0

mL) were added DBU (0.5 mL) slowly and the mixture was stirred at room temperature overnight. The reaction mixture was diluted with water (30 mL) and extracted with CH_2Cl_2 (2 × 30 mL). The combined organic phase was dried over anhydrous Na_2SO_4, filtered, and concentrated under reduced pressure. The crude product was purified by column chromatography starting from pure hexane to hexane/EtOAc (4/1) as the eluent to afford **10** as a yellow solid (0.335 g, 73% yield). ^{1}H NMR (400 MHz, $CDCl_3$): δ (ppm) 3.94 (s, 9H), 7.41 (d, 2H, *J* = 8.4 Hz), 7.58-7.66 (m, 10H), 7.81 (d, 2H,*J* = 8.0 Hz), 8.04-8.08 (m, 6H), 8.35 (s, 2H); ^{13}C NMR (100 MHz, $CDCl_3$): δ (ppm) 52.2, 52.3, 87.8, 90.0, 91.2, 93.3, 110.2, 115.0, 122.7, 123.2, 124.4, 126.9, 127.5, 128.4, 129.3, 129.57, 129.6, 129.9, 130.3, 131.4, 131.6, 133.5, 136.9, 140.8, 166.5, 166.6. MALDI-TOF m/z calcd for 717.215 found: 717.912.

2.3.13 Preparation of 11

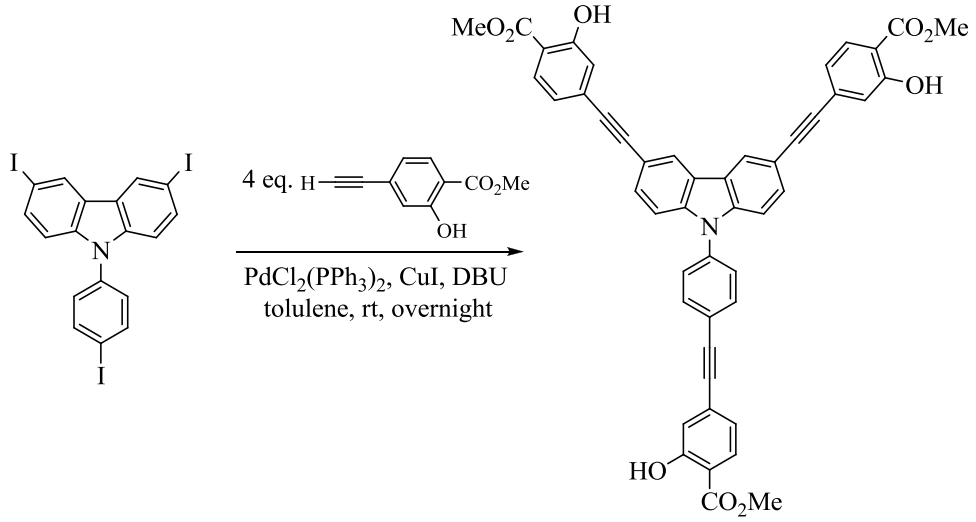

72%

To a mixture of **9** (0.3 g, 0.48 mmol), CuI (9.2 mg, 0.048 mmol), $PdCl_2(PPh_3)_2$ (33.9 mg, 0.048 mmol) and methyl 4-ethynyl-2-hydroxybenzoate (0.425 g, 2.42 mmol) in toluene (5.0 mL) were added DBU (0.4 mL) slowly and the mixture was stirred at room temperature overnight. The reaction mixture was diluted with water (30 mL) and

extracted with CH_2Cl_2 (2 × 50 mL). The combined organic phase was dried over anhydrous Na_2SO_4, filtered, and concentrated under reduced pressure. The crude product was purified by column chromatography starting from pure hexane to hexane/EtOAc (4/1) as the eluent to afford **11** as a yellow solid (0.27 g, 73% yield). ^{1}H NMR (400 MHz, $CDCl_3$): δ (ppm) 3.97 (s, 9H), 7.09 (d, 3H, *J* = 8.0 Hz), 7.19 (s, 3H), 7.40 (d, 2H, *J* = 8.4 Hz), 7.57-7.64 (m, 4H), 7.80-7.88 (m, 5H), 8.35 (s, 2H), 10.81 (s, 3H); ^{13}C NMR (100 MHz, $CDCl_3$): δ (ppm) 52.4, 52.5, 87.7, 89.8, 91.3, 93.5, 110.2, 111.9, 112.4, 114.9, 120.2, 120.5, 122.3, 122.4, 122.5, 123.2, 124.5, 126.9, 129.8, 129.9, 130.1, 130.4, 131.0, 133.6, 137.0, 140.9, 161.3, 170.1, 170.2. MALDI-TOF m/z calcd for 765.200 found: 765.114.

2.3.14 Preparation of 12

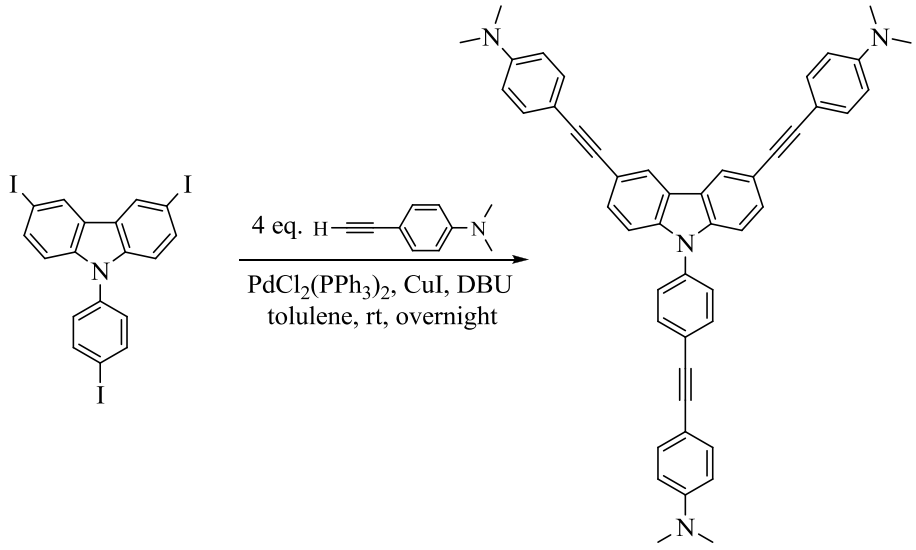

68%

To a mixture of **9** (0.32 g, 0.52 mmol), CuI (8.8 mg, 0.047 mmol), $PdCl_2(PPh_3)_2$ (32.6 mg, 0.047 mmol) and 4-ethynyl-*N,N*-dimethylaniline (0.3 g, 2.07 mmol) in toluene (5.0 mL) was added DBU (0.3 mL) slowly and the mixture was stirred at room temperature overnight. The reaction mixture was diluted with water (30 mL) and extracted with CH_2Cl_2 (2 × 30 mL). The combined organic phase was dried over anhydrous Na_2SO_4, filtered, and concentrated under reduced pressure. The crude product

was purified by column chromatography starting from pure hexane to hexane/EtOAc (4/1) as the eluent to afford **12** as a yellow solid (0.24 g, 68% yield). ^{1}H NMR (400 MHz, $CDCl_3$): δ (ppm) 3.01 (s, 18H), 6.69 (d, 6H, *J* = 8.4 Hz), 7.36 (d, 2H, *J* = 8.4 Hz), 7.45-7.48 (m, 6H) 7.52 (d, 2H, *J* = 8.4 Hz), 7.57 (d, 2H, *J* = 8.4 Hz), 7.72 (d, 2H, *J* = 8.8 Hz), 8.27 (s, 2H); The ^{13}C NMR (100 MHz, $CDCl_3$) cannot be obtained because the sample is unstable. MALDI-TOF m/z calcd for 672.325 found: 672.192.

2.3.15 Preparation of 13

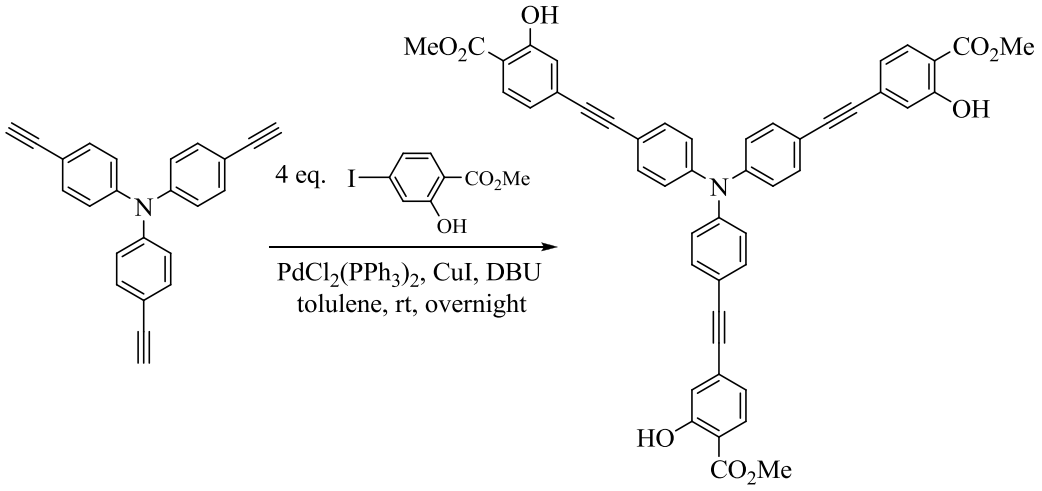

65%

To a mixture of tris(4-ethynylphenyl)amine (0.5 g, 1.58 mmol), CuI (30 mg, 0.16 mmol), $PdCl_2(PPh_3)_2$ (111 mg, 0.16 mmol) and methyl 2-hydroxy-4-iodobenzoate (2.19 g, 7.88 mmol) in toluene (10.0 mL) were added DBU (1.2 mL) slowly and the mixture was stirred at room temperature overnight. The reaction mixture was diluted with water (30 mL) and extracted with CH_2Cl_2 (2 × 50 mL). The combined organic phase was dried over anhydrous Na_2SO_4, filtered, and concentrated under reduced pressure. The crude product was purified by column chromatography starting from pure hexane to hexane/EtOAc (4/1) as the eluent to afford **13** as a yellow solid (0.78 g, 65% yield). ^{1}H NMR (400 MHz, $CDCl_3$): δ (ppm) 3.96 (s, 9H), 7.02 (d, 3H, *J* = 8.4 Hz), 7.08-7.12 (m, 9H), 7.45 (d, 6H, *J* = 8.4 Hz), 7.80 (d, 3H, *J* = 8.4 Hz), 10.78 (s, 3H); ^{13}C NMR (100

MHz, $CDCl_3$): δ (ppm) 52.4, 88.6, 92.4, 112.0, 117.5, 120.2, 122.3, 124.1, 129.8, 130.6, 133.1, 147.0, 161.3, 170.2. MALDI-TOF m/z calcd for 767.216 found: 766.807.

2.3.16 Preparation of 14

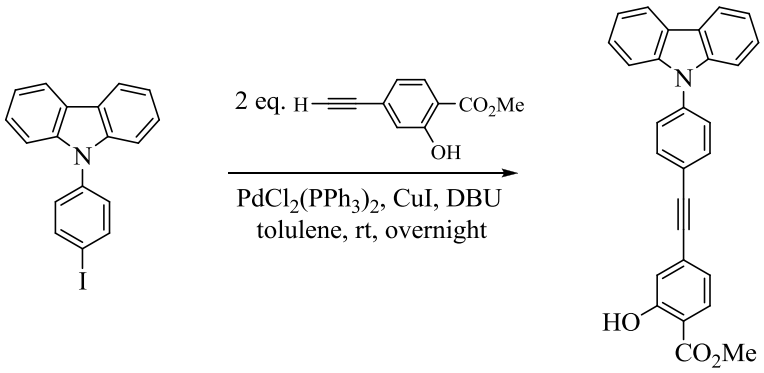

74%

To a mixture of **8** (0.3 g, 0.81 mmol), CuI (9 mg, 0.049 mmol), $PdCl_2(PPh_3)_2$ (34 mg, 0.049 mmol) and methyl 4-ethynyl-2-hydroxybenzoate (0.36 g, 2.03 mmol) in toluene (5.0 mL) were added DBU (0.3 mL) slowly and the mixture was stirred at room temperature overnight. The reaction mixture was diluted with water (30 mL) and extracted with CH_2Cl_2 (2 × 30 mL). The combined organic phase was dried over anhydrous Na_2SO_4, filtered, and concentrated under reduced pressure. The crude product was purified by column chromatography starting from pure hexane to hexane/CH_2Cl_2 (4/1) as the eluent to afford **14** as a white solid (0.25 g, 74% yield). ^{1}H NMR (400 MHz, $CDCl_3$): δ (ppm) 3.98 (s, 3H), 7.09 (d, 1H, J = 7.6 Hz), 7.20 (s, 1H), 7.30 (t, 2H, J = 6.4 Hz), 7.41-7.47 (m, 4H), 7.60 (d, 2H, J = 8.4 Hz), 7.78 (d, 2H, J = 8.4 Hz), 7.85 (d, 1H, J = 8.0 Hz), 8.15 (d, 2H, J = 7.6 Hz), 10.83 (s, 1H); ^{13}C NMR (100 MHz, $CDCl_3$): δ (ppm) 52.4, 89.3, 91.7, 109.7, 112.3, 120.3, 120.4, 120.5, 121.5, 122.4, 123.7, 126.1, 126.9, 129.9, 130.3, 133.4, 138.2, 140.5, 161.3, 170.1. MALDI-TOF m/z calcd for 417.136found: 416.453.

2.3.17 Preparation of 15

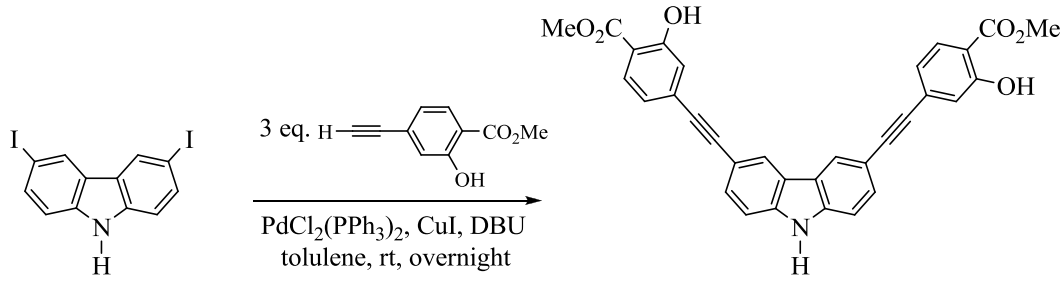

47%

To a mixture of **7** (0.3 g, 0.72 mmol), CuI (12.3 mg, 0.064 mmol), $PdCl_2(PPh_3)_2$ (45.2 mg, 0.064 mmol) and methyl 4-ethynyl-2-hydroxybenzoate (0.38 g, 2.15 mmol) in toluene (5.0 mL) was added DBU (0.32 mL) slowly and the mixture was stirred at room temperature overnight. The reaction mixture was diluted with water (30 mL) and extracted with CH_2Cl_2 (2 × 30 mL). The combined organic phase was dried over anhydrous Na_2SO_4, filtered, and concentrated under reduced pressure. The crude product was purified by column chromatography starting from pure hexane to hexane/EtOAc (2/1) as the eluent to afford **15** as a yellow solid (0.15 g, 47% yield). ^{1}H NMR (400 MHz, $CDCl_3$): δ (ppm) 3.90 (s, 6H), 7.01 (d, 2H, *J* = 7.2 Hz), 7.11 (s, 2H), 7.37 (d, 2H, *J* = 8.8 Hz), 7.57 (d, 2H, *J* = 8.0 Hz), 7.76 (d, 2H, *J* = 8.0 Hz), 8.23 (s, 2H), 10.74 (s, 2H); ^{13}C NMR (100 MHz, $CDCl_3$): δ (ppm) 52.3, 87.3, 93.8, 111.0, 111.8, 114.1, 120.1, 122.3, 123.0, 124.6, 129.8, 130.3, 131.1, 139.8, 161.3, 170.2. MALDI-TOF m/z calcd for 515.137 found: 514.514.

2.3.18 Preparation of 1

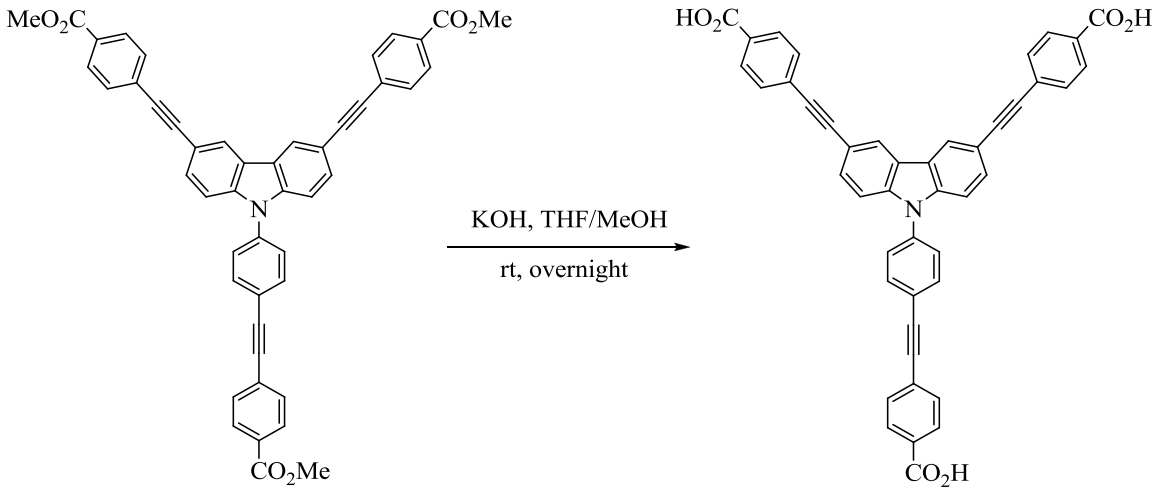

80%

To a mixture of **10** (0.5 g, 0.70 mmol) in THF (10 mL) and MeOH (10 mL) was added with saturated KOH aqueous solution (0.3 mL) and the mixture was stirred at room temperature overnight. The solution was evaporated and the residue dissolved in water (10 mL) and was added 1M HCl cool in ice-bath. The solution in suspension was centrifuged to afford **1** as a brown solid (0.38 g, 80% yield). ^{1}H NMR (400 MHz, DMSO-*d6*): δ (ppm) 7.45 (d, 2H, *J* = 8.4 Hz), 7.63-7.73 (m, 10H), 7.86 (d, 2H, *J* = 8.0 Hz), 7.92-7.96 (m, 6H), 8.60 (s, 2H); ^{13}C NMR (100 MHz, DMSO-*d6*): δ (ppm) 87.7, 89.7, 91.1, 93.2, 110.6, 114.0, 121.5, 122.7, 124.7, 126.3, 127.1, 129.6, 130.2, 130.5, 130.8, 131.3, 131.6, 132.7, 133.5, 136.4, 140.3, 166.6, 166.7. MALDI-TOF m/z calcd for 675.168 found: 674.886.

2.3.19 Preparation of 2

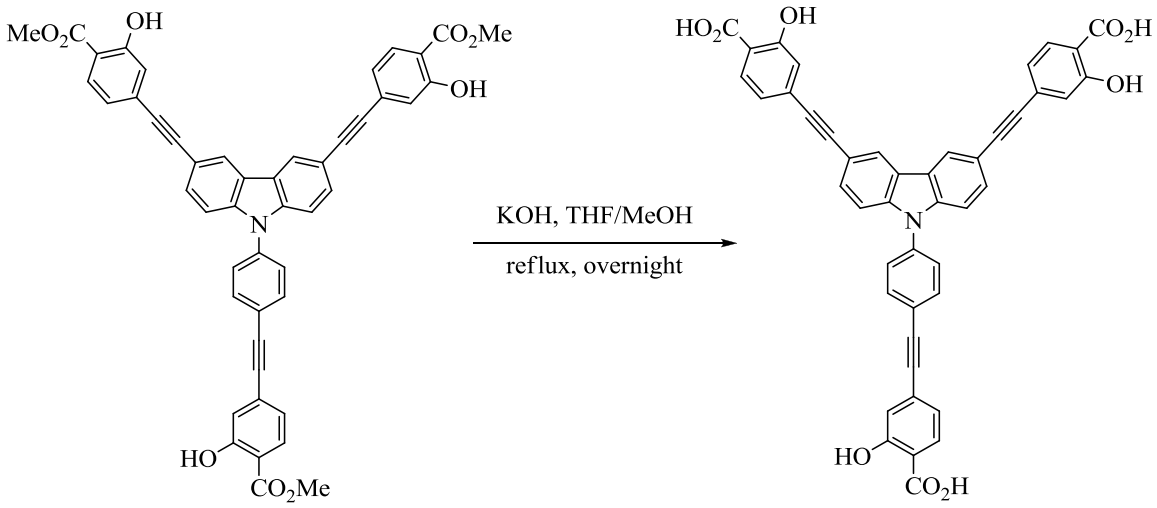

75%

To a mixture of **11** (0.3 g, 0.39 mmol) in THF (10 mL) and MeOH (10 mL) was added with saturated KOH aqueous solution (0.5 mL) and the mixture was stirred at 60 °C overnight. The solution was evaporated and the residue dissolved in water (10 mL) and was added 1M HCl cool in ice-bath. The solution in suspension was centrifuged to afford **2** as a yellow solid (0.21 g, 75% yield). ^{1}H NMR (400 MHz, acetone-d^{6}): δ (ppm) 7.15-7.21 (m, 6H), 7.55 (d, 2H, *J* = 8.8 Hz), 7.72 (d, 2H, *J* = 8.4 Hz), 7.80 (d, 2H, *J* = 8.8 Hz), 7.94-7.98 (m, 5H), 8.59 (s, 2H); ^{13}C NMR (100 MHz, DMSO-*d6*): δ (ppm) 87.5, 89.4, 91.1, 93.2, 110.6, 113.0, 113.9, 119.1, 119.6, 121.4, 122.0, 122.2, 122.7, 124.9, 127.0, 128.7, 128.8, 129.5, 130.5, 130.6, 130.7, 131.4, 131.5, 133.5, 136.4, 140.3, 160.8, 171.2. MALDI-TOF m/z calcd for 723.153 found: 723.430.

2.3.20 Preparation of 3

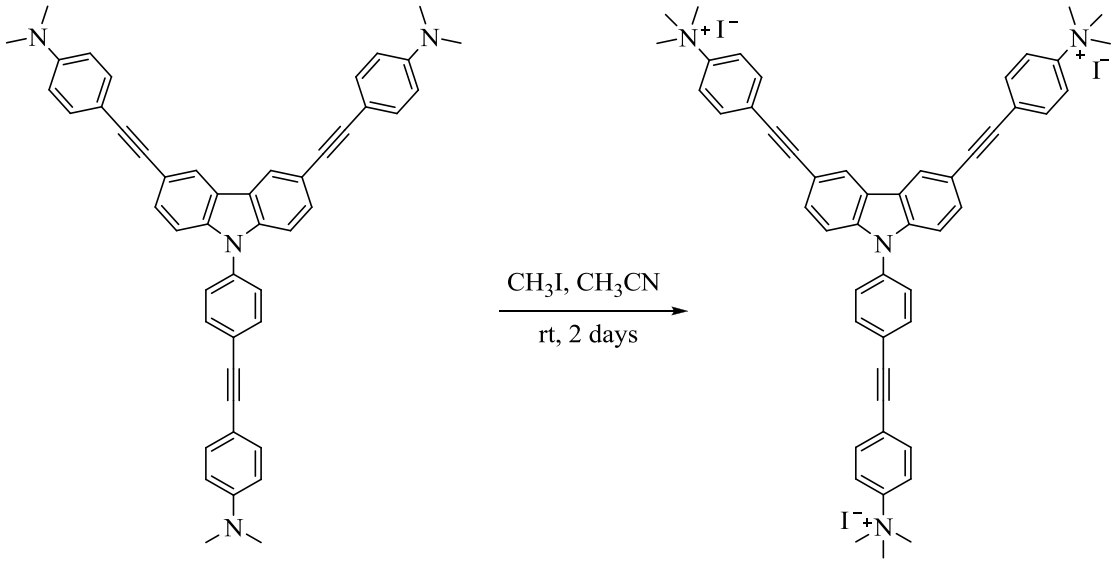

70%

To a mixture of **12** (0.3 g, 0.45 mmol) in CH_3CN (15 mL) was added CH_3I (0.5 mL) and the mixture was stirred at room temperature for 2 days. The solution was evaporated to afford **3** as a brown solid (0.225 g, 70% yield). ^{1}H NMR (400 MHz, CD_3OD): δ (ppm) 3.67 (s, 27H), 7.50 (d, 2H, *J* = 7.6 Hz), 7.68-7.72 (m, 4H), 7.82-7.88 (m, 6H), 7.91 (d, 2H, *J* = 8.4 Hz), 7.97-8.03 (m, 6H), 8.48 (s, 2H); ^{13}C NMR (100 MHz, DMSO-*d6*): δ (ppm) 56.4, 86.5, 88.5, 90.6, 92.5, 110.7, 111.9, 112.0, 113.9, 121.2, 121.3, 122.7, 123.9, 124.6, 124.8, 127.1, 130.6, 132.2, 132.5, 132.6, 132.9, 133.6, 136.4, 140.3, 146.6, 147.0.

2.3.21 Preparation of 4

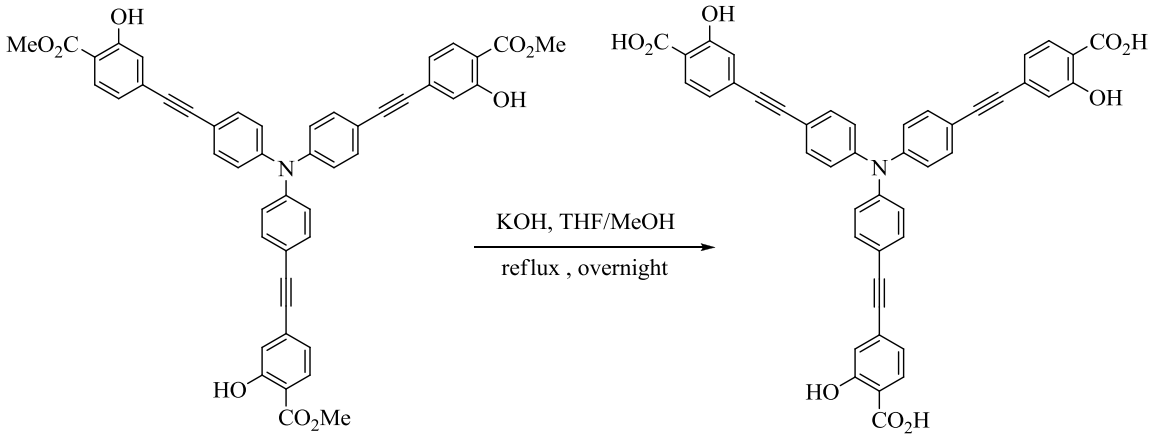

90%

To a mixture of **13** (0.3 g, 0.39 mmol) in THF (15 mL) and MeOH (15 mL) was added with saturated KOH aqueous solution (0.5 mL) and the mixture was stirred at 60 °C overnight. The solution was evaporated and the residue dissolved in water (10 mL) and was added 1M HCl cool in ice-bath. The solution in suspension was centrifuged to afford **4** as a yellow solid (0.25 g, 90% yield).^{1}H NMR (400 MHz, CD_3OD): δ (ppm) 6.95-7.03 (m, 12H), 7.42 (d, 6H, J = 8.4 Hz), 7.79 (d, 3H, J = 8.4 Hz); ^{13}C NMR (100 MHz, CD_3OD): δ (ppm) 89.5, 93.0, 113.8, 118.9, 120.6, 123.2, 125.3, 131.57, 131.6, 134.3, 148.4, 162.9, 173.0.

2.3.22 Preparation of 5

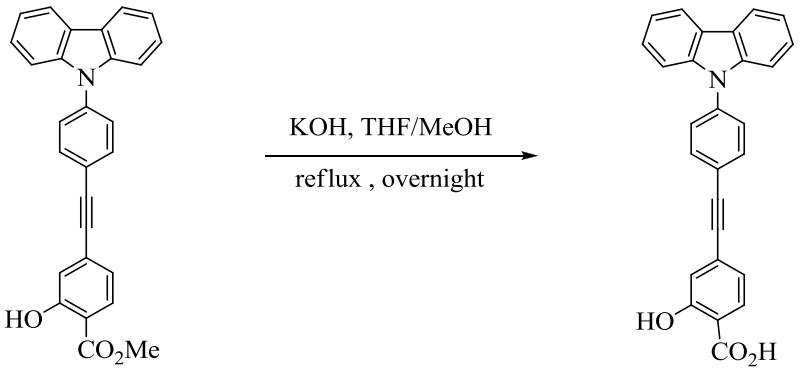

76%

To a mixture of **14** (0.2 g, 0.48 mmol) in THF (10 mL) and MeOH (10 mL) was added with saturated KOH aqueous solution (0.3 mL) and the mixture was stirred at 60 °C overnight. The solution was evaporated and the residue dissolved in water (10 mL) and was added 1M HCl cool in ice-bath. The solution in suspension was centrifuged to afford **5** as a white solid (0.15 g, 76% yield).^{1}H NMR (400 MHz, DMSO-*d6*): δ (ppm) 7.08-7.13 (m, 2H), 7.23 (s, 2H), 7.38-7.41 (m, 4H), 7.67 (d, 2H, *J* = 8.0 Hz), 7.77-7.83 (m, 3H), 8.20 (d, 2H, *J* = 7.6 Hz); ^{13}C NMR (100 MHz, DMSO-*d6*): δ (ppm) 89.1, 91.3, 109.7, 113.6, 119.5, 120.4, 120.6, 122.2, 123.0, 126.4, 126.8, 128.7, 130.7, 133.4, 137.5, 139.7, 160.8, 171.2. MALDI-TOF m/z calcd for 403.121 found: 402.390.

\

2.3.23 Preparation of 6

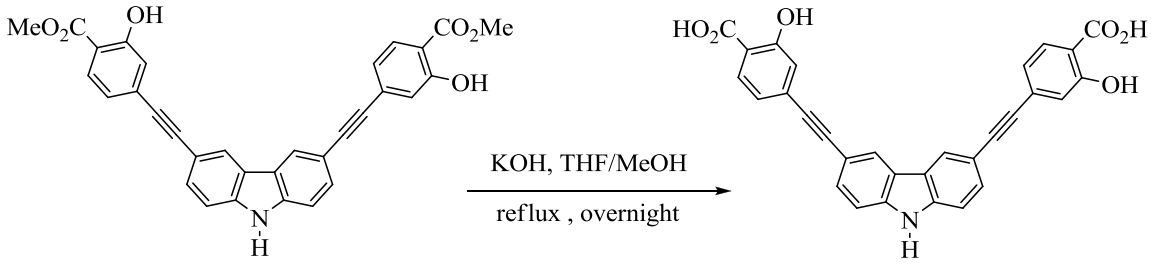

85%

To a mixture of **15** (0.1 g, 0.19 mmol) in THF (5 mL) and MeOH (5 mL) was added with saturated KOH aqueous solution (0.3 mL) and the mixture was stirred at 60 °C overnight. The solution was evaporated and the residue dissolved in water (10 mL) and was added 1M HCl cool in ice-bath. The solution in suspension was centrifuged to afford **6** as a brown solid (0.079 g, 85% yield). ^{1}H NMR (400 MHz, DMSO-*d6*): δ (ppm) 7.08-7.10 (m, 4H), 7.55-7.63 (m, 4H), 7.80 (d, 2H, *J* = 7.6 Hz), 8.5 (s, 2H), 12.01 (s, 2H); ^{13}C NMR (100 MHz, DMSO-*d6*): δ (ppm) 86.8, 94.0, 111.8, 112.0, 112.9, 119.0, 122.0, 122.1, 124.6, 129.7, 130.6, 140.3, 160.8, 171.2. MALDI-TOF m/z calcd for 487.106 found: 486.558.

2.4 Photophysical property study

The stock solutions of 150 μM fluorophores (**1**-**6**) diluted to 20 μM in 10 mM phosphate buffer (PB) pH 8.0 were prepared.

2.4.1 UV-Visible spectroscopy

The UV-Visible absorption spectra of the stock solutions of fluorophores were recorded from 250 nm to 700 nm at ambient temperature.

2.4.2 Fluorescence spectroscopy

The stock solutions of fluorophores were diluted to 1 μM, 10 mM phosphate buffer pH 8.0. The emission spectra of three compounds were recorded from 350 nm to 650 nm at ambient temperature using an excitation wavelength at 337, 343, 335, 377, 330 and 347 nm for fluorophores (**1**-**6**), respectively.

2.4.3 Fluorescence quantum yields

The fluorescence quantum yield of fluorophores were performed in 10 mM phosphate buffer pH 8.0 by using quinine sulfate in 0.1 M H_2SO_4 (Φ_F = 0.54) as a reference [45]. The UV-Visible absorption spectra of five analytical samples and five reference sample sat varied concentrations were recorded. The maximum absorbance of all samples should never exceed 0.1. The fluorescence emission spectra of the same solutions using appropriate excitation wavelengths selected were recorded based on the maximum absorption wavelength (λ_{max}) of each compound. Graphs of integrated fluorescence intensities were plotted against the absorbance at the respective excitation wavelengths. Each plot should be a straight line with 0 interception and gradient *m*.

In addition, the fluorescence quantum yield (Φ_F) was obtained from plotting of integrated fluorescence intensity *vs* absorbance represented into the following equation:

$$\Phi_X = \Phi_{ST}\left(\frac{Grad_X}{Grad_{ST}}\right)\left(\frac{\eta_X^2}{\eta_{ST}^2}\right)$$

The subscripts Φ_{ST} denote the fluorescence quantum yield of a standard as a reference with used quinine sulfate in 0.1 M H_2SO_4 (Φ_F = 0.54) and Φ_X is the fluorescence quantum yield of sample and η is the refractive index of the solvent.

2.5 Fluorescent sensor study

2.5.1 Metal ion sensor

The stock solutions of fluorophores (**1-6**) with a concentration of 10 mM in phosphate buffer pH 8.0 were prepared. The emission spectra of fluorophores (**1-6**) were recorded from 350 nm to 650 nm at ambient temperature. Their photophysical properties were studied in the presence of sixteen metal ions. The stock solutions of metal acetate were prepared by dissolving the salts in Milli-Q water (1000 μM) then diluted to 20 μM. The 20 μM of each stock metal solution were added (0-667 μL) to the fluorop solutions. The final volumes of the mixtures were adjusted to 1 mL to afford th concentration of 1 μM for the fluorophores and 0-10 μM for metal ions.

CHAPTER III

RESULTS AND DISCUSSION

3.1 Synthesis and characterization

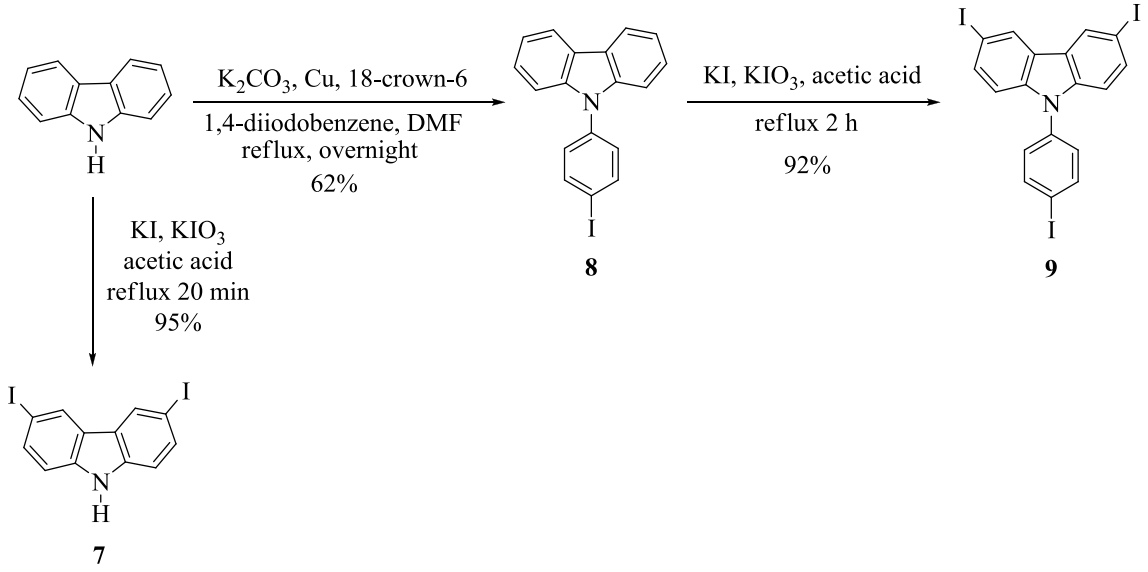

Scheme 3.1 Synthesis of 3,6-diiodo-9*H*-carbazole (**7**), 9-(4-iodophenyl)-9*H*-carbazole (**8**) and 3,6-diiodo-9-(4-iodophenyl)-9*H*-carbazole core (**9**)

The synthesis began with a regioselective diiodination of carbazole using KI/KIO_3 in refluxing acetic acid for 20 minutes to afford 3,6-diiodo-9*H*-carbazole (**7**) as a light brown solid in 95% yield after recrystallization. An *N*-arylation of carbazole using an excess amount of 1,4-diiodobenzene and copper bronze provided **8** in 62% yield. Diiodination of **8** yielded triiodo **9** in excellent yield of 92% as a single regioisomer. It is worth noting that attempt to perform triiodination of *N*-phenyl carbazole failed to give **9** as the iodination occurred only at the 3- and 6-positions of the carbazole ring (**Scheme 3.1**).

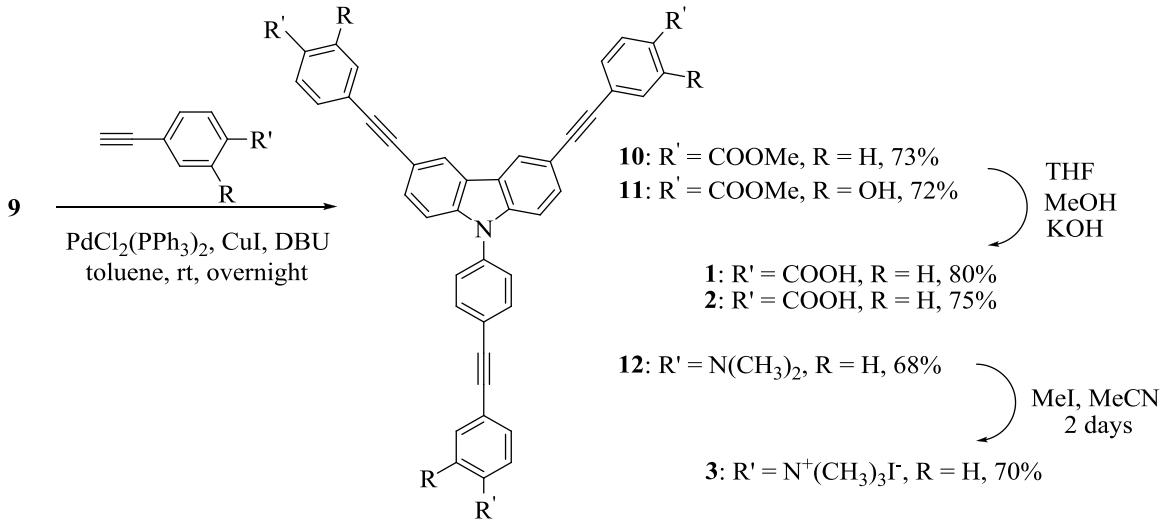

Scheme 3.2 Synthesis of fluorophore **1-3**

The Sonogashira coupling of **9** with methyl 4-ethynylbenzoate, methyl 4-ethynyl-2-hydroxybenzoate or 4-ethynyl-*N,N*-dimethylaniline produced tri-methylester **10**, tri-methylsalicylate **11** or tris-dimethylaniline **12** in 73, 72 and 68% yield, respectively. Finally, hydrolysis of the ester functional groups in **10** and **11** using saturated KOH in THF-MeOH or methylation of the dimethylamino group in **12** using by MeI in MeCN gave rise to fluorophore **1**, **2** and **3** in 80, 75 and 70% yield, respectively (**Scheme 3.2**).

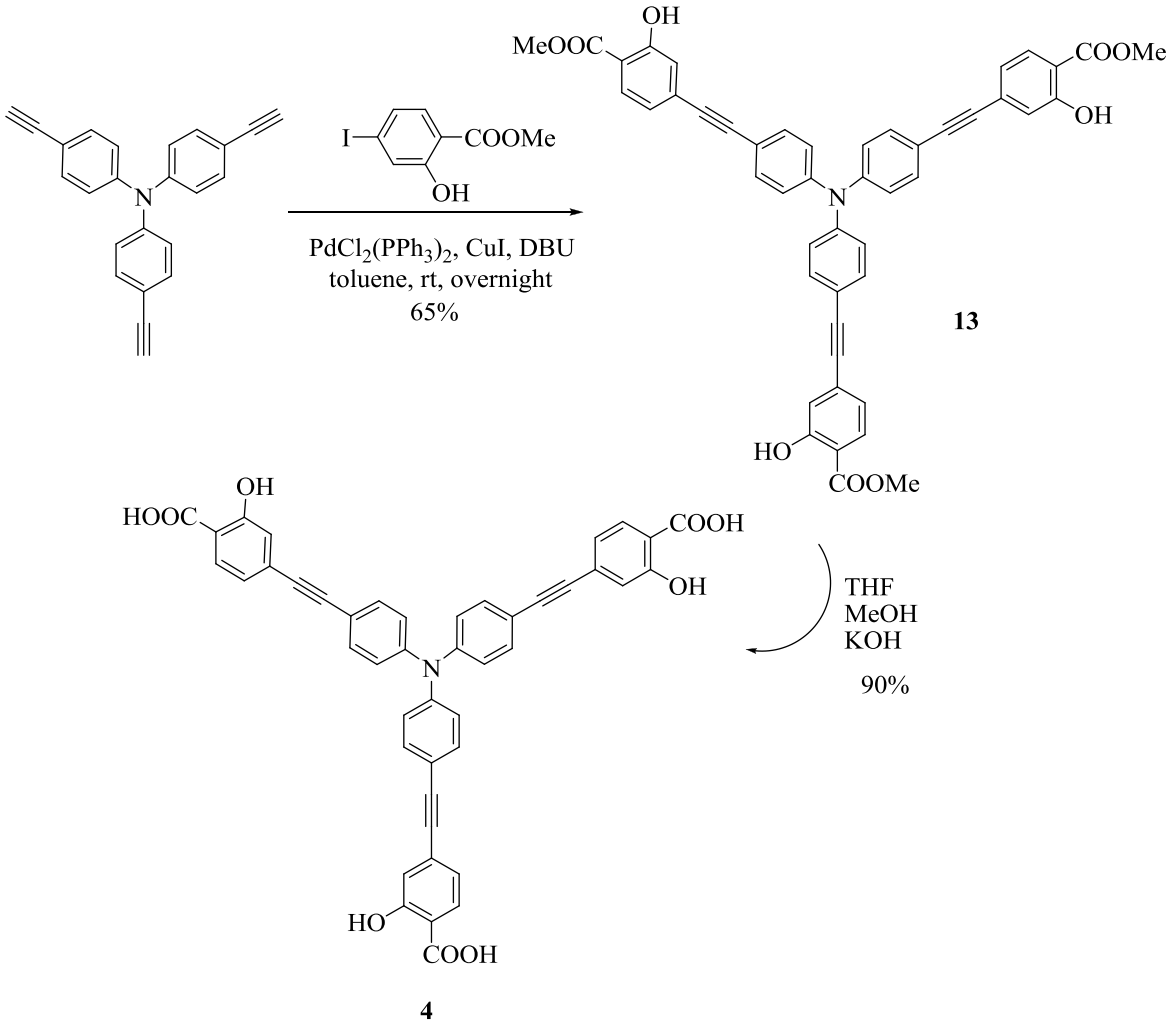

Scheme 3.3 Synthesis of fluorophore **4**

The Sonogashira coupling of tris(4-ethynylphenyl)amine with methyl 2-hydroxy-4-iodobenzoate produced tri-methylsalicylate **13** in 65% yield. After that, hydrolysis of the ester functional groups using saturated KOH in THF-MeOH gave rise to fluorophore **4** in 90% yield (**Scheme 3.3**). This fluorophore was synthesized in order to compare its photophysical properties to those of the more rigid analog (**2**).

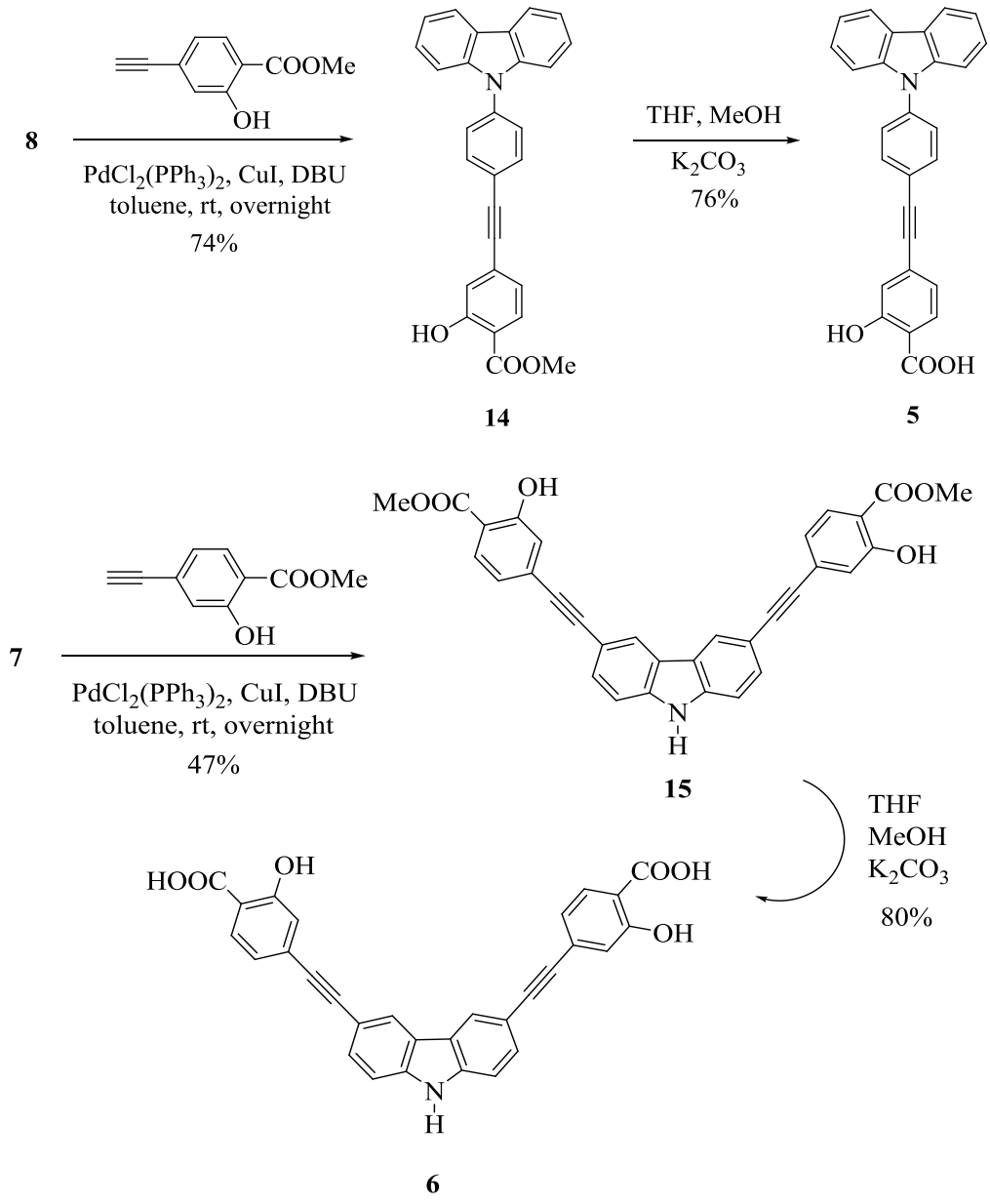

Scheme 3.4 Synthesis of fluorophore **5** and **6**

For the purpose of identifying which parts of fluorophore **2** are responsible for flurogenic response upon addition of analyte, fluorophore **5** and **6** were synthesized from iodo compound **8** and **7**. The Sonogashira coupling with methyl 4-ethynyl-2-hydroxybenzoate produced methylsalicylate **14** or di-methylsalicylate **15** in 74 and 47%

yield, respectively. Where upon, hydrolysis of the ester functional groups using saturated KOH in THF-MeOH gave rise to fluorophore **5** and **6** in 76 and 80% yield, respectively (**Scheme 3.4**).

The ^{1}H NMR spectra of **7- 9** and the signal assignments are shown in **Figure 3.1**. For compound **7**, two singlet peaks at 8.55 and 11.54 ppm were assigned for H(a) and H(d), respectively, whereas two doublet peaks at 7.33 and 7.64 ppm arose from for H(c) and H(b), respectively. For compound **8**, the protons in carbazole unit resonated at 8.15 ppm for H(a), 7.38-7.45 ppm for H(b-c), and 7.93 ppm for H(d), while the iodophenyl protons (H(f-e)) appeared at 7.29 and 7.35 ppm. For triiodo **9**, there were four signals for the aromatic protons at 7.12, 7.24, 7.67 and 7.93 ppm corresponding to H(e), H(d), H(c) and H(f), respectively, and a singlet peak at 8.38 ppm for H(a).

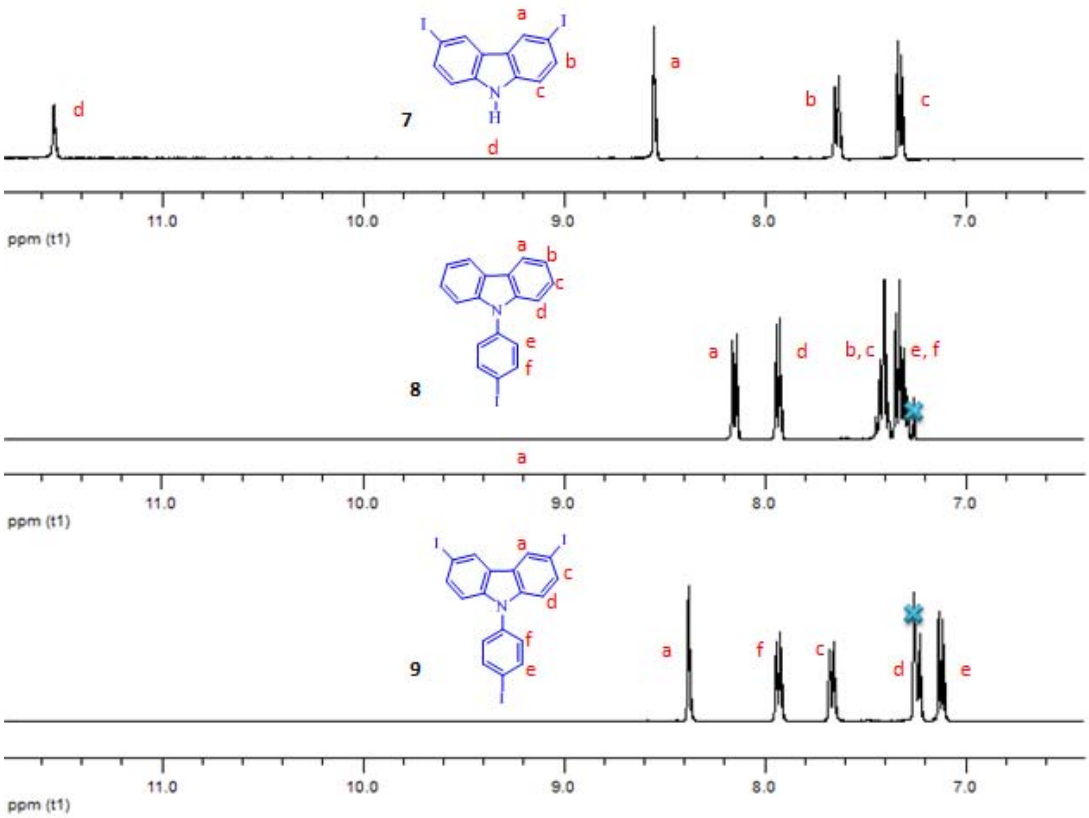

Figure 3.1 ^{1}H NMR spectra of iodo compound **7** (DMSO-*d6*), **8** and **9** ($CDCl_3$).

For the construction of fluorophore **1-3**, the Sonogashira coupling between three iodo groups in **9** with methyl 4-ethynylbenzoate, methyl 4-ethynyl-2-hydroxybenzoate, or 4-ethynyl-*N,N*-dimethylaniline produced methyl ester **10**, methyl salicylate **11**, or dimethylamine **12** in 73, 72, and 68% yield, respectively. The ^{1}H NMR spectra of these intermediates are shown in **Figure 3.2-3.4**. The methyl ester signal in **10** and **11** appeared as singlet peak at around 3.95 ppm. For **12**, a singlet signal at 3.0 ppm indicated the dimethylamino protons. Complete hydrolyses of **10** and **11** gave fluorophore **1** and **2** which could be noticed by the disappearance of the methyl ester singlet signal (**Figure 3.2** and **3.3**). The successful conversion of **12** to **3** by methylation using an excess amount of methyl iodide was evidenced by a new singlet signal of the methyl ammonium protons at 3.62 ppm (**Figure 3.4**).

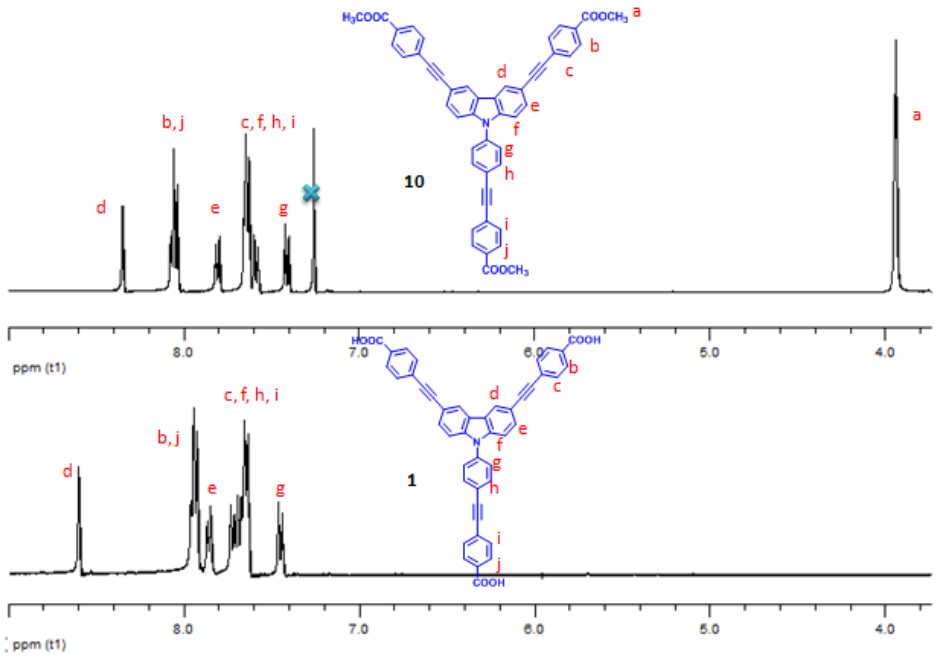

Figure 3.2 ^{1}H NMR spectra of **10** ($CDCl_3$) and **1** (DMSO-*d6*).

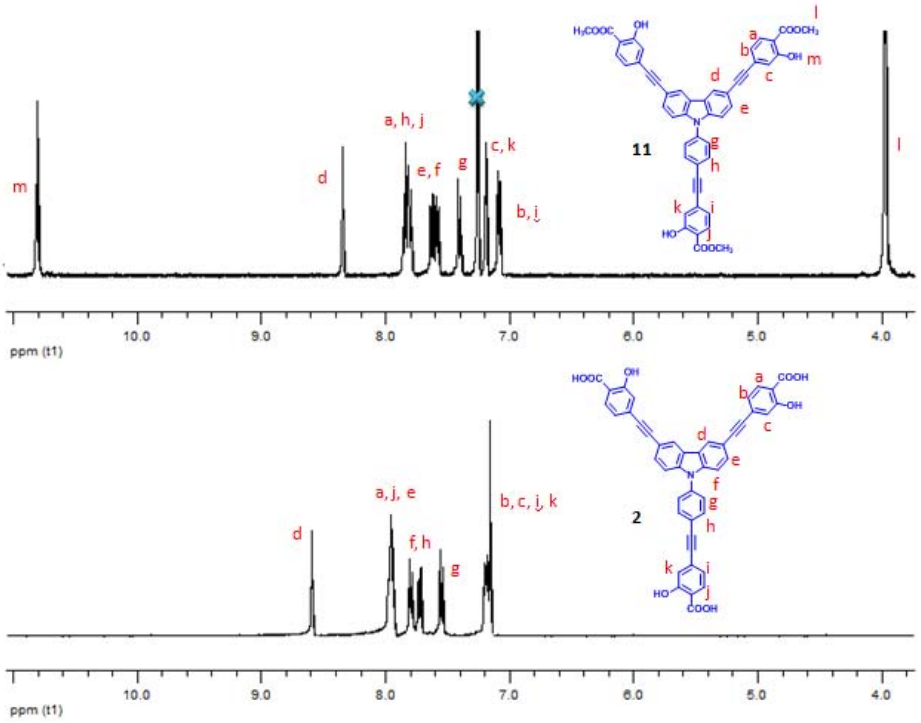

Figure 3.3 ^{1}H NMR spectra of **11** ($CDCl_3$) and **2** (acetone-d^6).

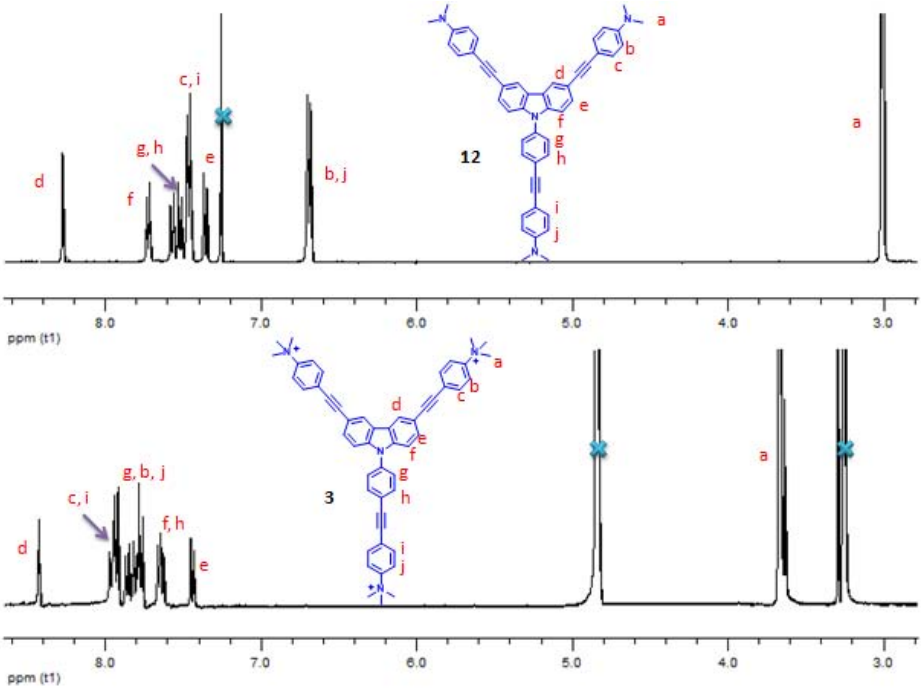

Figure 3.4 ^{1}H NMR spectra of **12** ($CDCl_3$) and **3** (CD_3OD).

In order to evaluate the effect of enhanced rigidity in **1-3**, the photophysical properties of their triphenylamine analogs must be retrieved. However, only the synthesis and characterization of **a** and **b** (**Figure 3.5**) have been reported in literature [45]. Therefore, the synthesis of fluorophore **4** was carried out in order to compare its photophysical properties with those of **2**. In addition, compound **5-6** were also synthesized since they will be used for assessment of the different salicylate moieties in **2**. Compound **4-6** were synthesized using the same Sonogashira-hydrolysis protocol described for **2**. (**Scheme 3.3** and **3.4**)

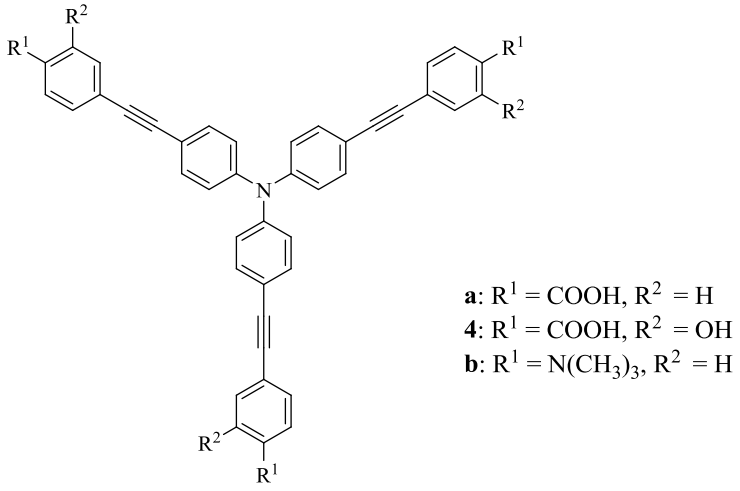

Figure 3.5 The structure of **a**, **4** and **b**.

The ^{1}H NMR spectra of compound **13-15** are shown in **Figure 3.6-3.8**. Before the hydrolysis, **13-15** showed signal of the methyl ester protons as a singlet at 3.96, 3.98 and 3.90 ppm, respectively, all of which would disappeared after the hydrolysis.

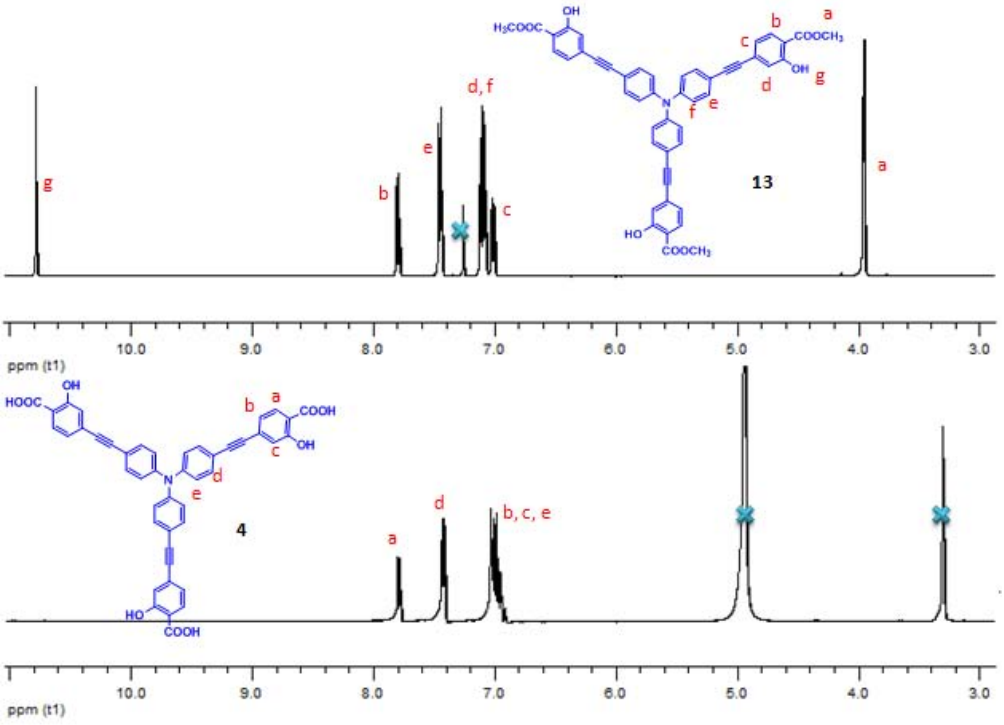

Figure 3.6 ^{1}H NMR spectra of **13** ($CDCl_3$) and **4** (CD_3OD).

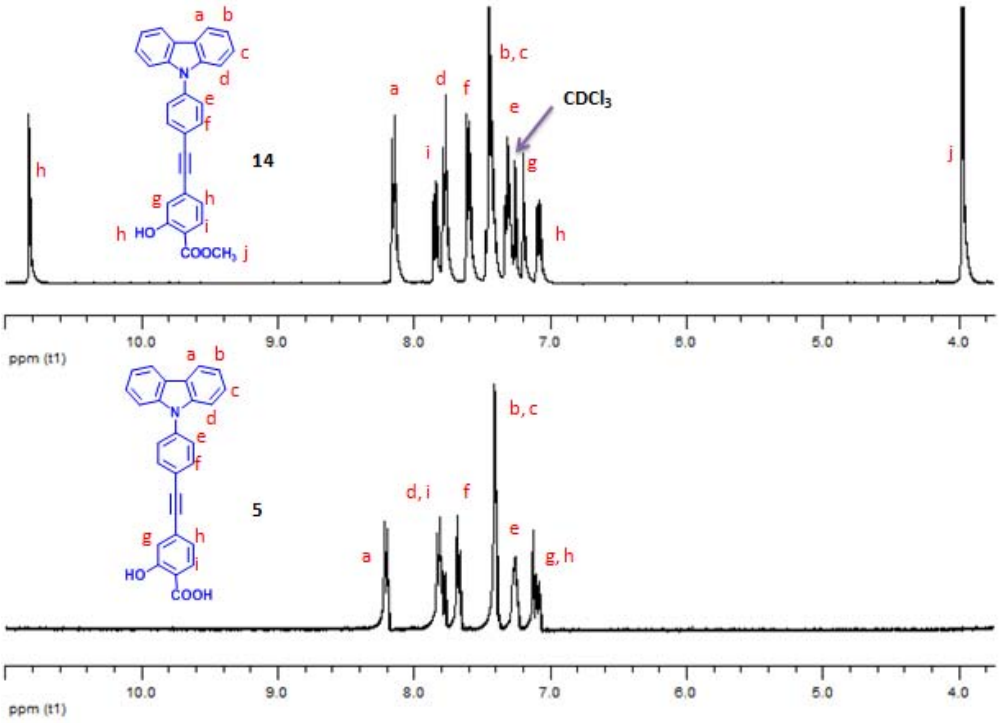

Figure 3.7 ^{1}H NMR spectra of **14** ($CDCl_3$) and **5** (DMSO-*d6*).

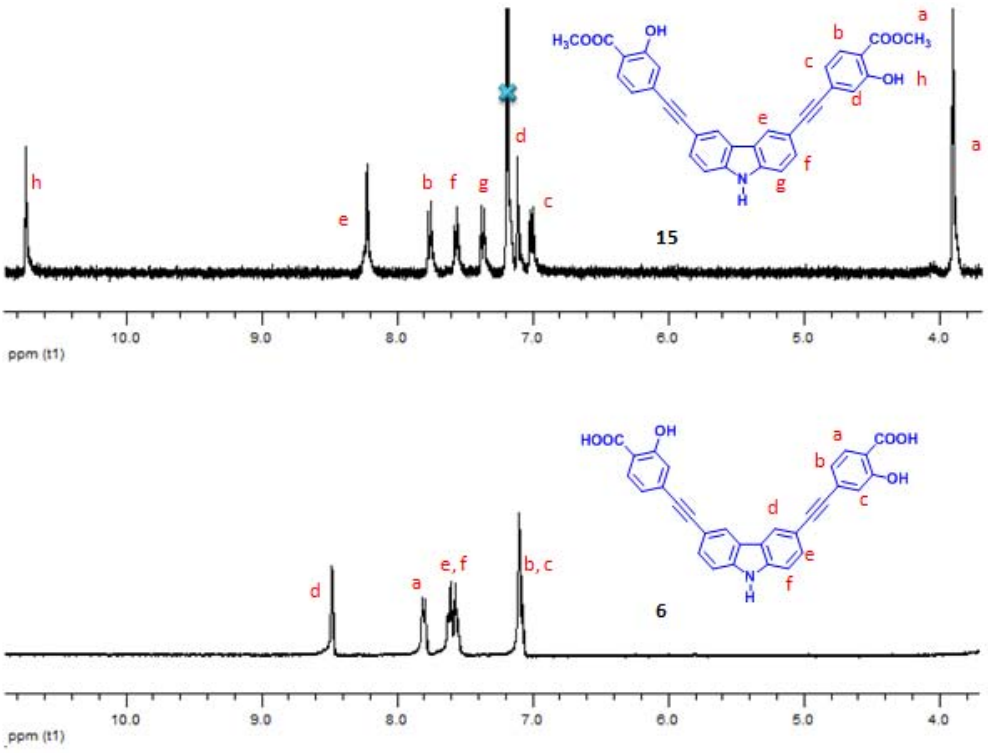

Figure 3.8 ^{1}H NMR spectra of **15** ($CDCl_3$) and **6** (DMSO-*d6*).

3.2 Photophysical properties

The photophysical properties of six fluorophores (**1**-**6**) were examined using their solutions in 10 mM phosphate buffer pH 8.0. All compounds displayed maximum absorption wavelength (λ_{max}) ranging from 335 to 377 nm and the maximum emission wavelengths in the range of 450 to 500 nm (**Figure 3.9** and **Table 3.1**). The absorption bands for fluorophores with *N*-phenyl carbazole (**1-3**) appear at short wavelengths (335-343 nm) whiles the fluorophores with triphenylamine core (**a**, **4**, **b**) exhibit maximum absorption peaks at 370-377 nm. This data indicates that fluorophores with *N*-phenyl carbazole core possess short or less continuous π-conjugation. The electron pair on the nitrogen atom locate in the carbazole unit in order to preserve the aromaticity. Since the overall structures of fluorophore **1-3** are similar, their molar absorptivities (ε) are of about the same magnitude. From the fluorescent spectra, it was found that the maximum

emission bands for **1** and **3** appeared at 450 and 456 nm, whereas fluorophore **2** emitted at 475 nm. The longer emission wavelength in **2** could result from the internal charge transfer (ICT) [47-49] process occurring between the electron-donating hydroxyl group and the electron-withdrawing carboxylate group, which is also evident by its lowest quantum yield (0.11).

Most importantly, the absolute quantum yields of **1**, **2** and **3** were approximately 3, 8 and 30% greater than those of their structurally related analogs which contain the triphenylamine core (the quantum yields of **a**, **4** and **b** were 0.09, 0.03 and 0.14, respectively). It was found that fluorophores with structurally flexible triphenylamine cores yielded relatively low quantum yields. This could cause by the fact that a portion of energy was lost in a non-radiative pathway such as a geometrical relaxation upon excitation. This small increase suggests that the replacement of two phenyl rings by one carbazole unit may decrease only a small magnitude of rotational mode. For molecules of this size, more rigidity may be needed in order to significantly improve the quantum yield. However, certain synthetic challenges as well as the expected low solubility should also be considered.

In terms of relative quantum yield enhancement, it was found that the incorporation of carbazole ring in **1** and **2** could increase quantum yield for only 3 and 8%, respectively. In contrast, a large enhancement of 30% was observed in the case of **3**. This could account for the fact that **a**, **1**, **2**, and **4** contain a π-conjugate electron-withdrawing carboxylic group which could cause an internal charge transfer (ICT). The core replacement of the triphenylamine (**a** and **4**) by the *N*-phenyl carbazole (**1** and **2**) would make the electron pair on the central nitrogen atom more localized in order to maintain the aromaticity of the carbazole units, hence, the ICT is less likely to occur. For **b** and **3**, the effect of increased rigidity is more apparent since the trimethylammonium groups do not participate in the ICT process. Therefore, it could be concluded that the ICT effect is the more important factor governing quantum yield of the fluorophores, whereas the rigidity effect is less dominant.

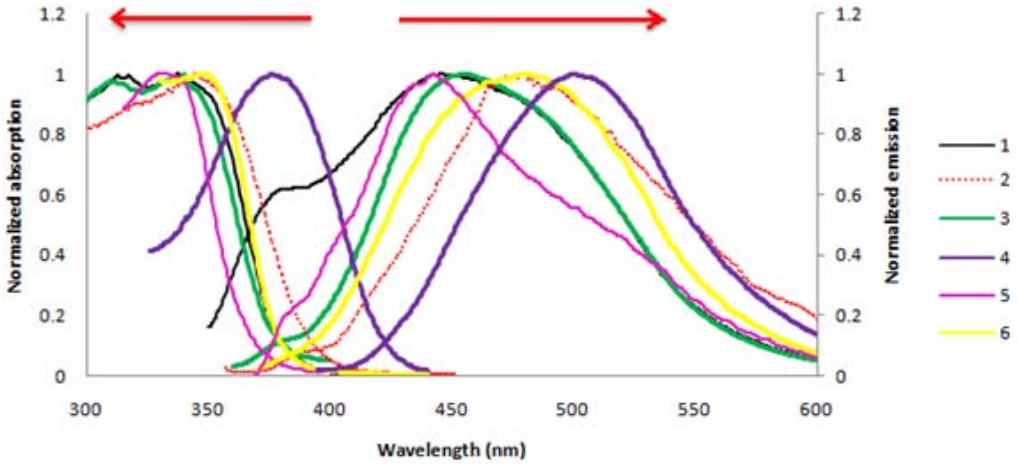

Figure 3.9 Normalized absorption and emission spectra of fluorophores **1-6** in 10 mM phosphate buffer pH 8.0.

Table 3.1 Photophysical properties of **1-6** in 10 mM phosphate buffer pH 8.0.

Compound	Absorption		Emission	
	λ_{max} (nm)	ε (M^{-1} cm^{-1})	λ_{max} (nm)	Φ_F[a]
1	337	44730	450	0.12
2	343	47776	475	0.11
3	335	38881	456	0.44
a*	374	5900	454	0.09
4	377	20412	500	0.03
b*	370	26823	485	0.14
5	330	32846	442	0.09
6	347	35802	480	0.05

[a]quinine sulfate in 0.1 M H_2SO_4 (Φ= 0.54) was the reference, *see in [45]

3.3 Sensing application

Next, the fluorogenic behaviors of **1-3** for metal ions, the fluorescent signal of solutions of each fluorophore in 10 mM phosphate buffer pH 8.0 were monitored in the presence of sixteen metal ions including Ba^{2+}, Ca^{2+}, Cd^{2+}, Co^{2+}, Cu^{2+}, Hg^{2+}, Mg^{2+}, Mn^{2+}, Ni^{2+}, Pb^{2+}, Zn^{2+}, Ag^{+}, K^{+}, Li^{+}, Na^{+} and Al^{3+}. It was found that the fluorescent signals of **1** and **3** (**Figure 3.10** and **3.12**) could not be altered by any of these metal ions. In contrast, the fluorescent signal of **2** was selectively quenched by Cu^{2+} ion (**Figure 3.11**, **3.13** and **3.14**). The selectivity of the fluorescence quenching may cause by the high complexation or chelation affinity between salicylate and Cu^{2+} [50].

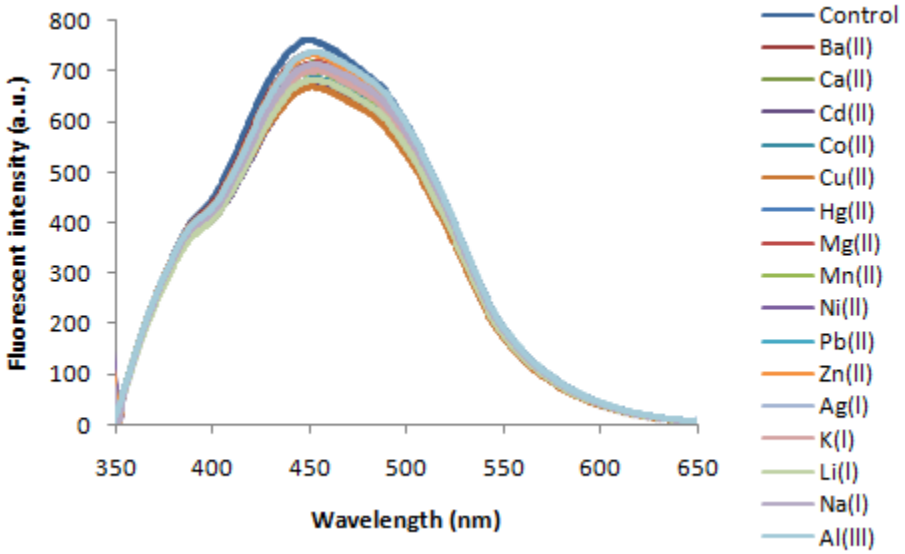

Figure 3.10 Emission spectra of **1** (1 μM) in the presence of sixteen metal ions (10 μM).

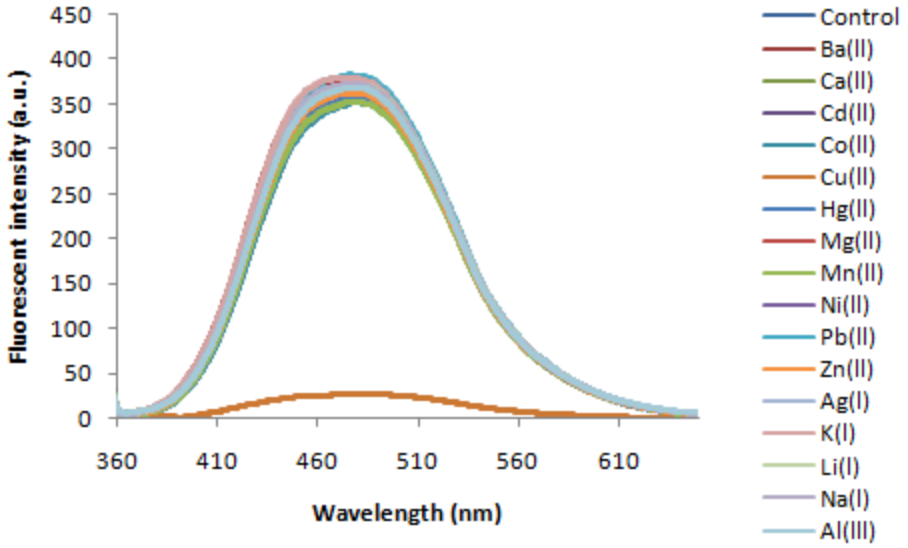

Figure 3.11 Emission spectra of **2** (1 μM) in the presence of sixteen metal ions (10 μM).

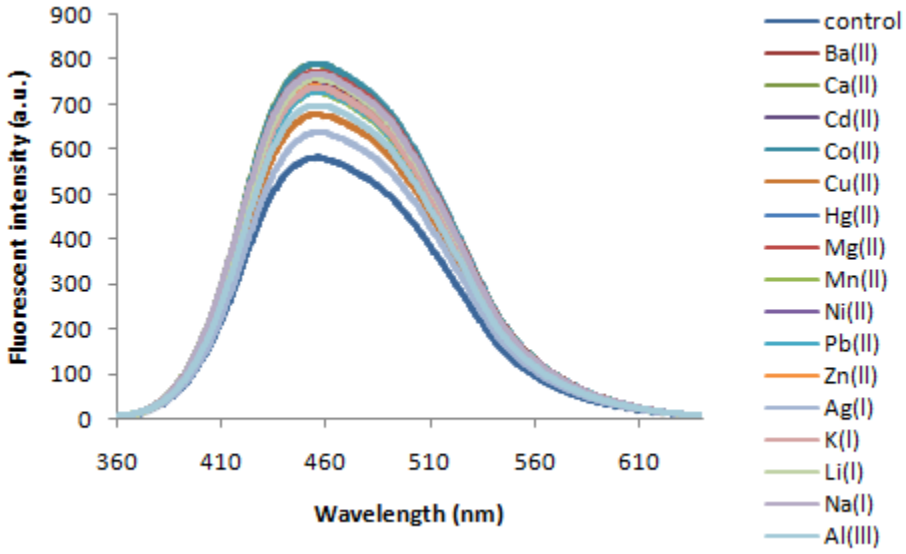

Figure 3.12 Emission spectra of **3** (1 μM) in the presence of sixteen metal ions (10 μM).

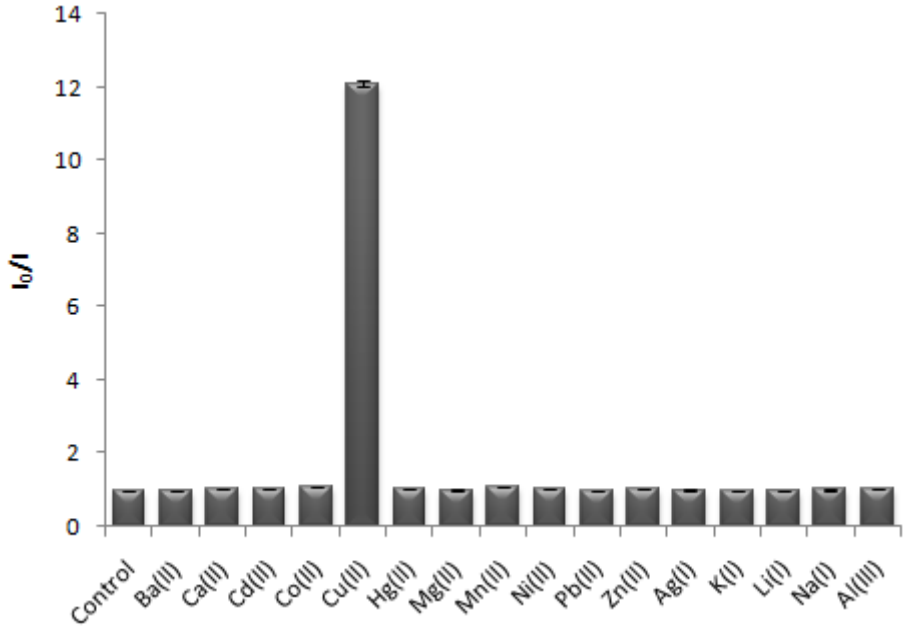

Figure 3.13 Fluorogenic responses of **2** (1μM) with Cu^{2+} ions over metal ions (10 μM in 10 mM phosphate buffer pH 8.0) in the presence of sixteen metal ions (10 μM).

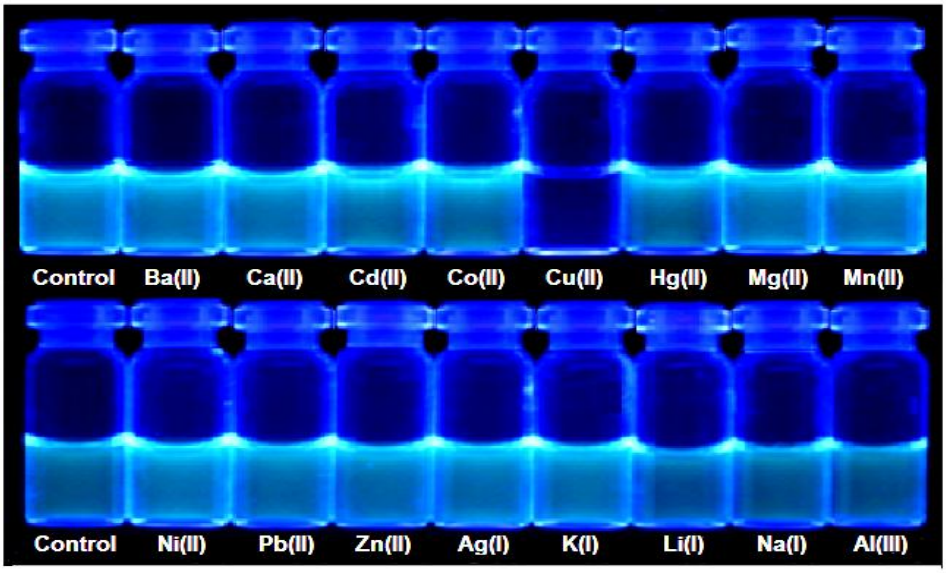

Figure 3.14 Photographs of **2** (10 μM) in the presence of sixteen metal ions (30 μM) under a UV lamp.

3.4 Interference test

A series of competitive experiments were performed in order to examine the selectivity for fluorophore **2** toward Cu^{2+}. The solution of **2** (1 μM) in 10 mM phosphate buffer pH 8 in the presence of Cu^{2+} (10 equiv) was used as a blank. The quenching efficiencies in the presence of additional metal ions (100 equiv) were not significantly different from the blank, which indicated that fluorophore **2** can be used as a selective sensor for Cu^{2+} without the interfering by a ten-fold concentration of another metal ion in the same solution.

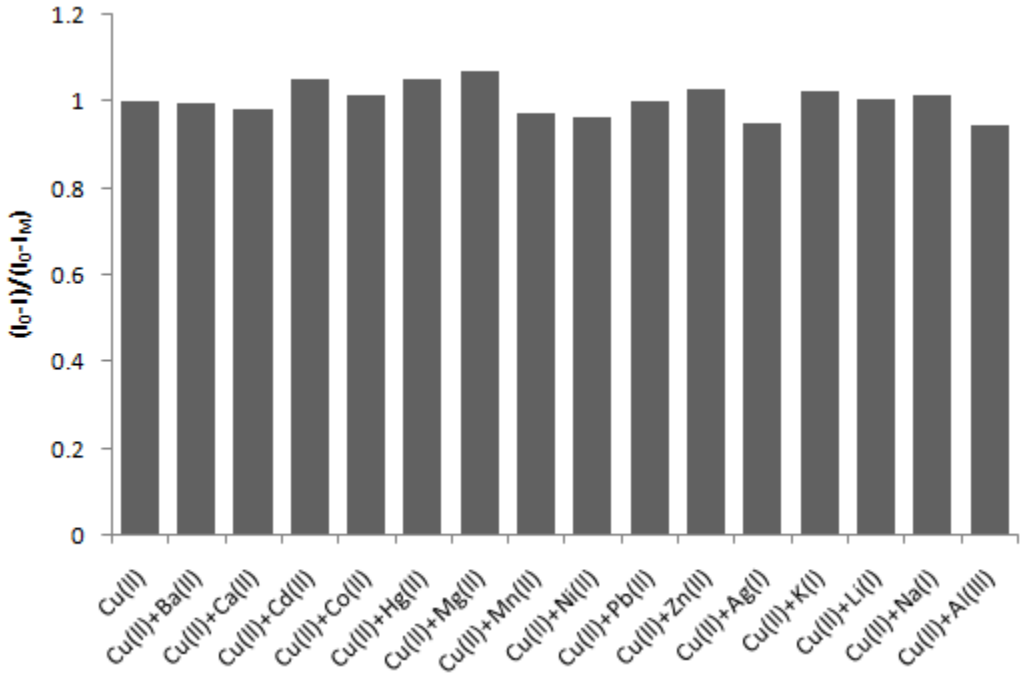

Figure 3.15 Interference experiments of **2** (1 μM) and Cu^{2+} (10 μM) with sixteen interfering metal ions (100 μM).

3.5 Fluorescent titration of 2 with Cu^{2+}

The fluorescent titration of fluorophore **2** (1 μM) with Cu^{2+} (0-10 μM) was conducted and the data was presented in **Figure 3.16**. During the addition of Cu^{2+} of 1-5 equivalents, the fluorescent intensity gradually decreased. The intensity changes were less noticeable when the concentration of Cu^{2+} was above 6 equivalents. As reported in several literatures [46, 50], the mechanism of fluorescent quenching should involve the chelation of the salicylate peripheries with Cu^{2+}. That the addition of more than one equivalent of Cu^{2+} is required in order to reach a complete fluorescent quenching state suggests that some of the free fluorophores are still available in the solution. Since one molecule of **2** possesses three salicylate units, each of them may be able to bind with Cu^{2+} with the same binding constant.

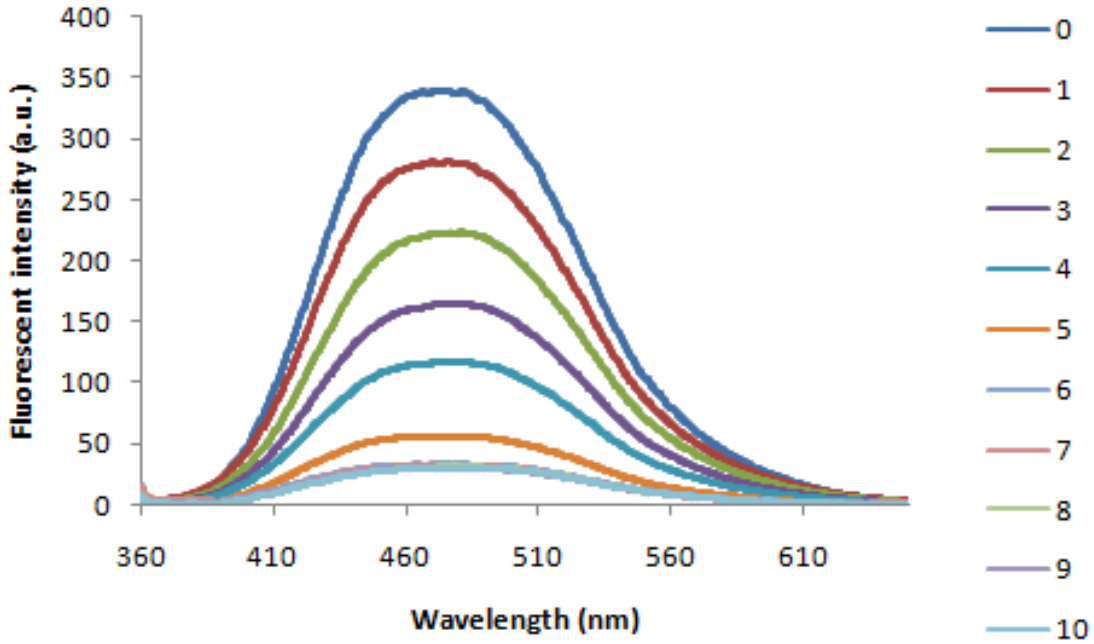

Figure 3.16 The fluorescent intensity of **2** (1 μM) with Cu^{2+} titration (0-10 μM) in 10 mM phosphate buffer pH 8.0.

3.6 The Stern-Volmer plot for fluorescent quenching of 2 by Cu^{2+}

A Stern-Volmer plot as shown in **Figure 3.17** was obtained by variation of Cu^{2+}concentration, acquisition of the fluorescent intensity, and construction of a plot between (I_0/I) and the Cu^{2+} concentrations. In this S-curve plot, the quenching efficiency increased gradually at the concentration range of Cu^{2+} between 1-3 μM. When the concentration of Cu^{2+} reached 4 μM, a fluorescent switching-off effect was observed. This sudden increase in quenching efficiency could account for a superquenching behavior [51-54], in which one Cu^{2+} ion complexes with two salicylate groups from two molecules of fluorophore **2**, resulting in Cu^{2+}-linked dimeric or oligomeric aggregation of the fluorophore and thus a greater quenching was observed.

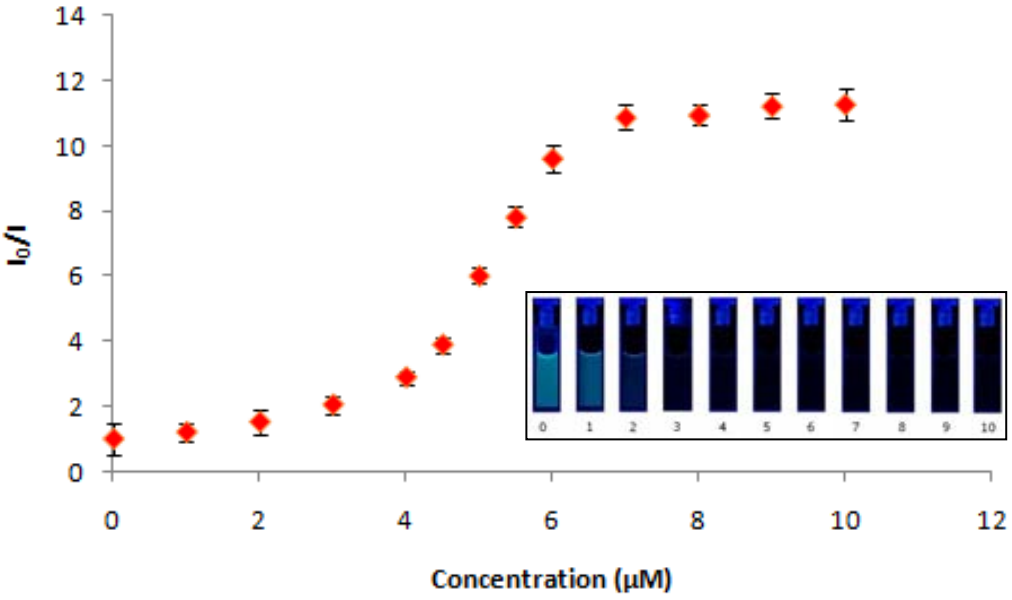

Figure 3.17 The Stern-Volmer plot for fluorescent quenching of **2** (1μM) by various concentration of Cu^{2+} (0-10 equivalents). Inset is the photographs of samples of **2** (10μM) with 0-10 equivalents of Cu^{2+}.

3.7 Fractional investigation of fluorophore 2

Since there was a non-linear Stern-Volmer relationship in the fluorescent quenching of **2** by Cu^{2+}, it was believed that the two kinds of peripheries (on the carbazole or on the phenyl ring) may response differently towards Cu^{2+}. In order to prove this hypothesis, fluorophore **5** (one ethynyl salicylate group on phenyl ring) and **6** (two ethynyl salicylate groups in carbazole) were then prepared as described in **Scheme 3.4**. Their photophysical properties are also tabulated in **Table 3.1**.

Upon addition of Cu^{2+}, approximately up to 60% of fluorescent intensity of **5** was quenched whereas the quenching effect by the copper ion was insignificant. These results indicated that the ethynyl salicylate on the phenyl ring is more sensitive towards Cu^{2+} than those groups on the carbazole. In other words, the ethynyl salicylate on the phenyl ring in **2** could behave as a sensitive binding site for Cu^{2+} while the ethynyl salicylate groups on the carbazole ring function as the fluorescent signal amplifiers.

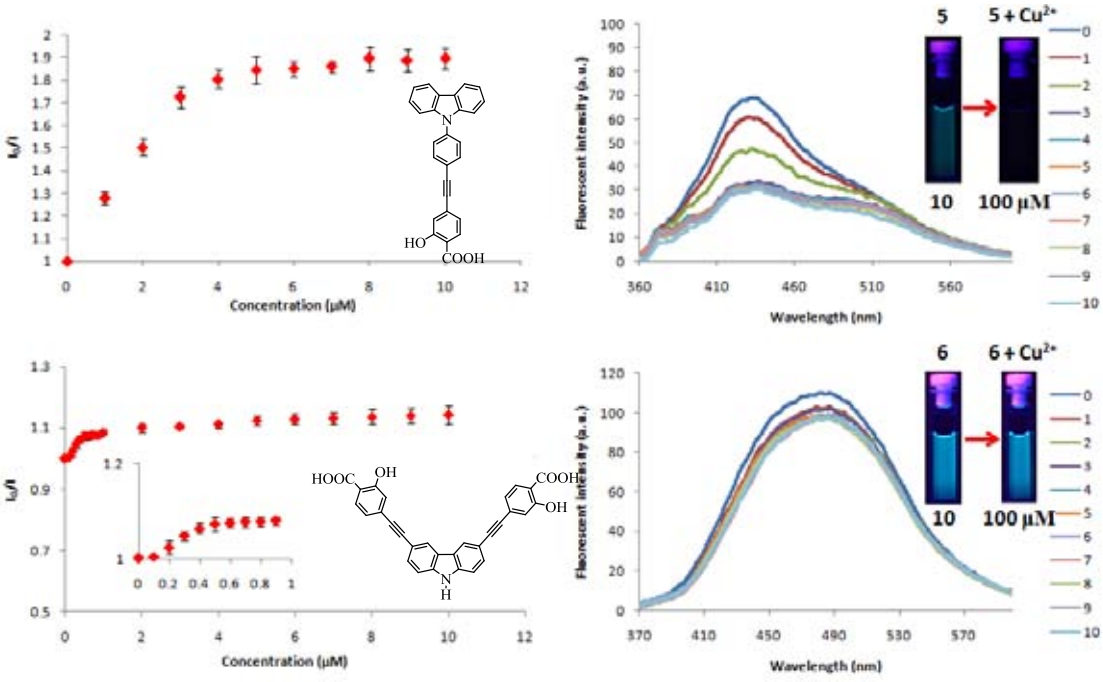

Figure 3.18 The Stren-Volmer plot and fluorescent spectra for fluorescent quenching of **5** and **6** by Cu^{2+}.

CHAPTER IV

CONCLUSION

4.1 Conclusion

In summary, six new water soluble fluorophores (**1**-**6**) were successfully synthesized. The synthesis relied on the Sonogashira coupling between the triiodophenylcarbazole and the acetylenic aromatic ester. In terms of relative quantum yield enhancement, the incorporation of rigidity into molecules is proven to be an efficient approach. However, the internal charge transfer (ICT) effect is the more important factor governing quantum yield of the fluorophores, whereas the rigidity effect is less dominant.

In addition, it was found that the fluorescent signal of **2** can be selectively quenched by copper (II) ion. The non-linear relationship between fluorescent intensity and concentration of copper (II) ion reveals a turn-off fluorescent switching property for the copper (II) ion at 4 micromolar and above. The fractional investigation of **2** indicates that the ethynyl salicylate on the phenyl ring of the core is responsible for fluorogenic response towards copper (II) ion, as where other parts of molecule function as fluorescent signal amplification units.

REFERENCES

[1] Martinez-Máñez, R.; and Sancenón, F. Fluorogenic and chromogenic chemosensors and reagents for anions. *Chem. Rev.* 103 (2003): 4419-4478.

[2] Silva, A.P.; and others. Signaling recognition events with fluorescent sensors and switches. *Chem. Rev.* 97 (1997): 1515-1566.

[3] Skoog, D.A. Molecular fluorescence, phosphorescence and chemiluminescence spectroscopy. In Principles of instrumental analysis. Third Edition. pp. 225-244. USA: Saunders College Publishing, 1985.

[4] Lakowicz, J.R. Introduction to fluorescence. In Principles of fluorescence spectroscopy. Third Edition. pp. 1-25. USA: Springer Science+Business Media, LLC: 233 Spring Street, 2006.

[5] Valeur, B.; and Leray, I. Design principles of fluorescent molecular sensors for cation recognition. *Coord. Chem. Rev*. 205 (2000): 3-40.

[6] Gunnlaugsson, T.; Glynn, M.; Tocci, G.M.; Kruger, P.E.; and Pfeffer, F.M. Anion recognition and sensing in organic and aqueous media using luminescent and colorimetric sensor. *Coord. Chem. Rev*. 250 (2006): 3094-3117.

[7] Jiang, P.; and Guo, Z. Fluorescent detection of zinc in biological systems: recent development on the design of chemosensors and biosensors. *Coord. Chem. Rev*. 248 (2004): 205-229.

[8] Liu, Y.; Ogawa, K.; and Schanze, K.S. Conjugated polyelectrolytes as fluorescent sensors. *J. Photoch. Photobio. C*. 10 (2009): 173-190.

[9] Burn, P.L.; and others. Chemical tuning of the electronic properties of poly(*p*-phenylenevinylene)-based copolymers. *J. Am. Chem. Soc.* 115 (1993): 10117-10124.

[10] Kraft, A.; Grimsdale, A.C.; and Holmes, A.B. Electroluminescent conjugated polymers-seeing polymers in a new light. *Angew. Chem. Int. Ed.* 37 (1998): 402-427.

[11] Alan, J.H. Semiconducting and metallic polymers: the fourth generation of polymeric materials (nobel lecture). *Angew*. *Chem. Int. Ed*. 40 (2001): 2591-2611.

[12] Pei, Q.B.; Yu, G.; Zhang, C.; Yang, Y.; and Heeger, A.J. Polymer light-emitting electrochemical-cells. *Science* 269 (1995): 1086-1088.

[13] Dimitrakopoulos, C.D.; and Malenfant, P.R.L. Organic thin film transistors for large area electronics. *Adv. Mater*. 14 (2002): 99-117.

[14] Torsi, L.; Dodabalapur, A.; Rothberg, L.J.; Fung, A.W.P.; and Katz, H.E. Intrinsic transport properties and performance limits of organic field-effect transistors. *Science* 272 (1996): 1462-1464.

[15] Sirringhaus, H. Device physics of solution-processed organic field-effect transistors. *Adv. Mater.* 17 (2005): 2411-2425.

[16] Arango, A.C.; and others. Efficient titanium oxide/conjugated polymer photovoltaics for solar energy conversion. *Adv. Mater.* 12 (2000): 1689-1692.

[17] McDonald, S.A.; and others. Solution-processed PbS quantum dot infrared photodetectors and photovoltaics. *Nat. Mater.* 4 (2005): 138-142.

[18] Coakley, K.M.; and McGehee, M.D. Conjugated polymer photovoltaic cells. *Chem. Mater.* 16 (2004): 4533-4542.

[19] Ramos, A.M.; Rispens, M.T.; Duren, J.K.J.; Hummelen, J.C.; and Janssen, R.A.J. Photoinduced electron transfer and photovoltaic devices of a conjugated polymer with pendant fullerenes. *J. Am. Chem. Soc*. 123 (2001): 6714-6715.

[20] Jager, E.W.H.; Inganäs O.; and Lundström I. Perpendicular actuation with individually controlled polymer microactuators. *Adv. Mater.* 13 (2001): 76-79.

[21] Burgmayer, P.; and Murray, R.W. An ions gate membrane: electrochemical control of ion permeability through a membrane with an embedded electrode. *J. Am. Chem. Soc*. 104 (1982): 6139-6140.

[22] Gangopadhyay, R.; and De, A. Conducting polymer nanocomposites: a brief overview. *Chem. Mater*. 12 (2000): 608-622.

[23] Meyer, W.H. Polymer electrolytes for lithium-ion batteries. *Adv. Mater*. 10 (1998): 439-448.

[24] Hide, F.; DiazGarcia, M.A.; Schwartz, B.J.; and Heeger, A.J. New developments in the photonic applications of conjugated polymers. *Acc. Chem. Res*. 30 (1997): 430–436.

[25] Gunes, S.; Neugebauer, H.; and Sariciftci, N.S. Conjugated polymer-based organic solar cells. *Chem, Rev*. 107 (2007): 1324-1338.

[26] McQuade, D.T.; Pullen, A.E.; and Swager, T.M. Conjugated polymer-based chemical sensor. *Chem. Rev*. 100 (2000): 2537-2574.

[27] Thomas, S.W.; Joly, G.D.; and Swager, T.M. Chemical sensors based on amplifying fluorescent conjugated polymers. *Chem. Rev*. 107 (2007): 1339-1386.

[28] Nquyen, T.Q.; Wu, J.J.; Doan, V.; Schwartz, B.J.; and Tolbert, S.H. Control of energy transfer in oriented conjugated polymer–mesoporous silica composites. *Science*. 288 (2000): 652–656.

[29] Gierscher, J.; Cornil, J.; and Egelhaaf, H.J. Optical bandgaps of pi-conjugated organic materials at the polymer limit: experiment and theory. *Adv. Mater*. 19 (2007): 173-191.

[30] Tang, Y.L.; and others. Direct visualization of glucose phosphorylation with a cationic polythiophene. *Adv. Mater*. 20 (2008): 703-705.

[31] Grimsdale, A.C.; and Mullen, K. Polyphenylene-type emissive materials: poly(paraphenylene)s, polyfluorenes, and ladder polymers. *Emiss. Mater. Nanomater*. 199 (2006): 1-82.

[32] Bunz, U.H.F. Poly(aryleneethynylene)s: syntheses, properties, structures, and applications. *Chem. Rev*. 100 (2000): 1605-1644.

[33] Perepichka, I.F.; Perepichka, D.F.; Meng, H.; and Wudl, F. Light-emitting polythiophenes. *Adv. Mater*. 17 (2005): 2281-2305.

[34] Patil, A.O.; Heeger, A.J.; and Wudl, F. Optical-properties of conducting polymers. *Chem. Rev*. 88 (1988): 183-200.

[35] MacDiarmid, A.G. Synthetic metals: a novel role for organic polymers (nobel-lecture). *Angew. Chem. Int. Ed*. 40 (2001): 2581-2590.

[36] Scherf, U.; and List, E.J.W. Semiconducting polyfluorenes-towards reliable structure-property relationships. *Adv. Mater*. 14 (2002): 477-487.

[37] Nijegorodov, N.; Zvolinsky, V.; and Luhahga, P.V.C. Photonics and photochemical stability of aromatic molecules, family related in π-structure but different in planarity, rigidity and molecule symmetry. *J. Photochem. Photobio. A*. 196 (2008): 219-226.

[38] Brunel, J.; and others. Propeller-shaped octupolar molecules derived from triphenylbenzene for nonlinear optics: synthesis and optical studies. *Chem. Mater.* 15 (2003): 4139-4148.

[39] Zhang, W.-B.; Jin, W.-H.; Zhou, X.-H.; and Pei, J. Star-shaped oligo(p-phenylene)-functionalized truxenes as blue-light-emitting materials: synthesis and the structure-property relationship. *Tetrahedron*. 63 (2007): 2907-2914.

[40] Wang, H.; and others. The synthesis and characterization of novel dipolar fluorescent materials based on a quinoxaline core. *Dyes Pigments*. 83 (2009): 269-275.

[41] Kim, B. I.; and Bunz, F. H. Modulating the sensory response of a conjugated polymer by proteins: An agglutination assay for mercury ions in water. *J. Am. Chem. Soc*. 128 (2006): 2818-2819.

[42] Li, Z.; Lou, X.; Yu, H.; Li, Z.; and Qin, J. An imidazole-functionalized polyfluorene derivative as sensitive fluorescent probe for metal ions and cyanide. *Macromolecules*. 41 (2008): 7433-7439.

[43] Kim, M.H.; Noh, J.H.; Kim, S.; Ahn, S.; and Chang, S.-K. The synthesis of crown ether-appended dichlorofluoresceins and their selective Cu^{2+} chemosensing. *Dyes Pigments*. 82 (2009): 341-346

[44] Xu, Z.; Pan, J.; Spring, D.R.; Cui, J.; and Yoon, J. Ratiometric fluorescent and colorimetric sensors for Cu^{2+} based on 4,5-disubstituted-1,8-naphthalimide and sensing cyanide via Cu^{2+} displacement approach. *Tetrahedron*. 66 (2010): 1678-1683.

[45] Niamnont, N.; Siripornnoppakhun, W.; Rashatasakhon, P.; and Sukwattanasinitt, M. A Polyanionic Dendritic Fluorophore for Selective Detection of Hg^{2+} in Triton X-100 Aqueous Media. *Org. Lett*. 11 (2009): 2768-2771.

[46] Sirilaksanapong, S.; Sukwattanasinitt, M.; and Rashatasakhon, P. 1,3,5-Triphenylbenzene fluorophore as a selective Cu^{2+} sensor in aqueous media. *Chem. Commun.* 48 (2012): 293-295.

[47] Zachariasse, K.A.; Druzhinin, S.I.; Bosch, W.; and Machinek R. Intramolecular charge transfer with the planarized 4-aminobenzonitrile. *J. Am. Chem. Soc.* 126 (2004): 1705-1715.

[48] Chakraborty, A.; Kar, S.; Nath, D.; and Guchhait N. Photoinduced intramolecular charge-transfer reactions in 4-amino-3-methyl benzoic acid methyl ester: A fluorescence study in condensed phase and jet-cooled molecular beams. *J. Chem. Sci*. 119 (2007): 195-204.

[49] Galievsky, V.A.; and others. Ultrafast intramolecular change transfer with N-(4-cyanophenyl)carbazole Evidence for a LE precursor and dual LE + ICT fluorescence. *J. Phys. Chem. A*. 114 (2010): 12622-12638.

[50] Sundari, R.; Ahmad, M.; and Heng, L.Y. Development of an optical fibre reflectance sensor for copper (II) detection based on immobilized salicylic acid. *Sens. Actuators. B*. 113 (2006): 201-206.

[51] Lu, L.; Jones, R. M.; McBranch, D.; and Whitten, D. Superquenching in cyanine pendant poly(L-lysine) dyes: Dependence on molecular weight, solvent, and aggregation. *J. Am. Chem. Soc.* 124 (2002): 483-488.

[52] Lu, L.; Jones, R. M.; McBranch, D.; and Whitten, D. Surface-enhanced superquenching of cyanine dyes as J-aggregates on laponite clay nanoparticles. *Langmuir* 18 (2002): 7706-7713.

[53] Chen, L.; and others. Highly sensitive biological and chemical sensors based on reversible fluorescence quenching in a conjugated polymer. *Proc. Natl. Acad. Sci. USA* 96 (1999): 12287-12292.

[54] Jones, R. M.; and others. Building highly sensitive dye assemblies for biosensing from molecular building blocks. *Proc. Natl. Acad. Sci. USA* 98 (2001): 14769-14772.

APPENDICES

APPENDIX A

APPENDEX A

^{1}H NMR and ^{13}C NMR spectra

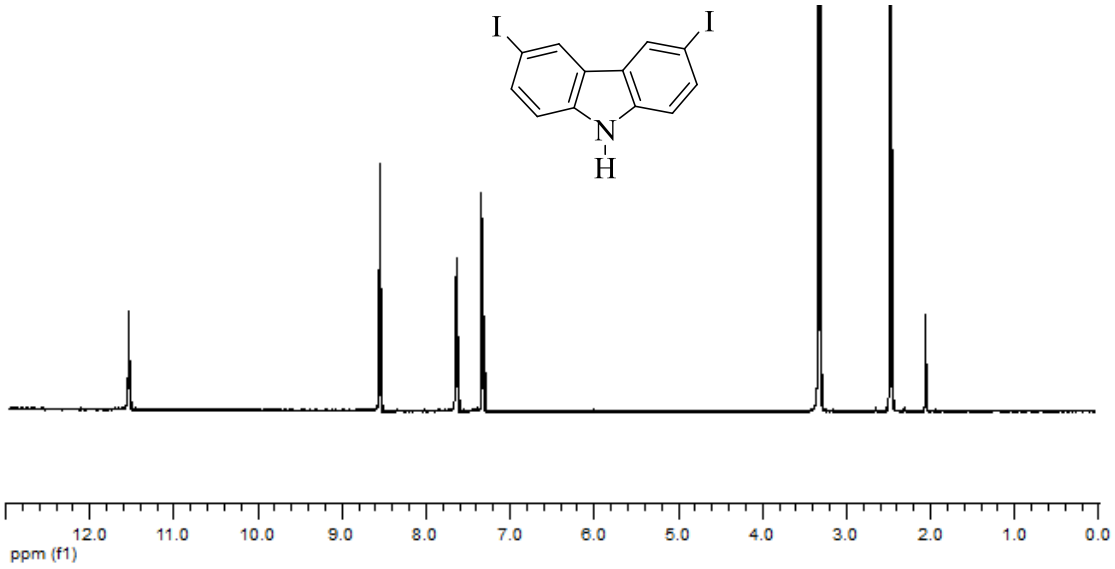

Figure A.1 ^{1}H NMR spectrum of 3,6-diiodo-*9H*-carbazole (**7**) in DMSO-*d6*.

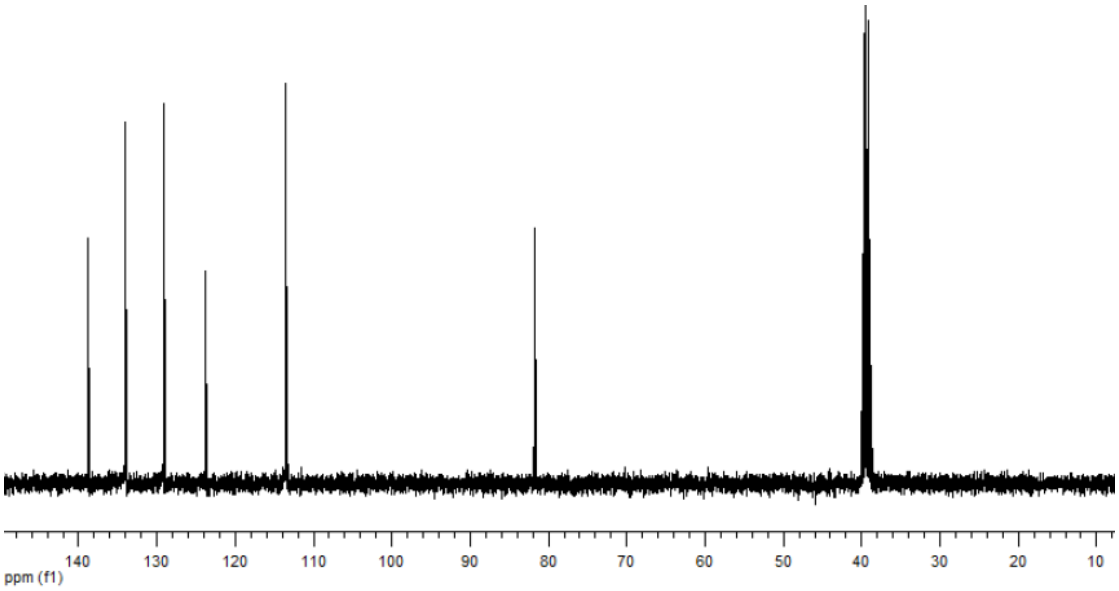

Figure A.2 ^{13}C NMR spectrum of 3,6-diiodo-*9H*-carbazole (**7**) in DMSO-*d6*.

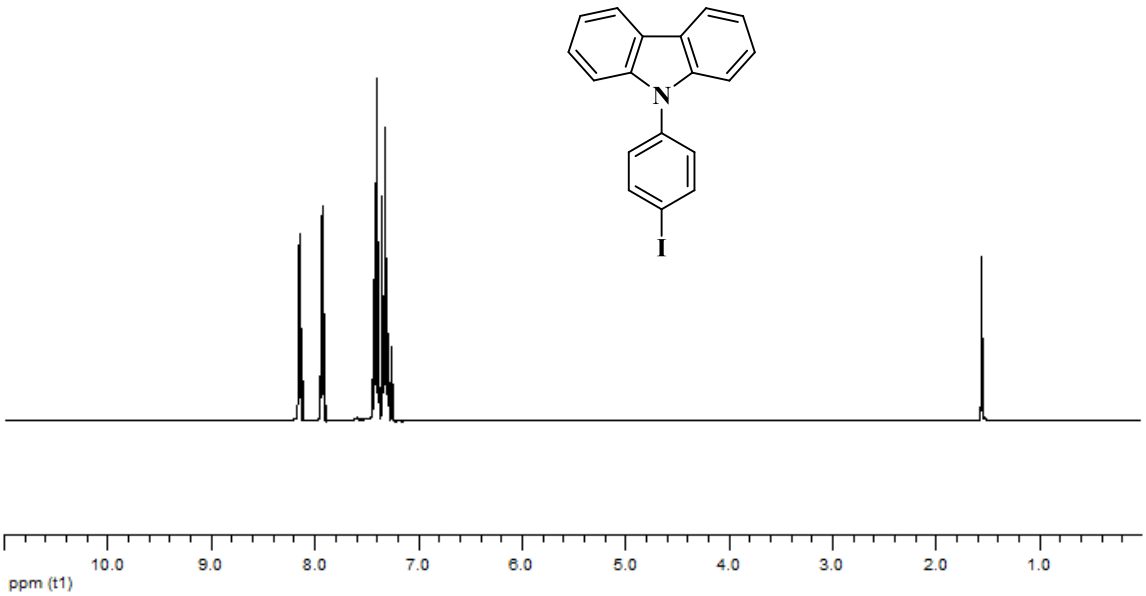

Figure A.3 ^{1}H NMR spectrum of 9-(4-iodophenyl)-9*H*-carbazole (**8**) in $CDCl_3$.

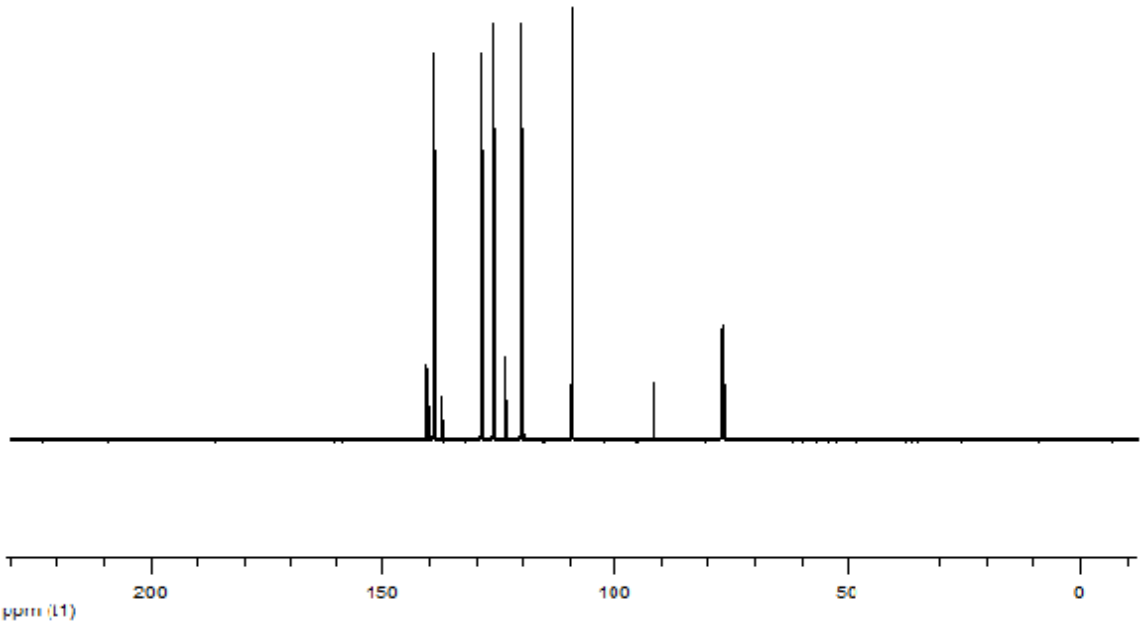

Figure A.4 ^{13}C NMR spectrum of 9-(4-iodophenyl)-9*H*-carbazole (**8**) in $CDCl_3$.

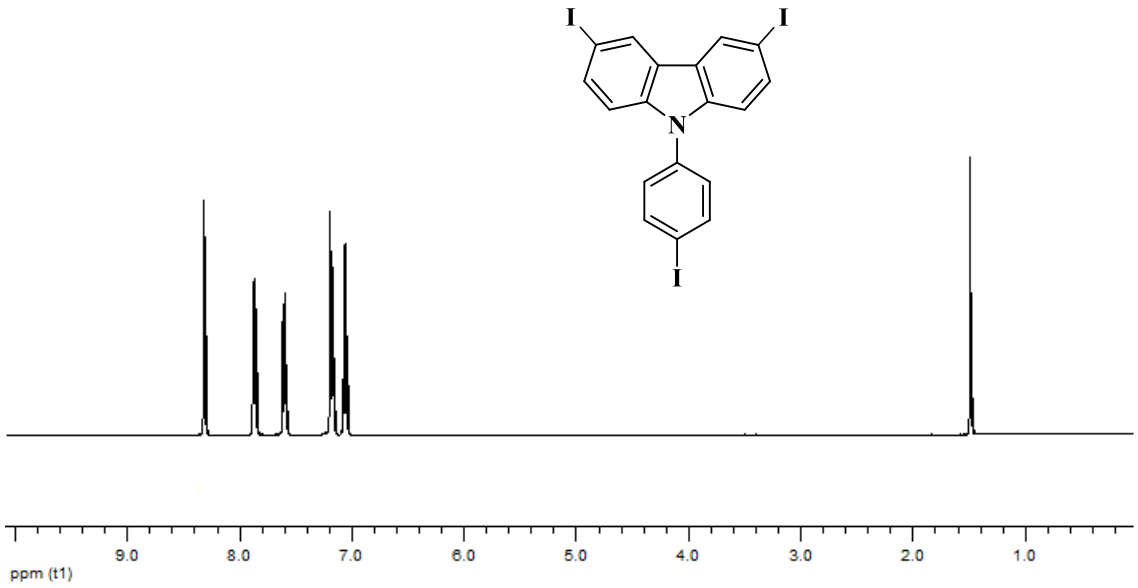

Figure A.5 ^{1}H NMR spectrum of 3,6-diiodo-9-(4-iodophenyl)-9*H*-carbazole (**9**) in $CDCl_3$.

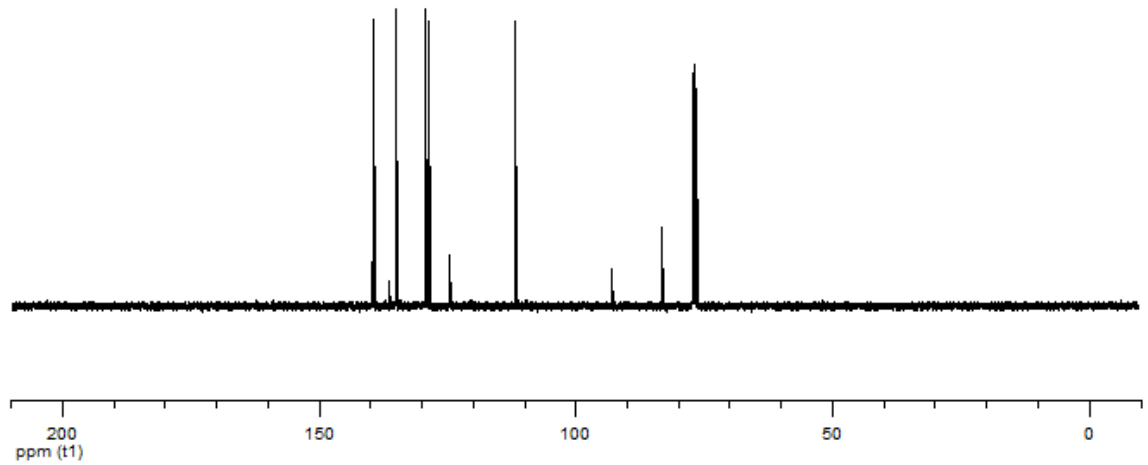

Figure A.6 ^{13}C NMR spectrum of 3,6-diiodo-9-(4-iodophenyl)-9*H*-carbazole (**9**) in $CDCl_3$.

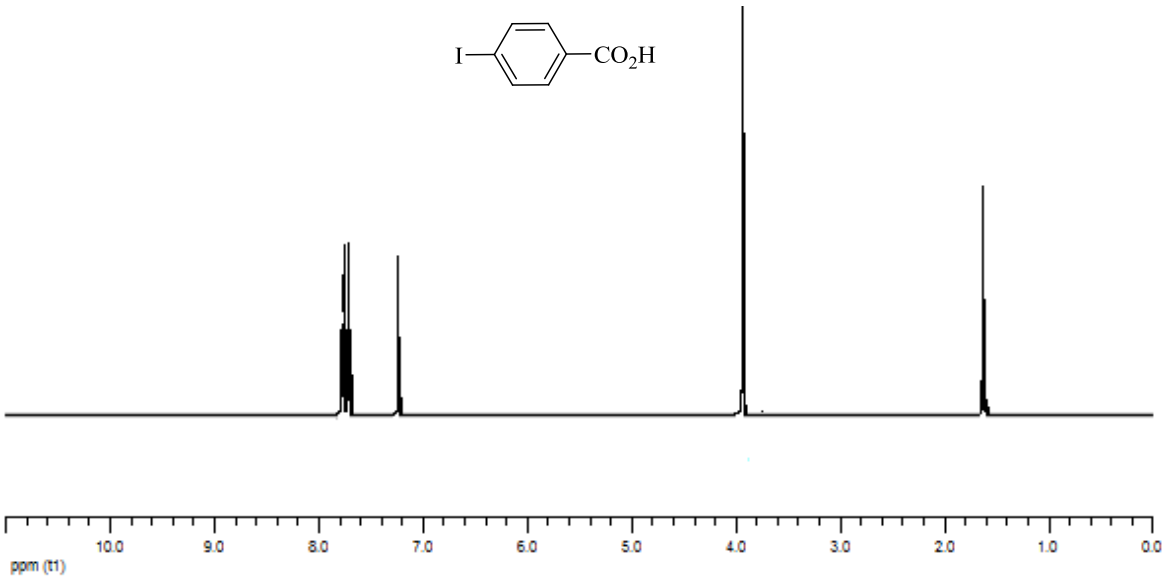

Figure A.7 ^{1}H NMR spectrum of methyl 4-iodobenzoate in $CDCl_3$.

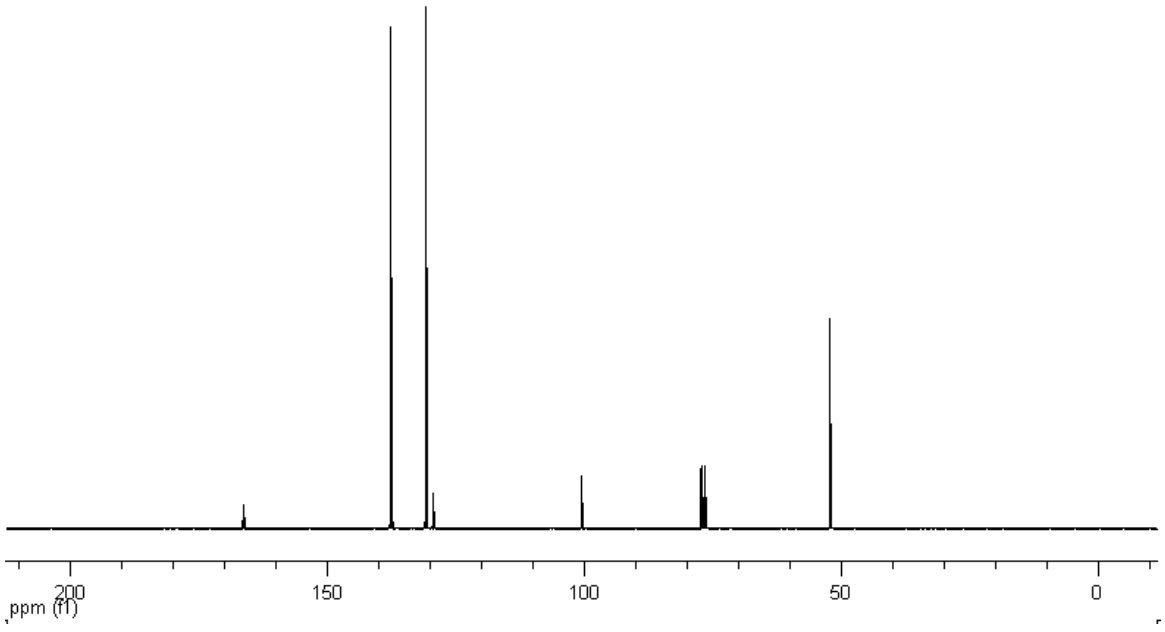

Figure A.8 ^{13}C NMR spectrum of methyl 4-iodobenzoat in $CDCl_3$.

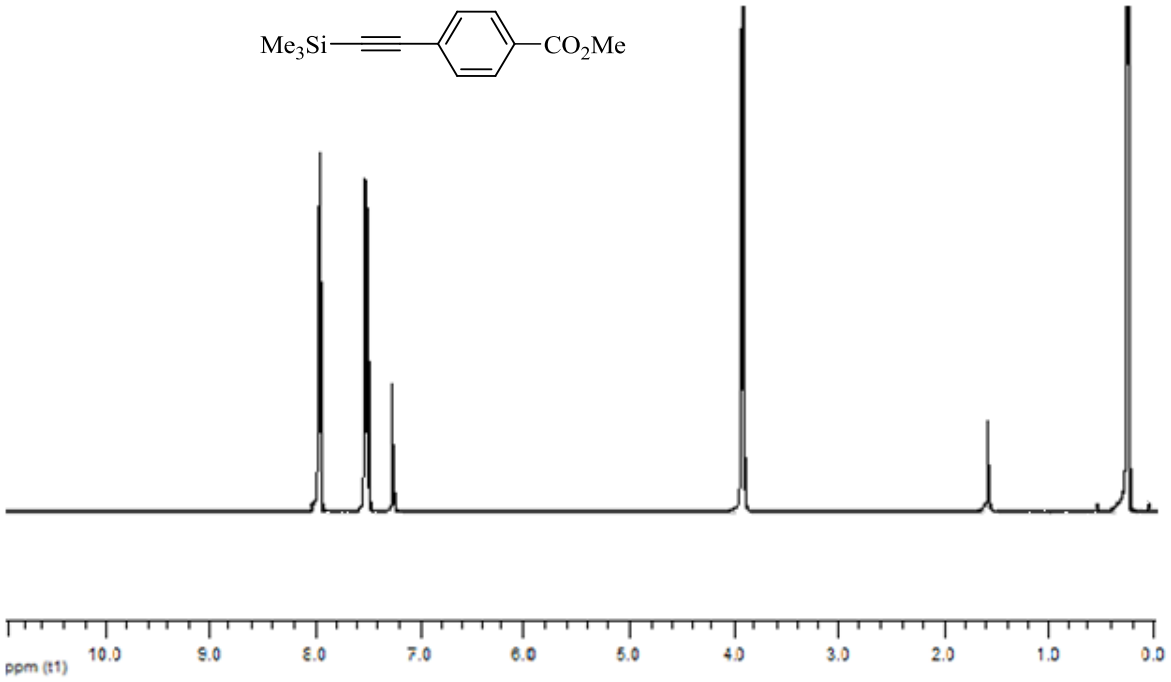

Figure A.9 ^{1}H NMR spectrum of methyl 4-((trimethylsilyl)ethynyl)benzoate in $CDCl_3$.

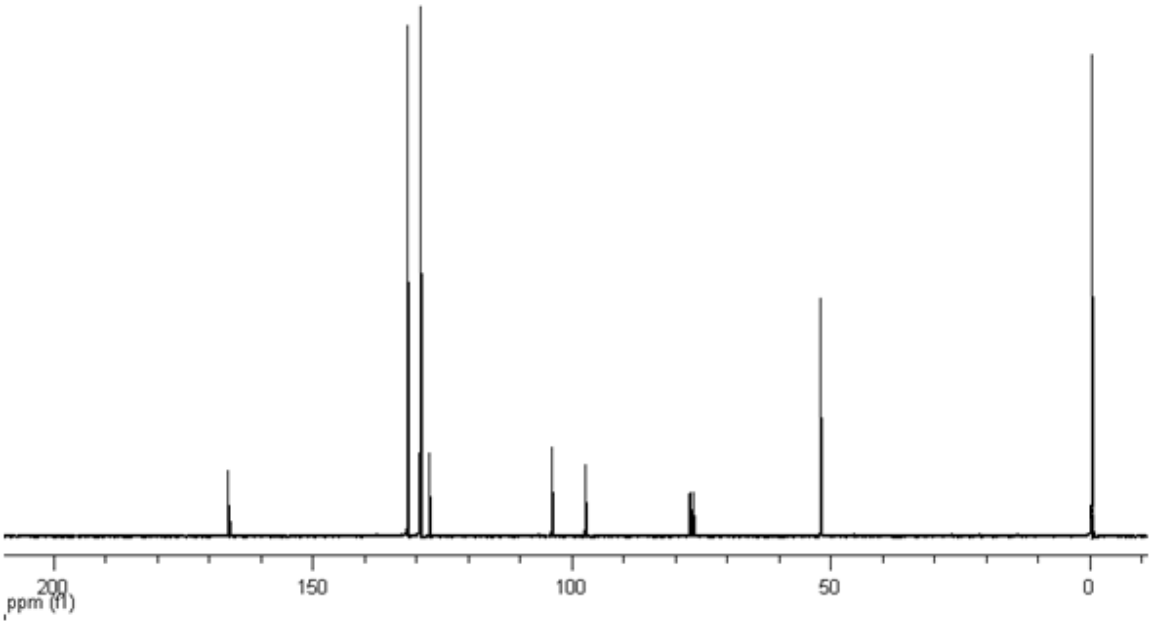

Figure A.10 ^{13}C NMR spectrum of methyl 4-((trimethylsilyl)ethynyl)benzoate in $CDCl_3$.

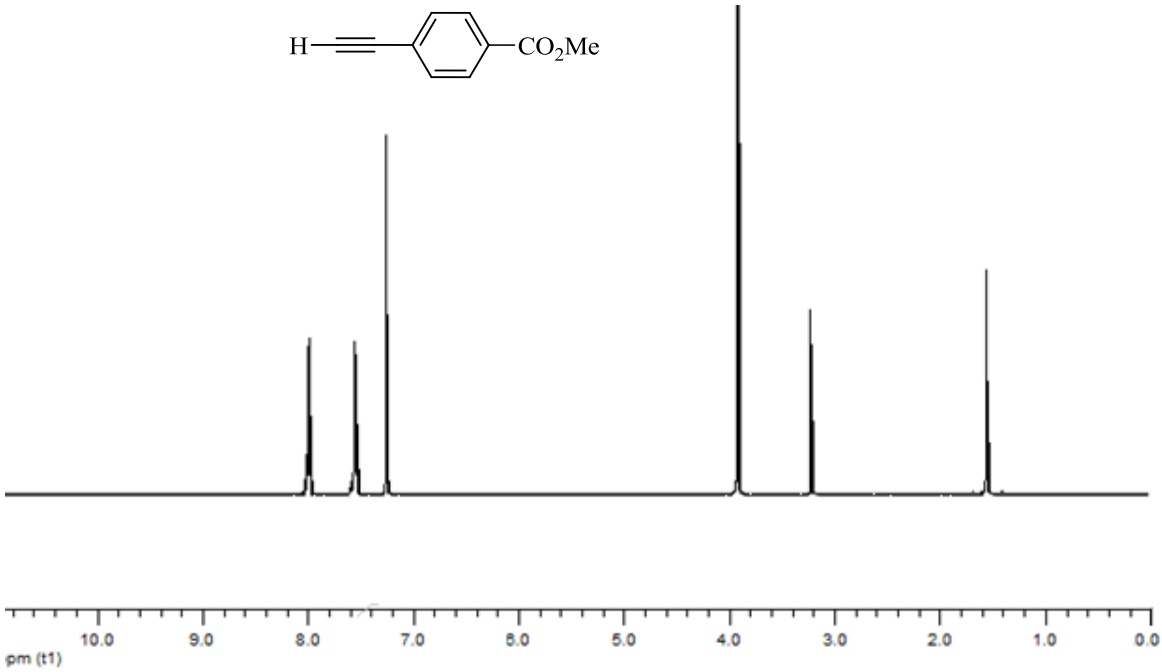

Figure A.11 ^{1}H NMR spectrum of methyl 4-ethynylbenzoate in $CDCl_3$.

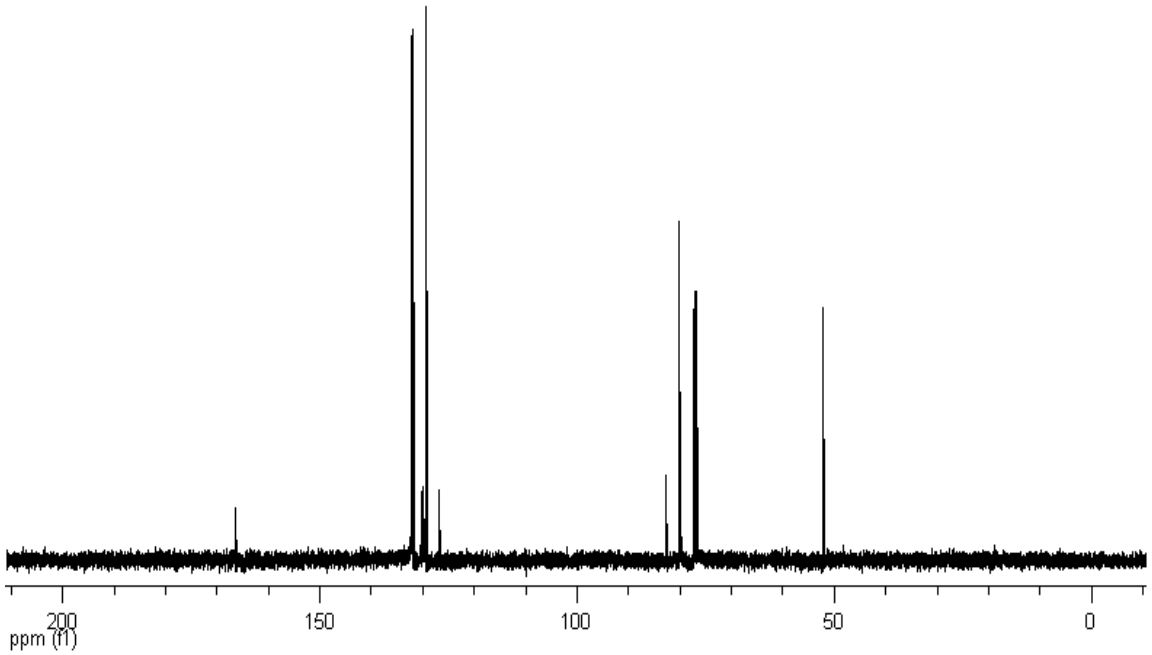

Figure A.12 ^{13}C NMR spectrum of methyl 4-ethynylbenzoate in $CDCl_3$.

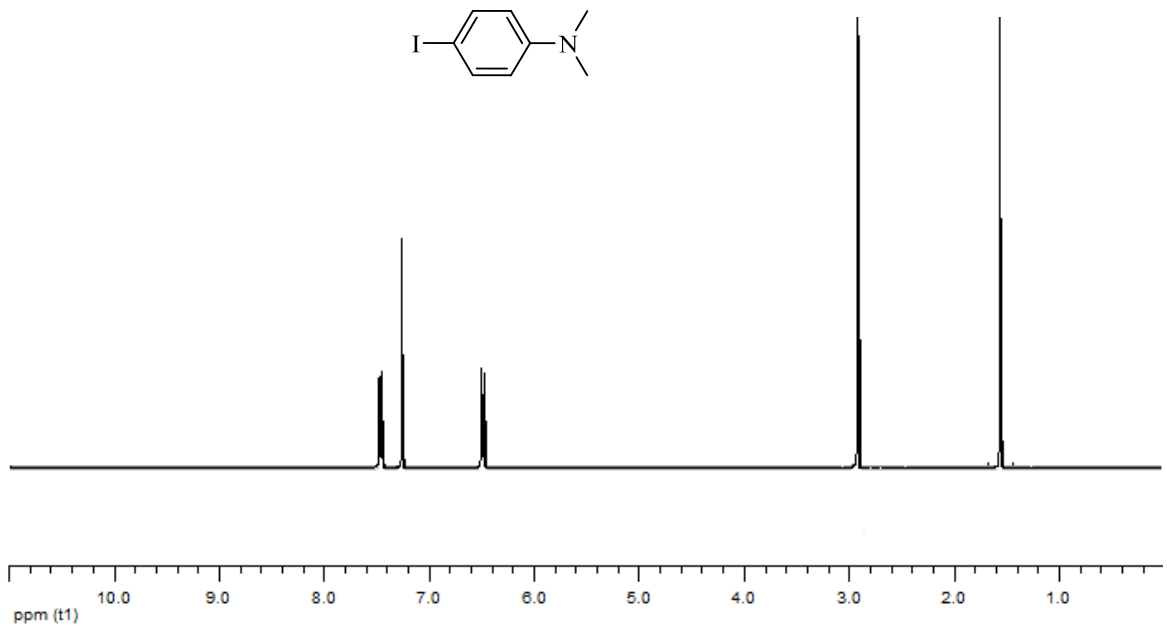

Figure A.13 ^{1}H NMR spectrum of 4-iodo-*N*,*N*-dimethylaniline in $CDCl_3$.

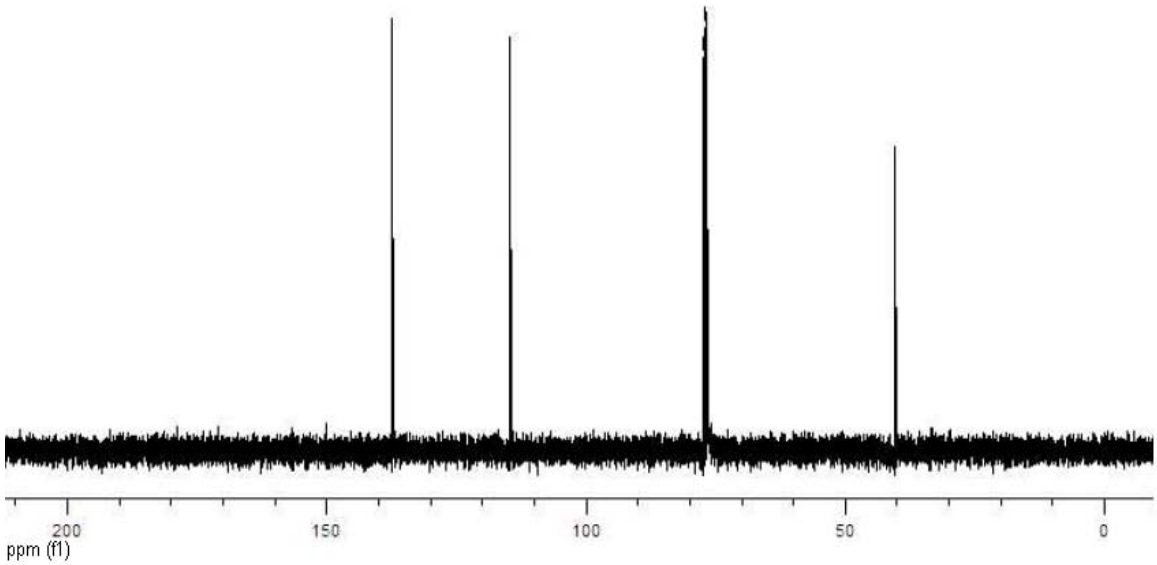

Figure A.14 ^{13}C NMR spectrum of 4-iodo-*N*,*N*-dimethylaniline in $CDCl_3$.

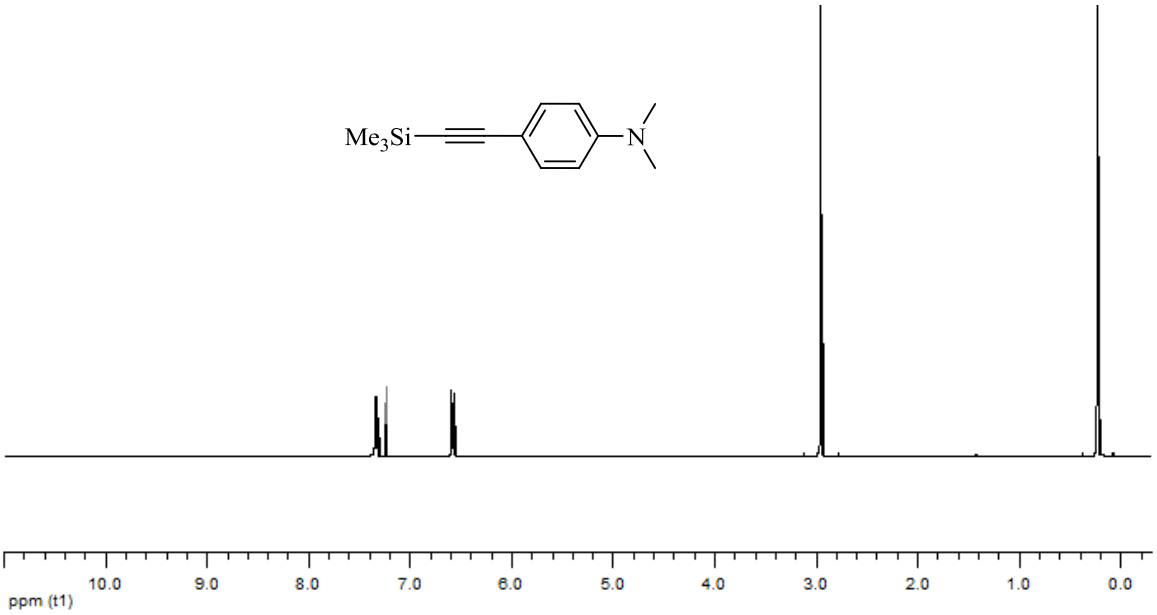

Figure A.15 ^{1}H NMR spectrum of *N*,*N*-dimethyl-4-((trimethylsilyl)ethynyl)aniline in $CDCl_3$.

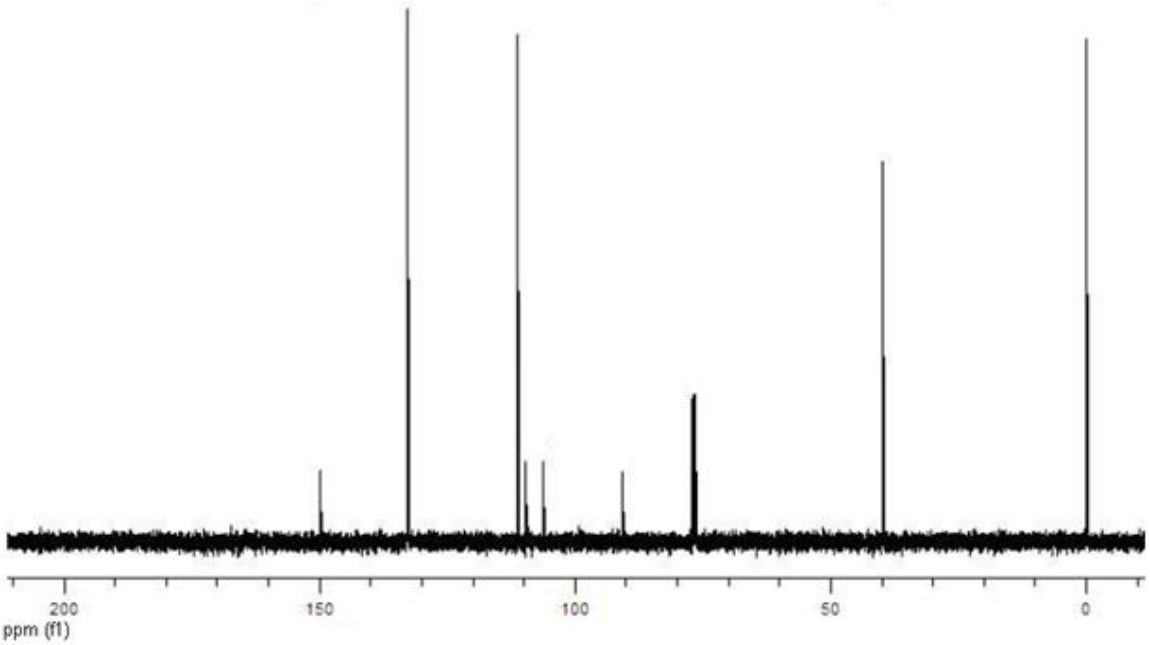

Figure A.16 ^{13}C NMR spectrum of *N*,*N*-dimethyl-4-((trimethylsilyl)ethynyl)aniline in $CDCl_3$.

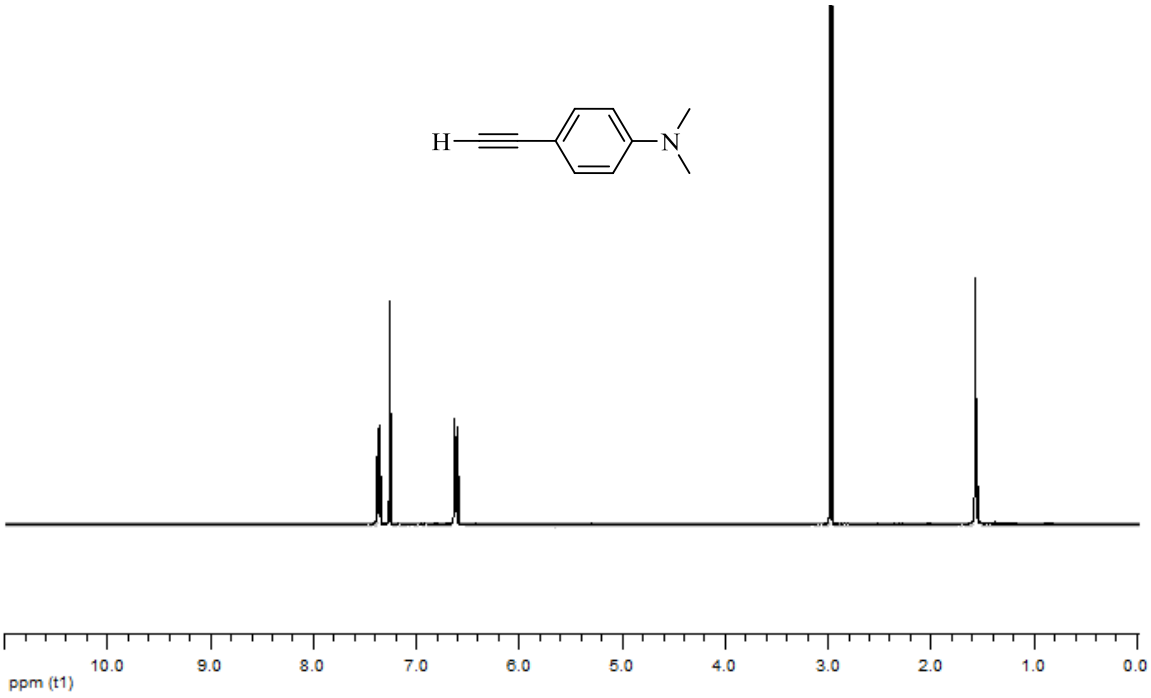

Figure A.17 ^{1}H NMR spectrum of 4-ethynyl-*N*,*N*-dimethylaniline in $CDCl_3$.

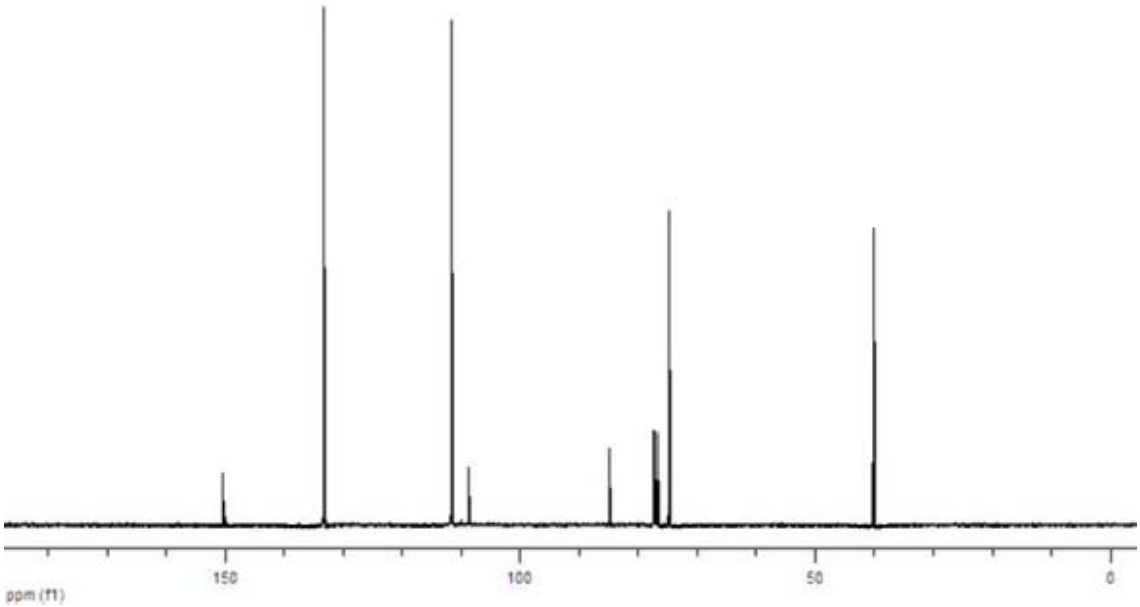

Figure A.18 ^{13}C NMR spectrum of 4-ethynyl-*N*,*N*-dimethylaniline in $CDCl_3$.

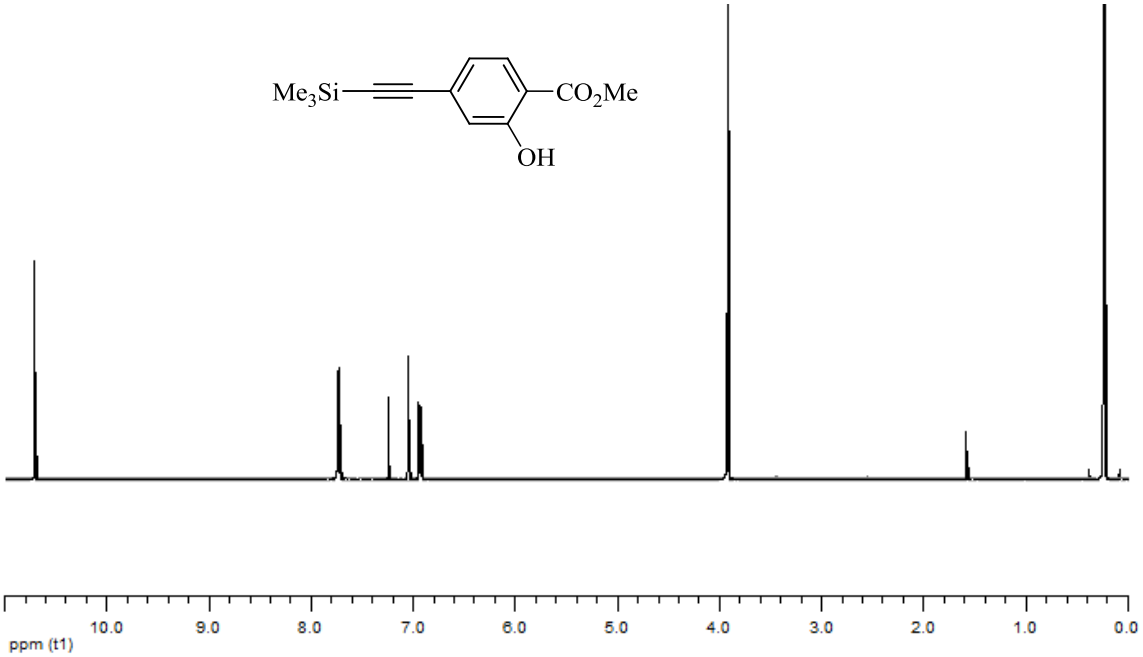

Figure A.19 ^{1}H NMR spectrum of methyl 2-hydroxy-4-((trimethylsilyl)ethynyl)benzoate in $CDCl_3$.

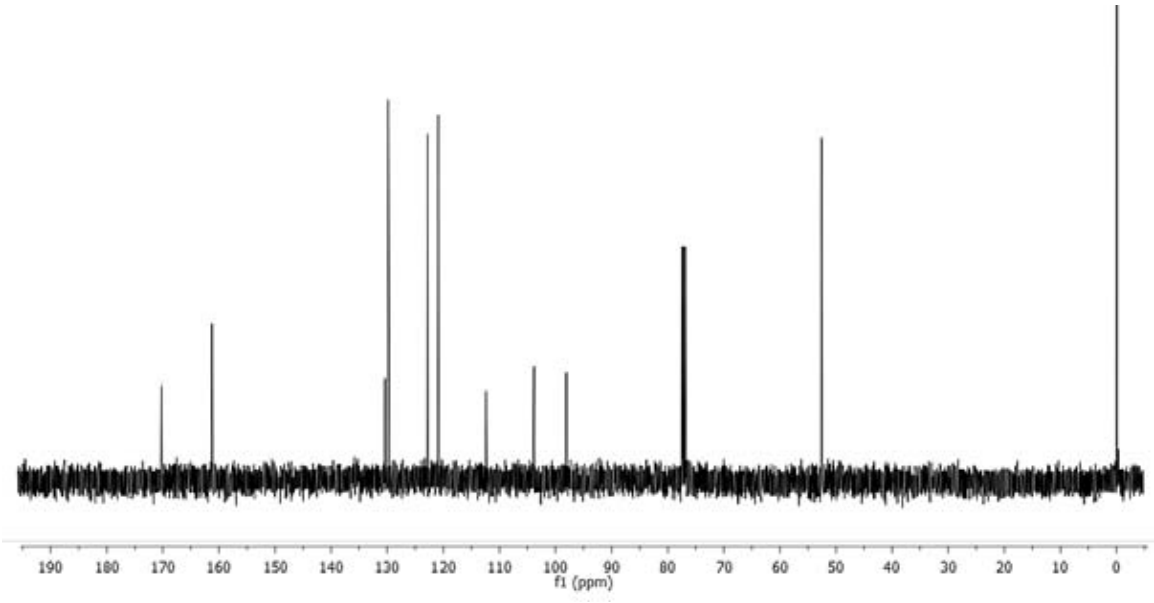

Figure A.20 ^{13}C NMR spectrum of methyl 2-hydroxy-4((trimethylsilyl)ethynyl)benzoate in $CDCl_3$.

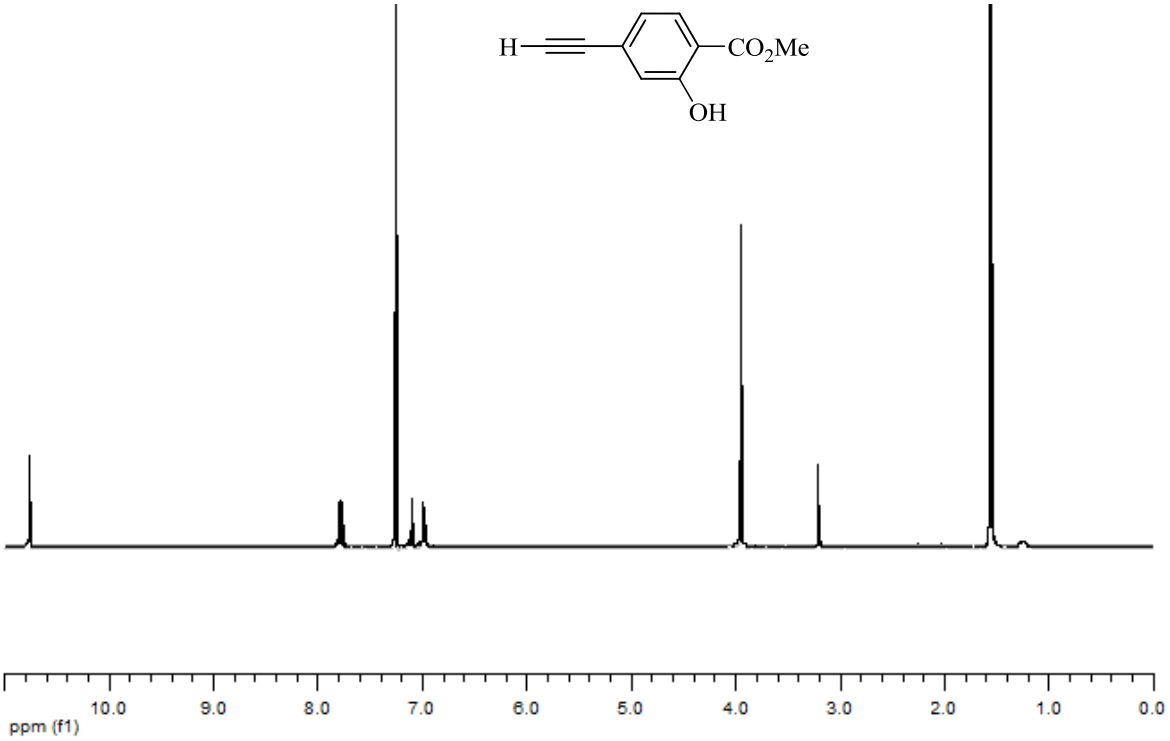

Figure A.21 ^{1}H NMR spectrum of methyl 4-ethynyl-2-hydroxybenzoate in $CDCl_3$.

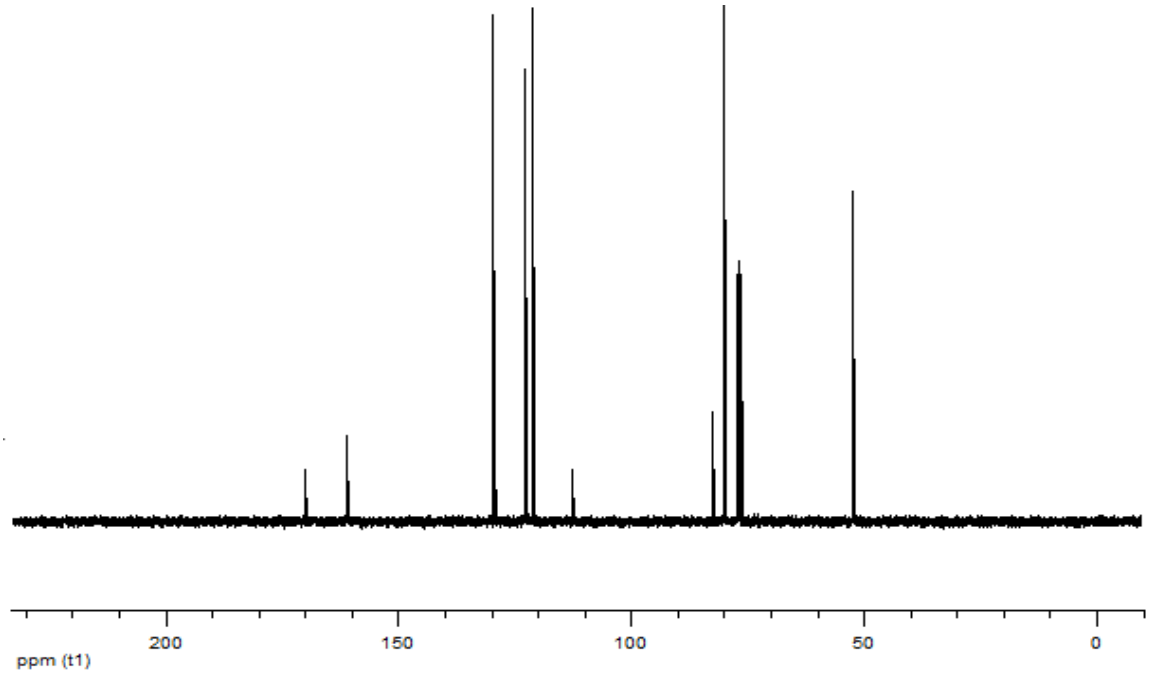

Figure A.22 ^{13}C NMR spectrum of methyl 4-ethynyl-2-hydroxybenzoate in $CDCl_3$.

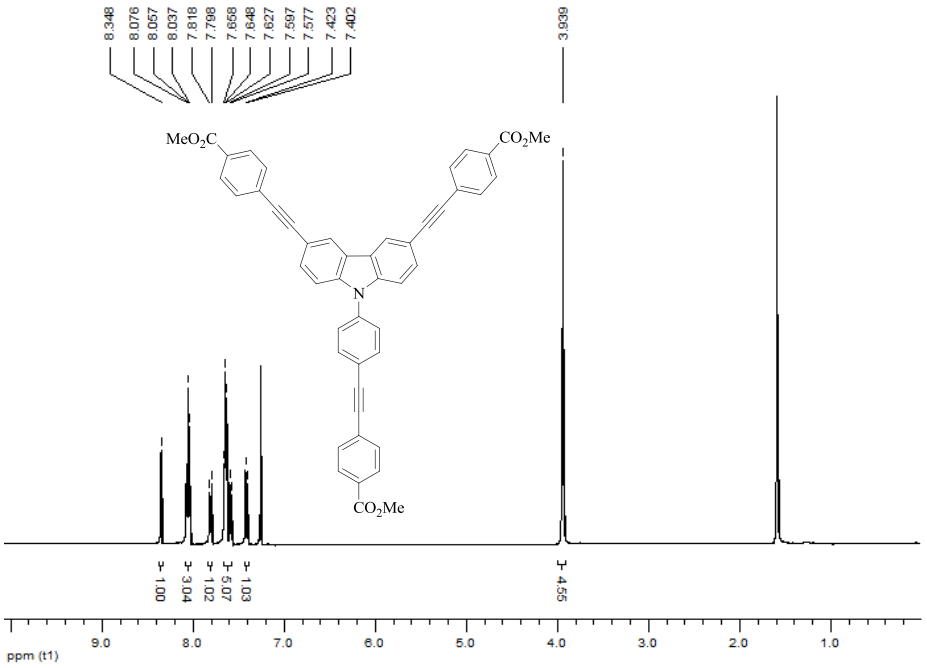

Figure A.23 ^{1}H NMR spectrum of **10** in $CDCl_3$.

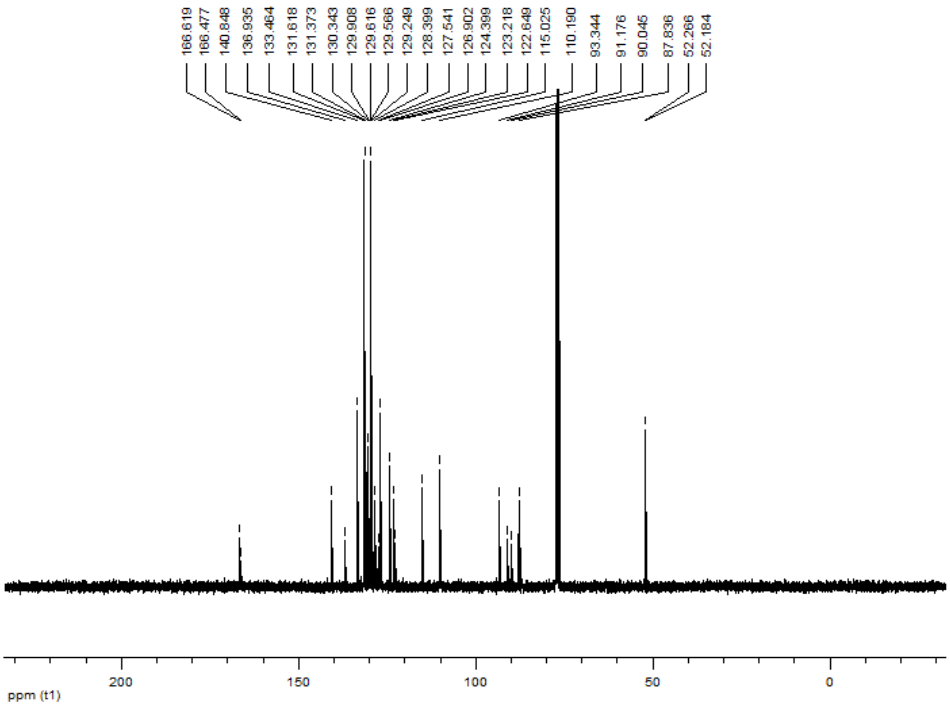

Figure A.24 ^{13}C NMR spectrum of **10** in $CDCl_3$.

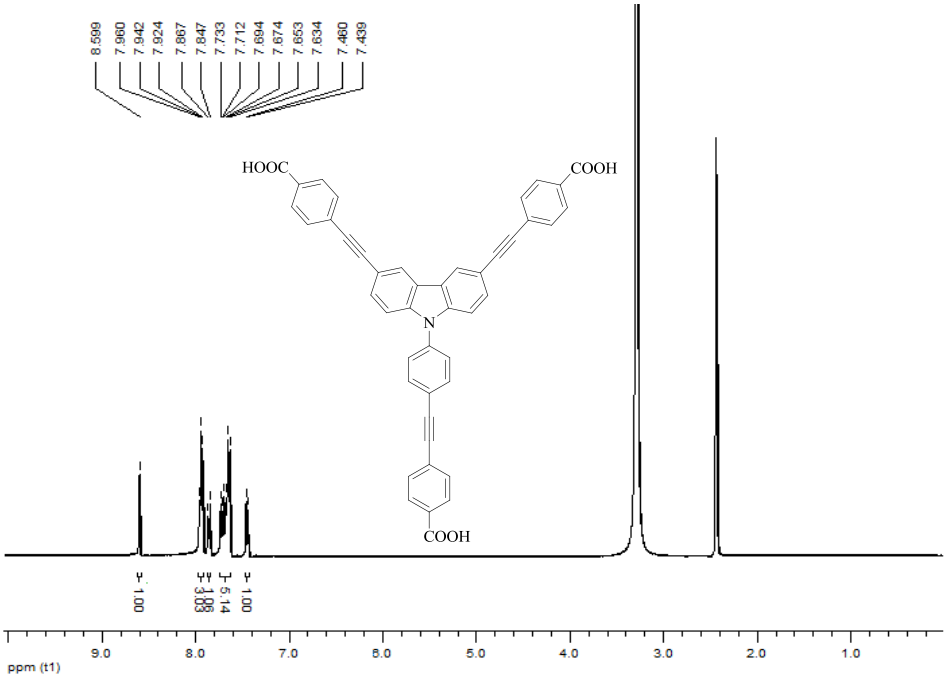

Figure A.25 ^{1}H NMR spectrum of **1** in DMSO-*d6*.

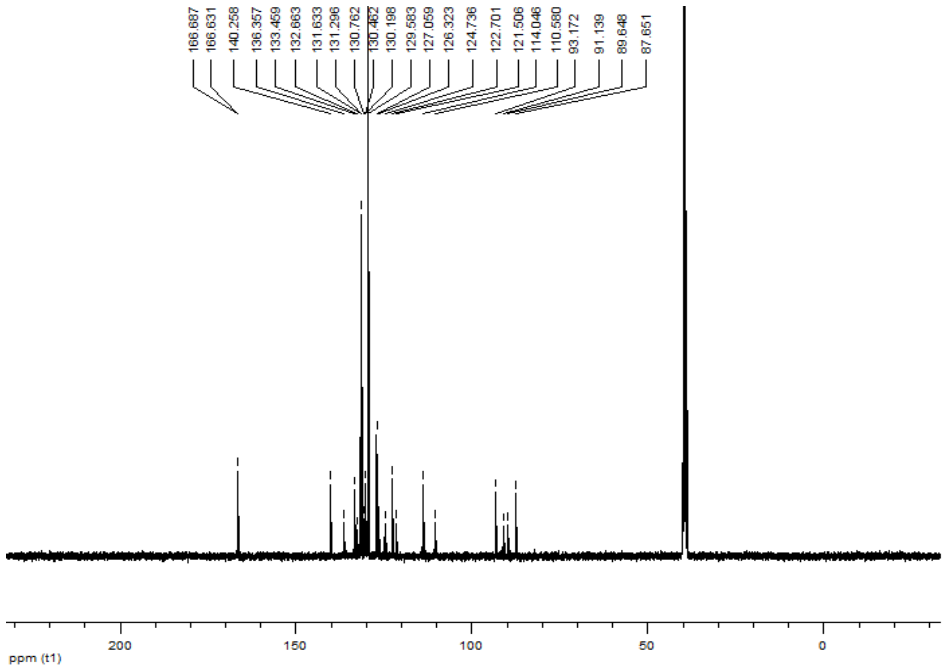

Figure A.26 ^{13}C NMR spectrum of **1** in DMSO-*d6*.

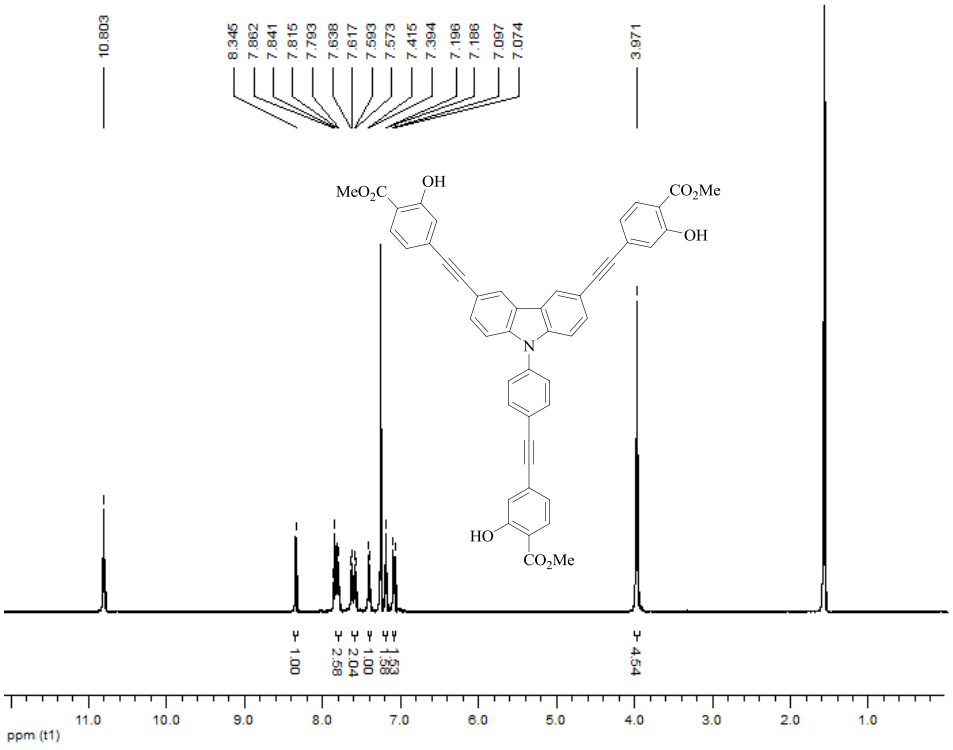

Figure A.27 ^{1}H NMR spectrum of **11** in $CDCl_3$.

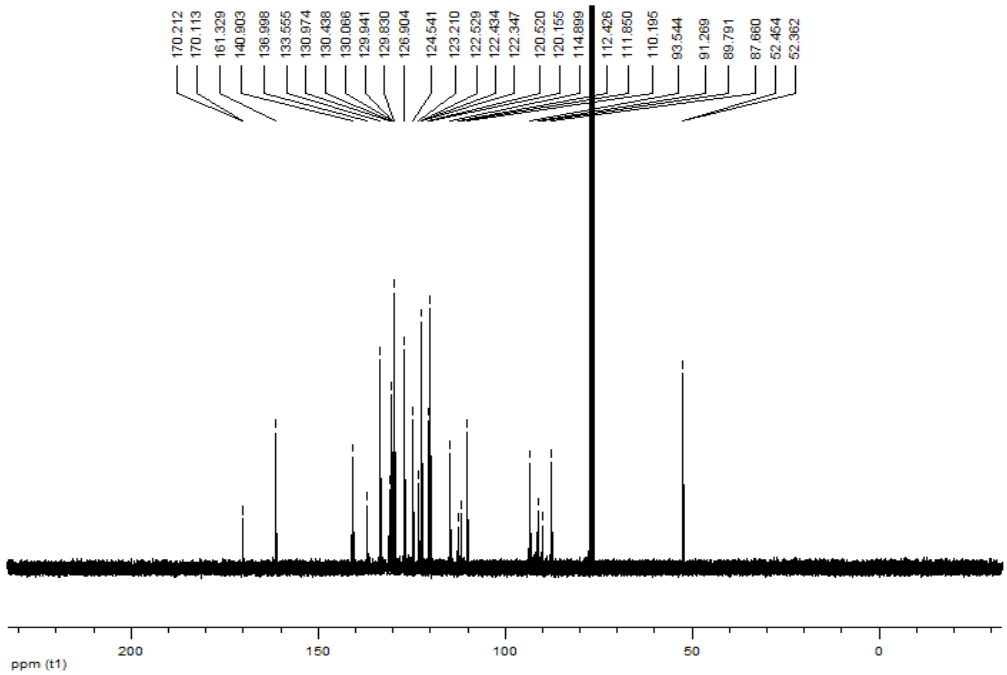

Figure A.28 ^{13}C NMR spectrum of **11** in $CDCl_3$.

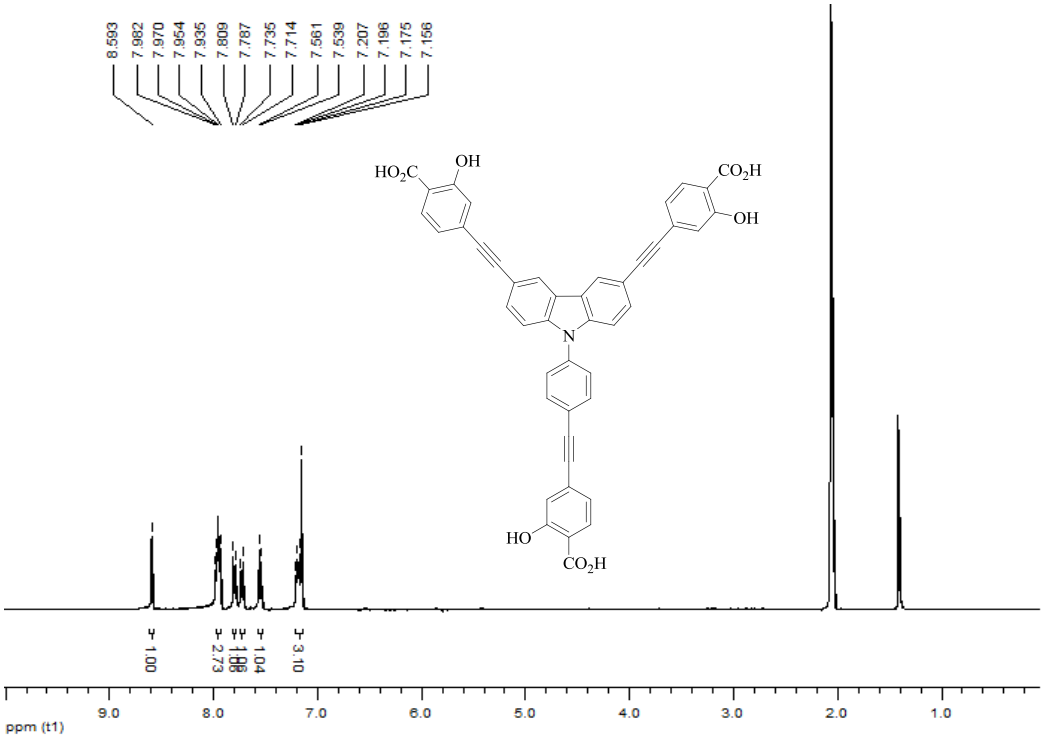

Figure A.29 ^{1}H NMR spectrum of **2** in acetone-d^{6}.

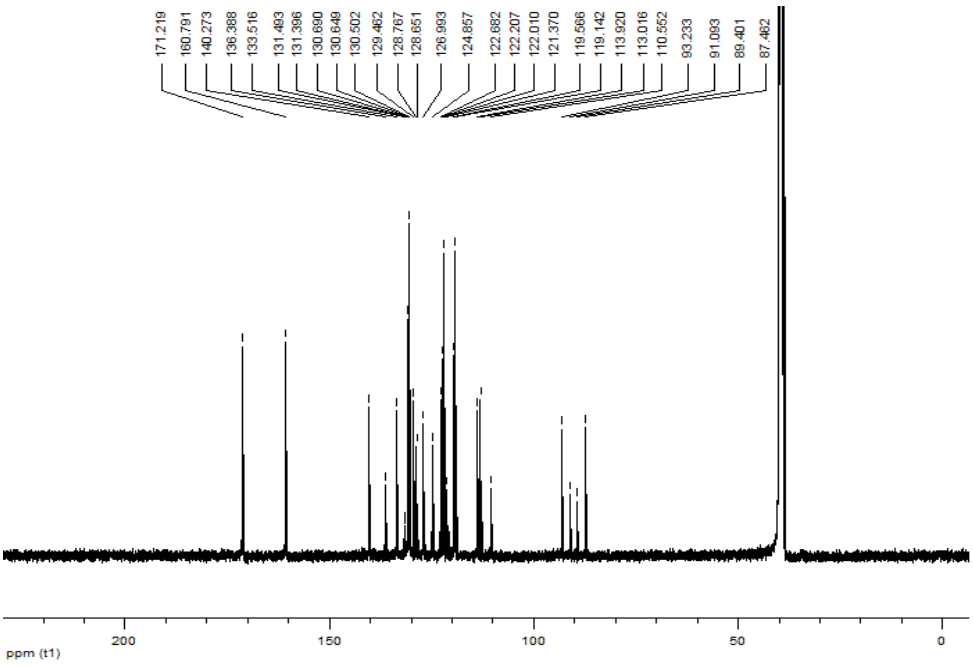

Figure A.30 ^{13}C NMR spectrum of **2** in DMSO-*d6*.

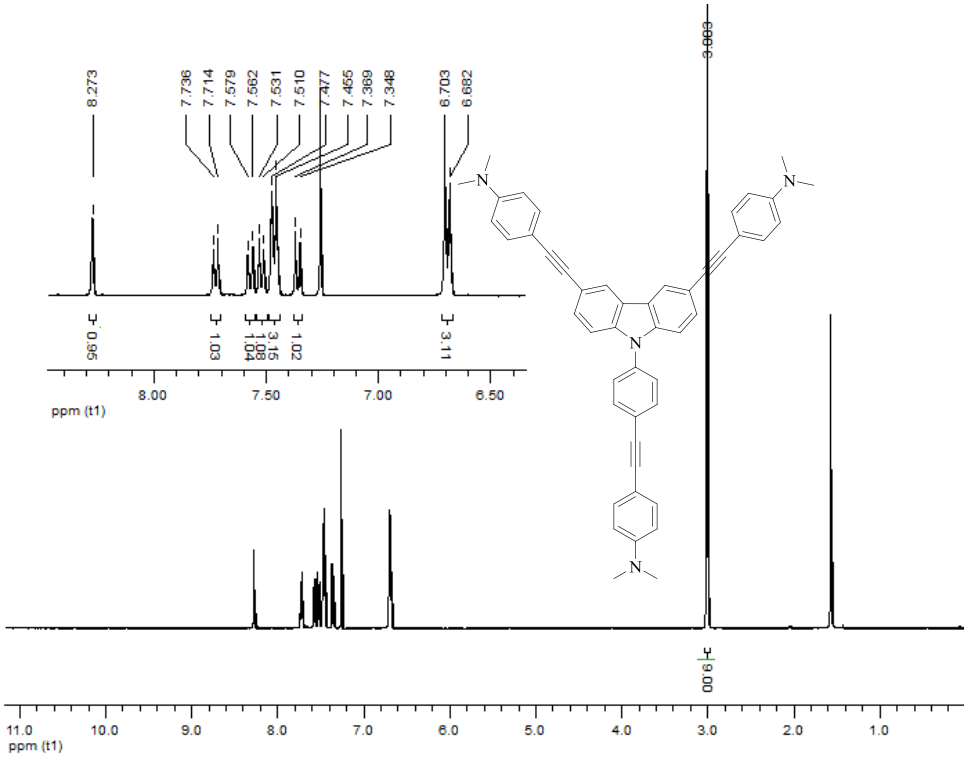

Figure A.31 ^{1}H NMR spectrum of **12** in $CDCl_3$.

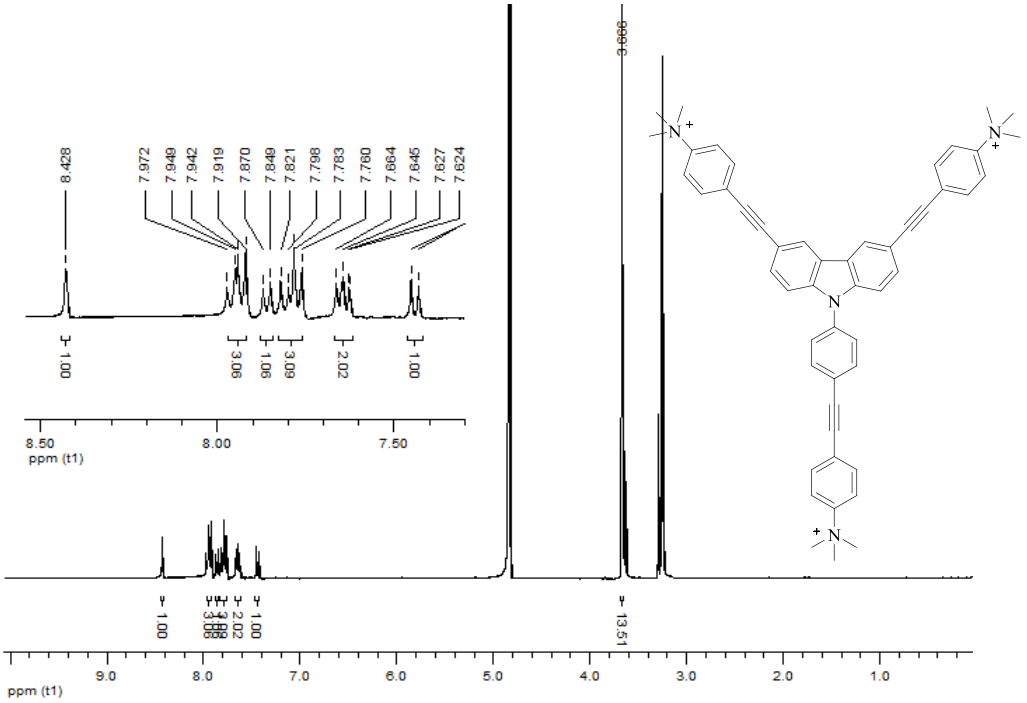

Figure A.32 ^{1}H NMR spectrum of **3** in CD_3OD.

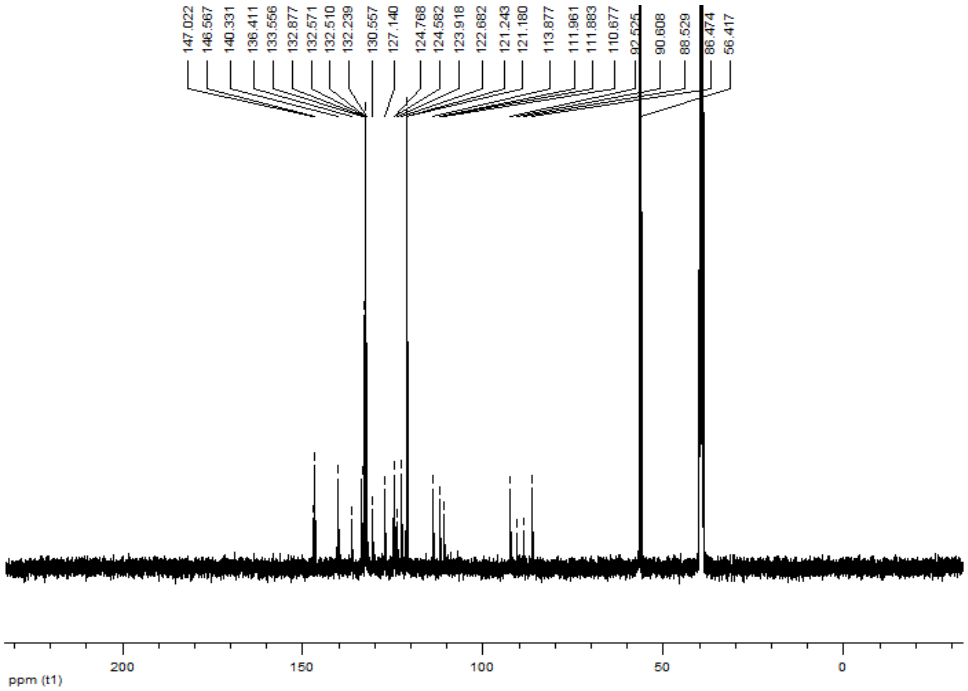

Figure A.33 ^{13}C NMR spectrum of **3** in CD_3OD.

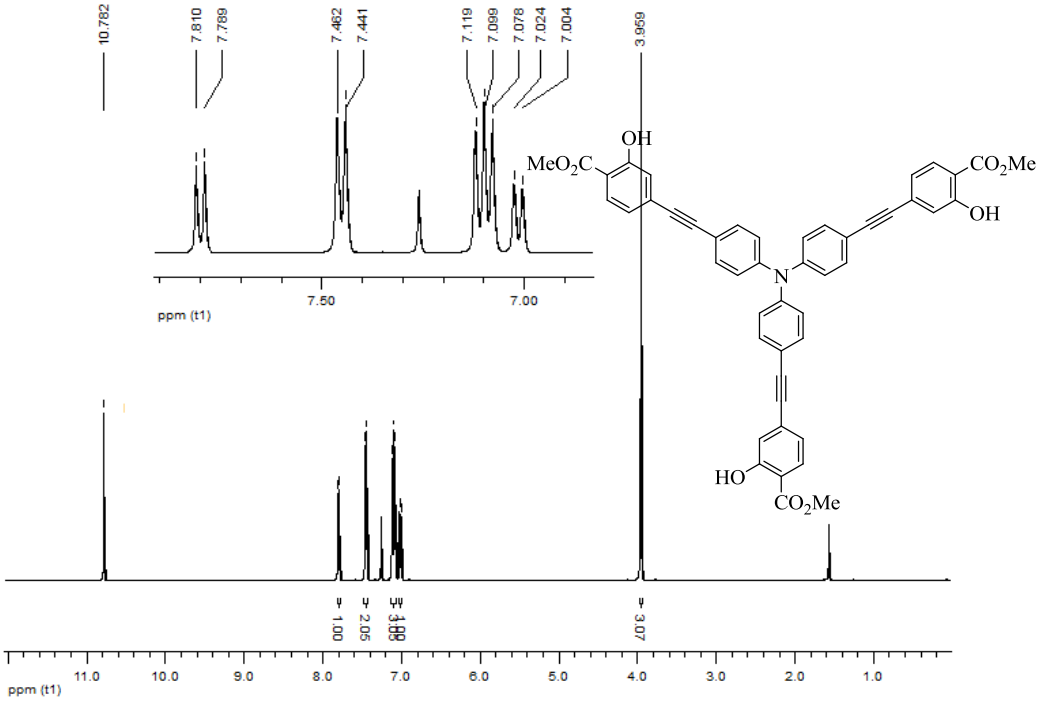

Figure A.34 ^{1}H NMR spectrum of **13** in $CDCl_3$.

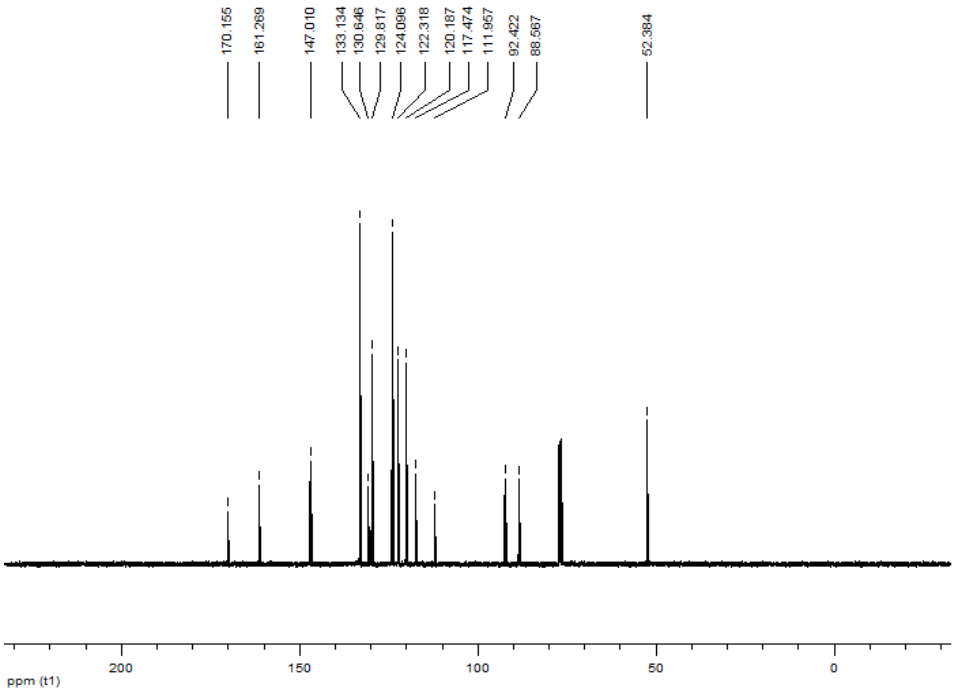

Figure A.35 ^{13}C NMR spectrum of **13** in $CDCl_3$.

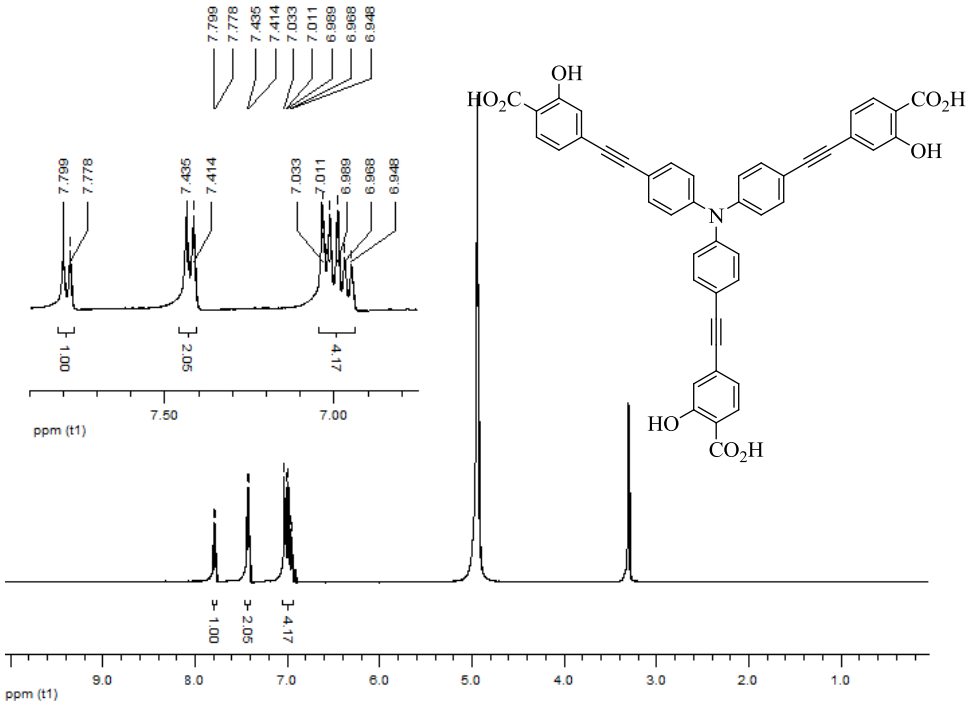

Figure A.36 ^{1}H NMR spectrum of **4** in CD_3OD.

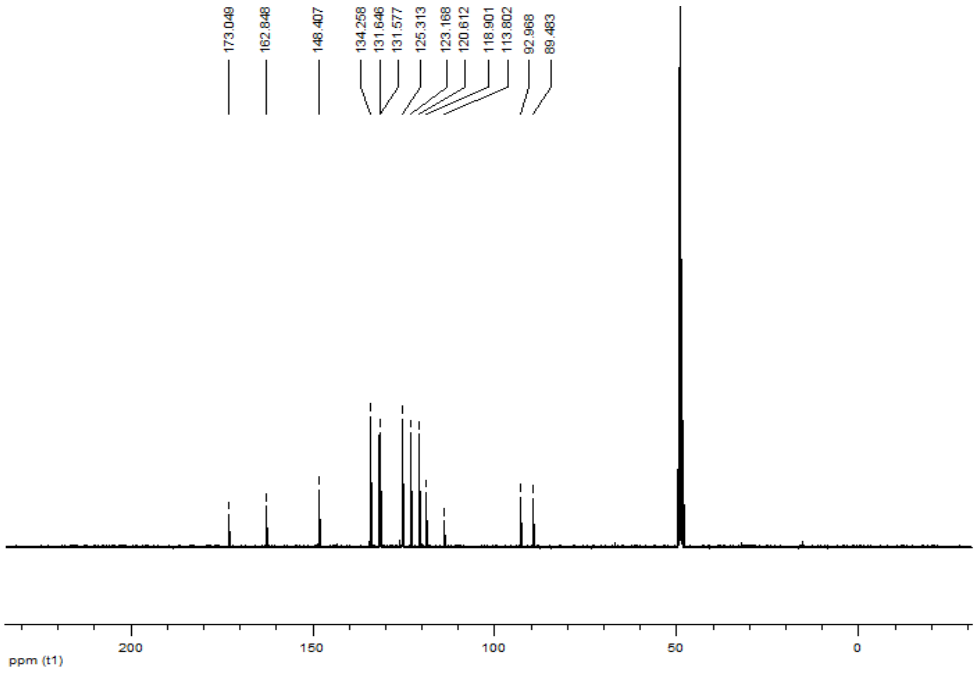

Figure A.37 ^{13}C NMR spectrum of **4** in CD_3OD.

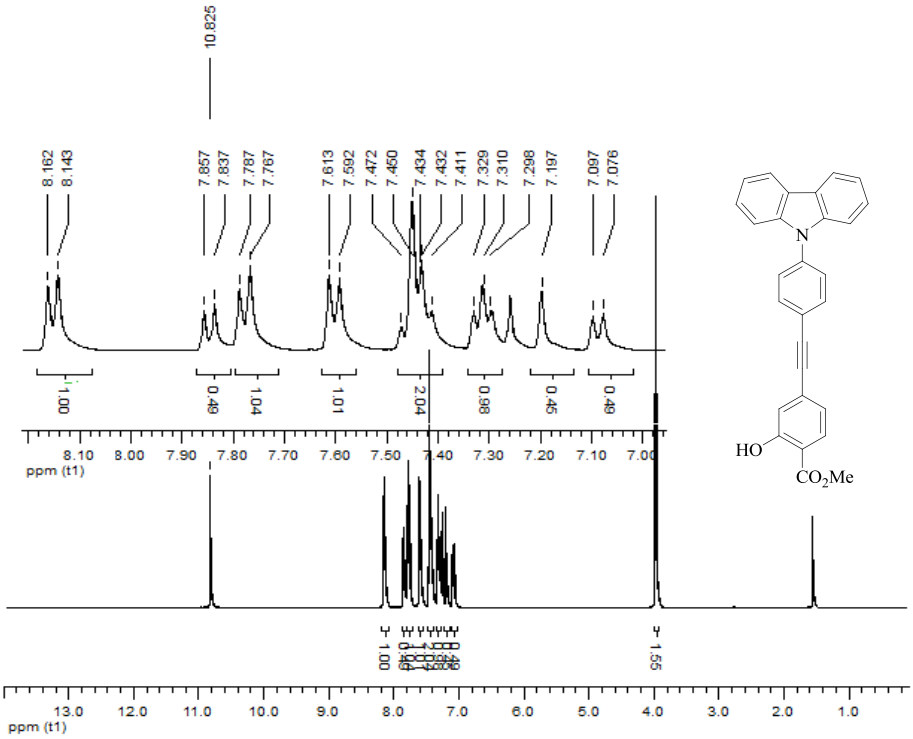

Figure A.38 ^{1}H NMR spectrum of **14** in $CDCl_3$.

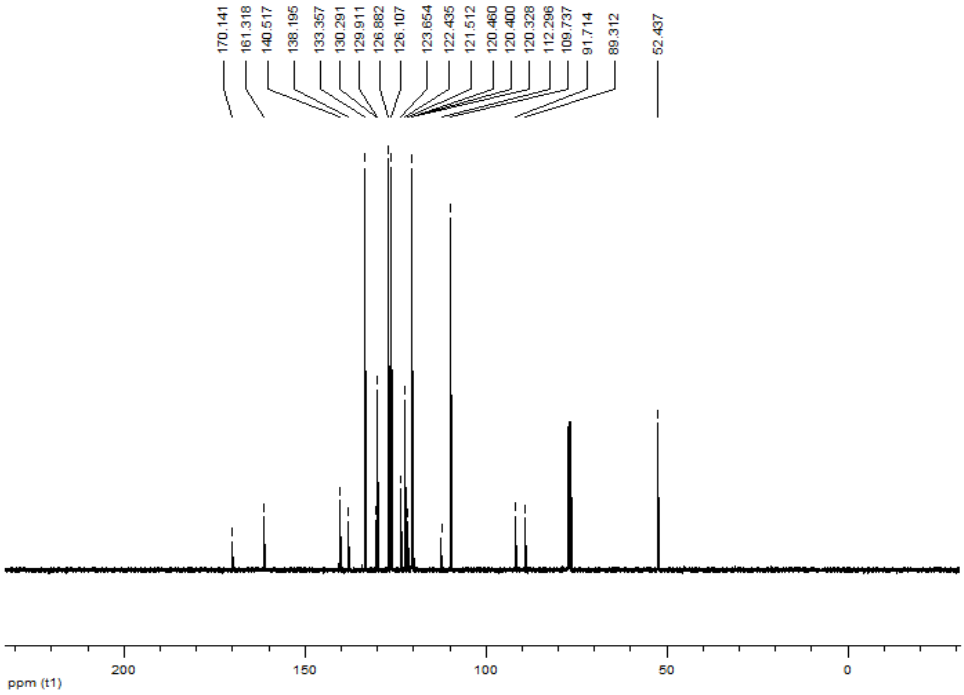

Figure A.39 ^{13}C NMR spectrum of **14** in $CDCl_3$.

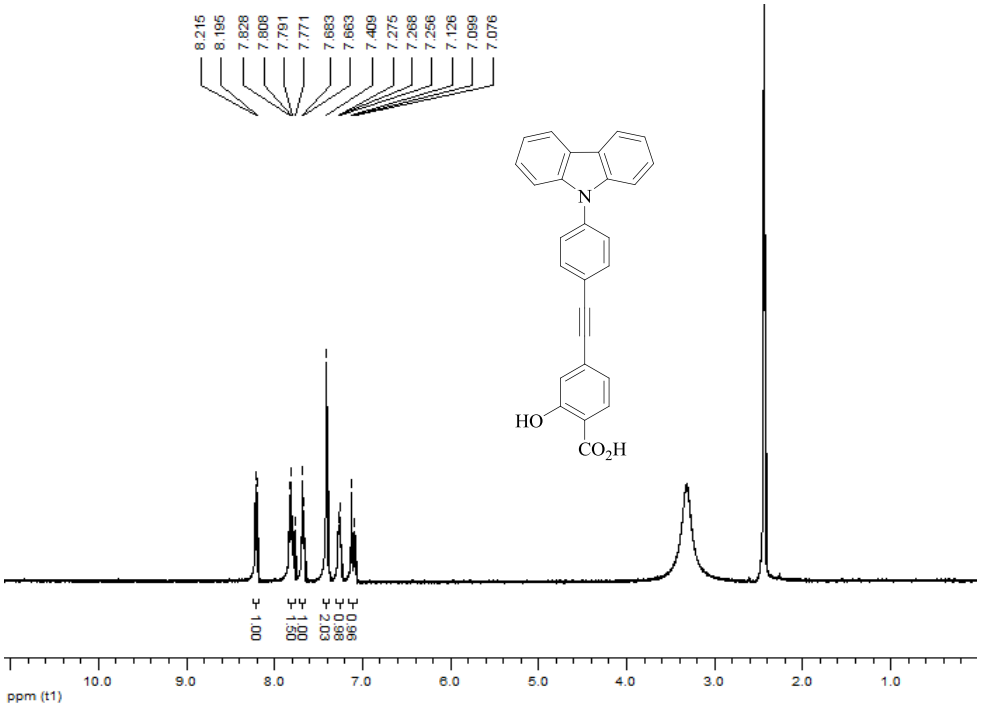

Figure A.40 ^{1}H NMR spectrum of **5** in DMSO-*d6*.

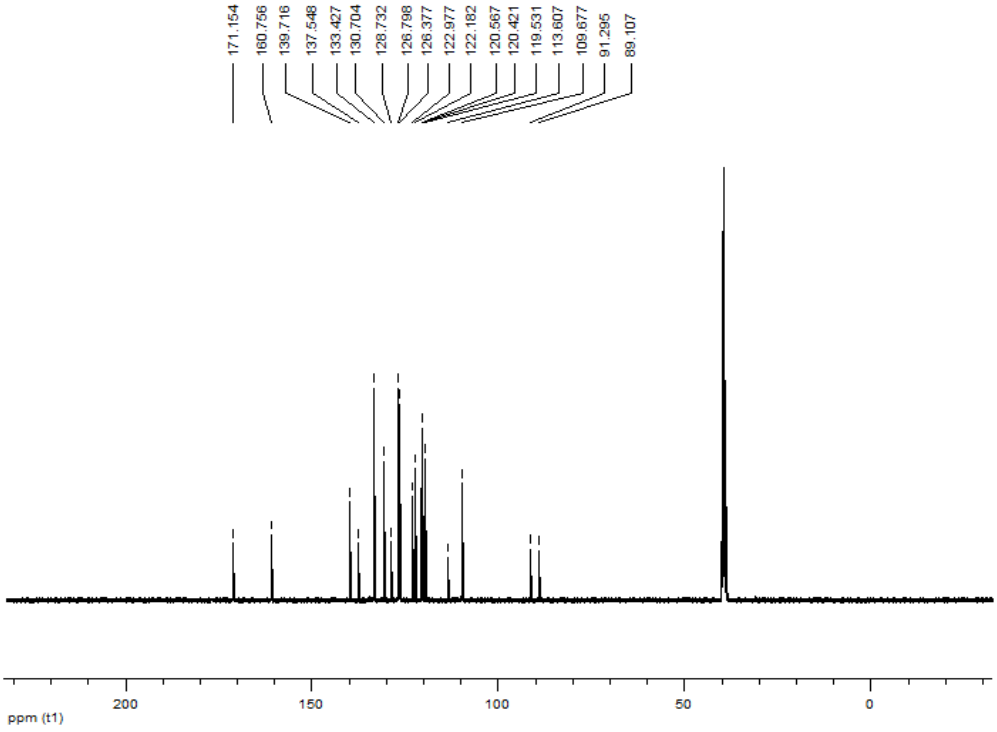

Figure A.41 ^{13}C NMR spectrum of **5** in DMSO-*d6*.

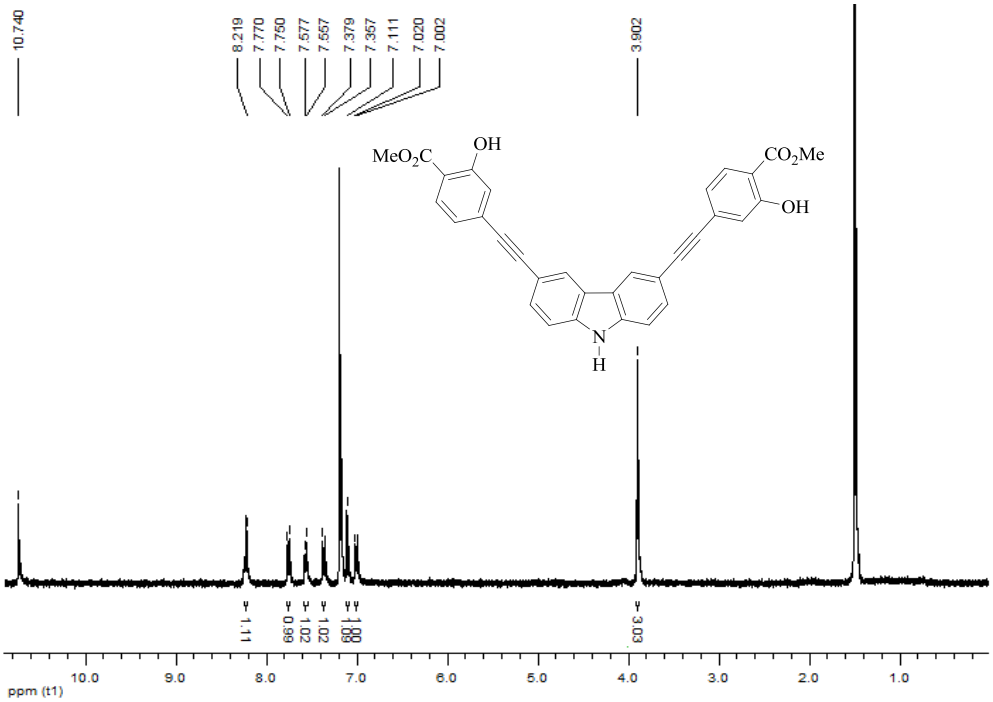

Figure A.42 ^{1}H NMR spectrum of **15** in $CDCl_3$.

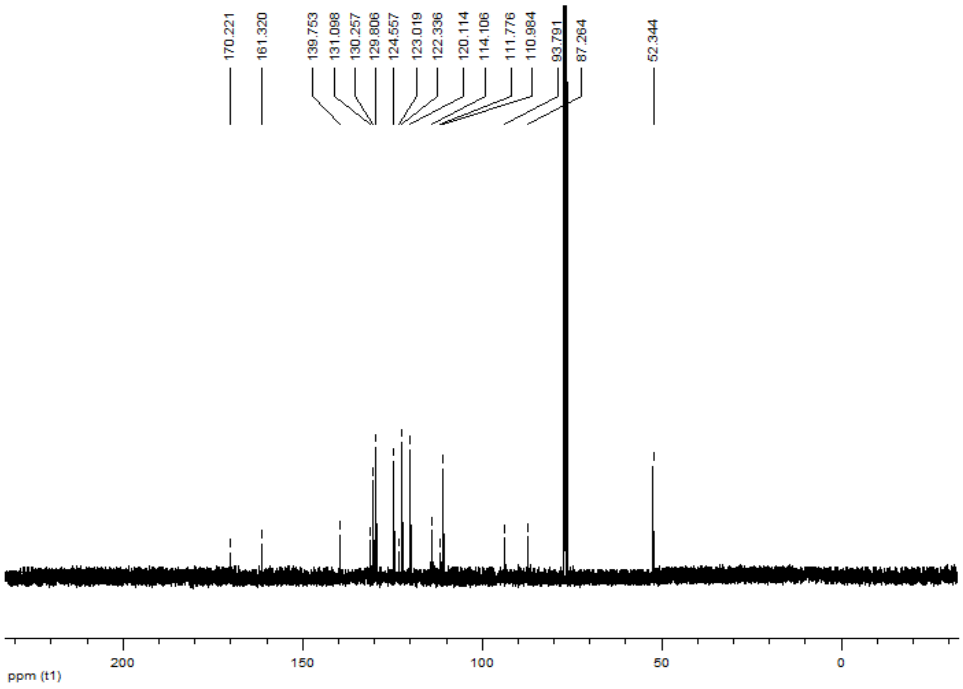

Figure A.43 ^{13}C NMR spectrum of **15** in $CDCl_3$.

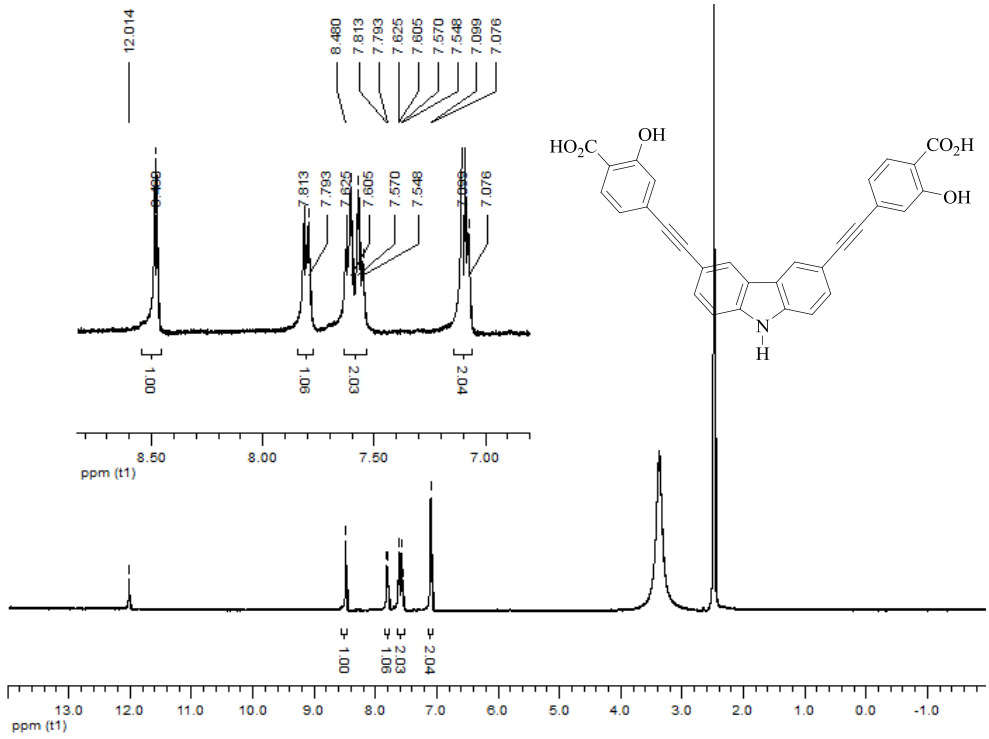

Figure 44 ^{1}H NMR spectrum of **6** in DMSO-*d6*.

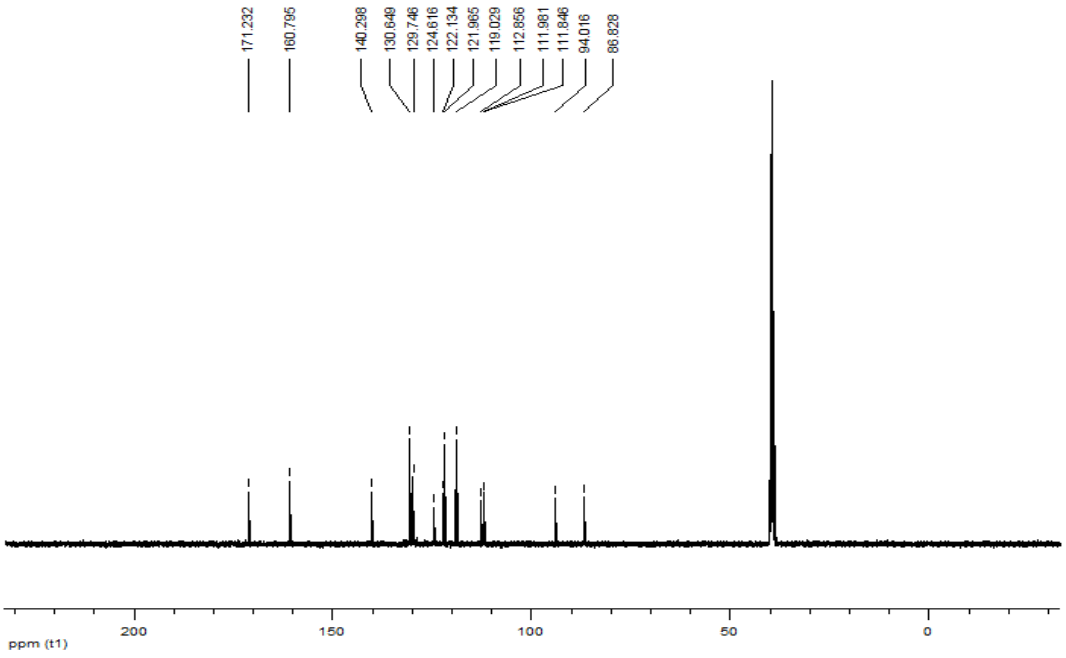

Figure 45 ^{13}C NMR spectrum of **6** in DMSO-*d6*.

APPENDIX B

APPENDEX B

MALDI-TOF

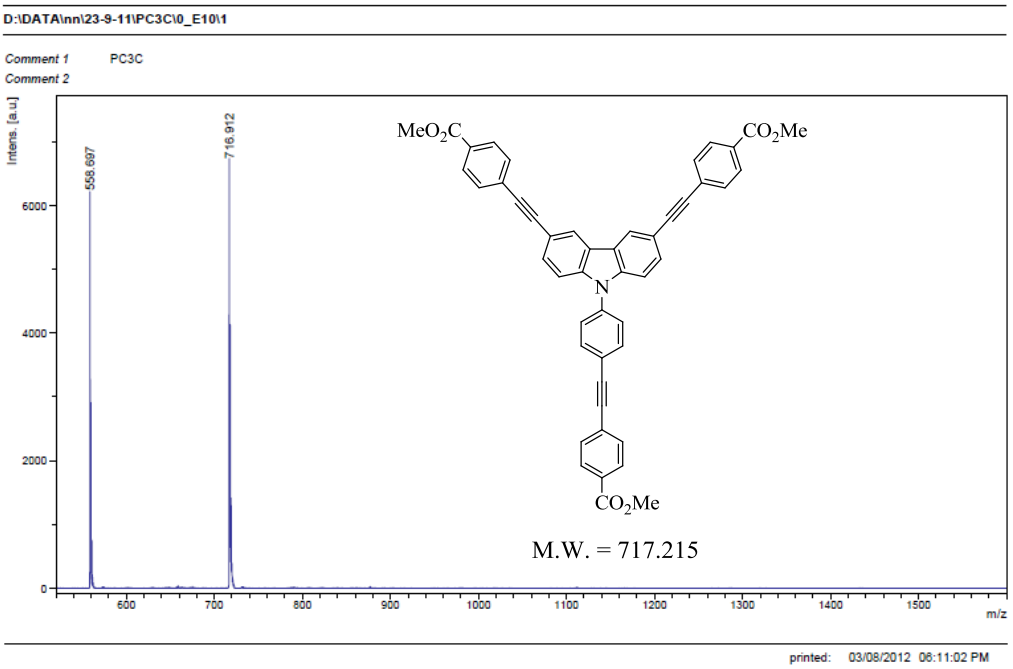

Figure B.1 MALDI-TOF of **10**.

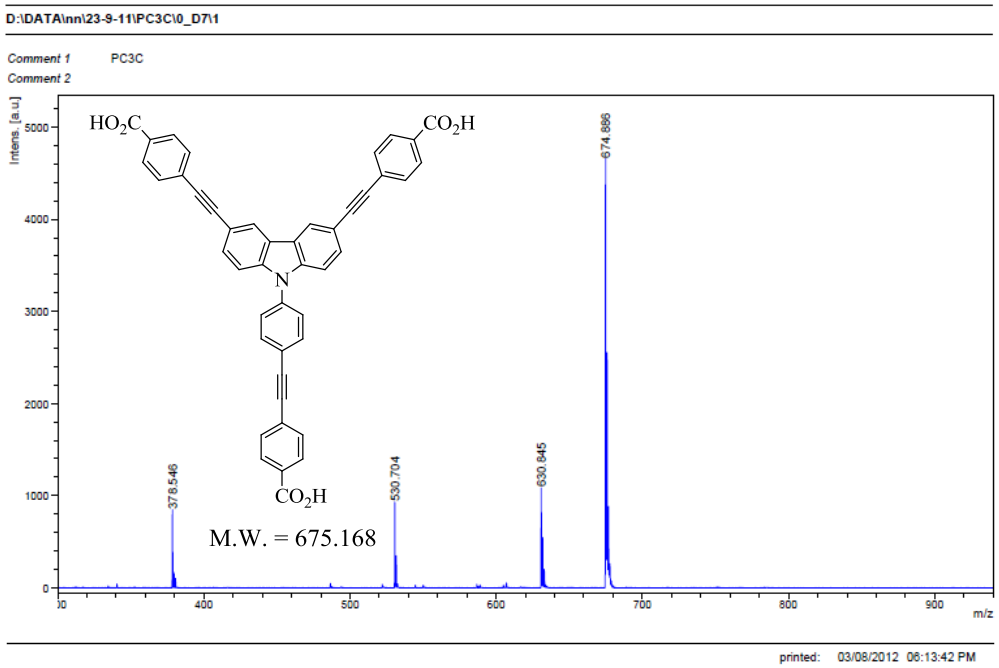

Figure B.2 MALDI-TOF of **1**.

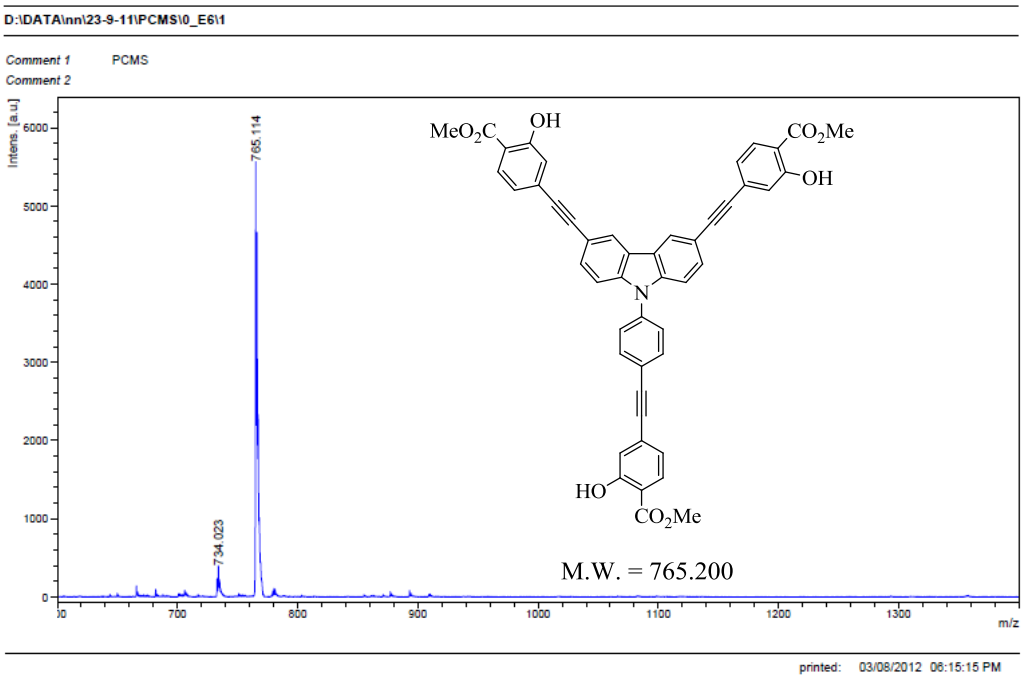

Figure B.3 MALDI-TOF of **11**.

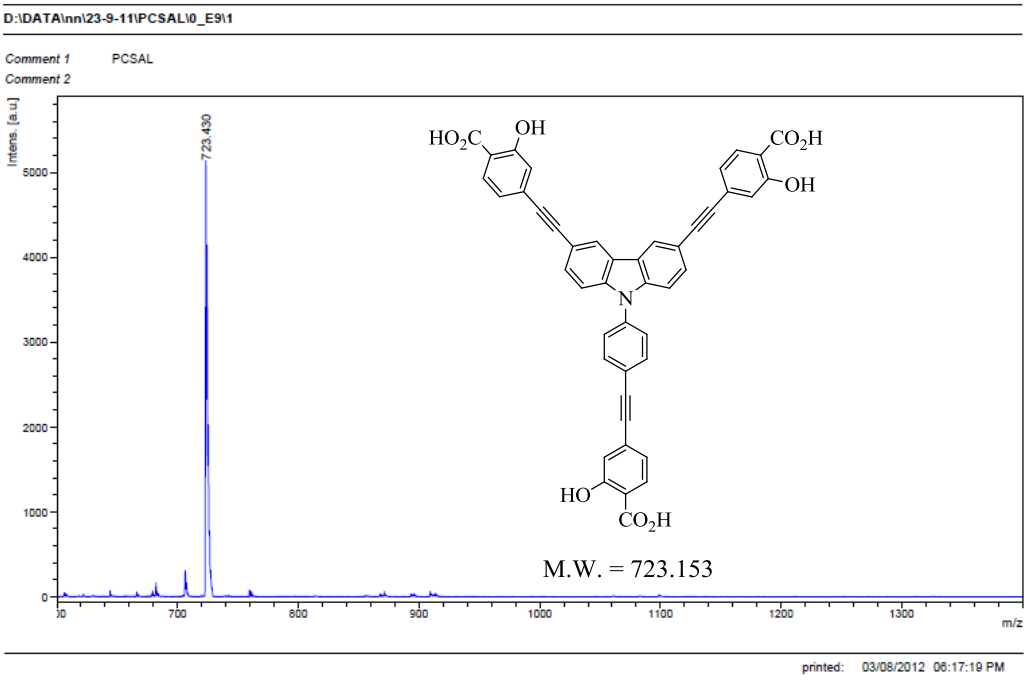

Figure B.4 MALDI-TOF of **2**.

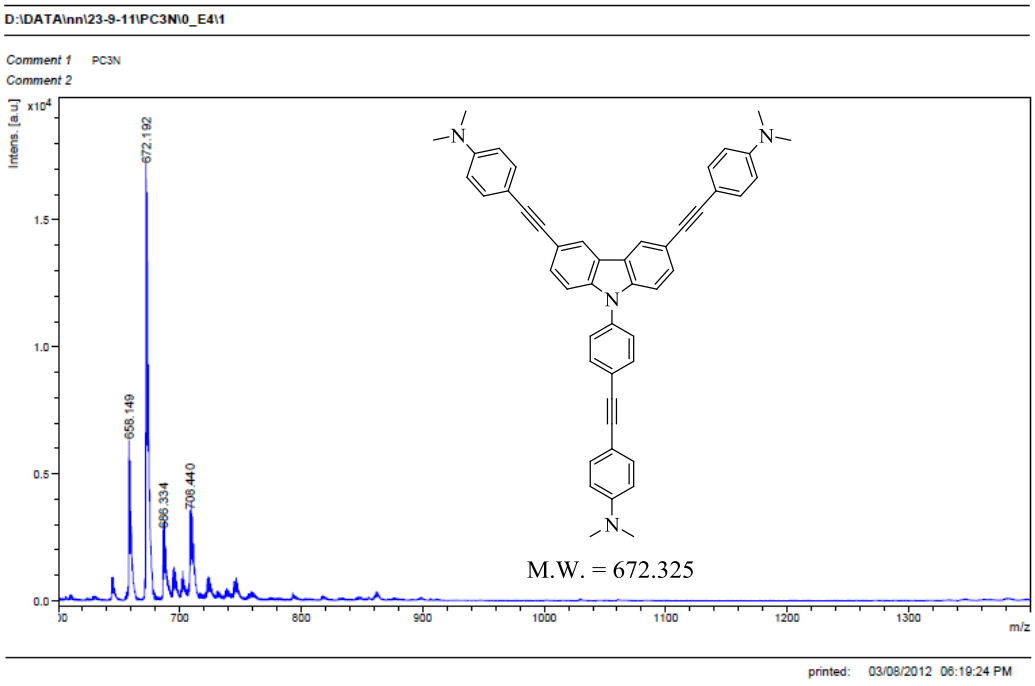

Figure B.5 MALDI-TOF of **12**.

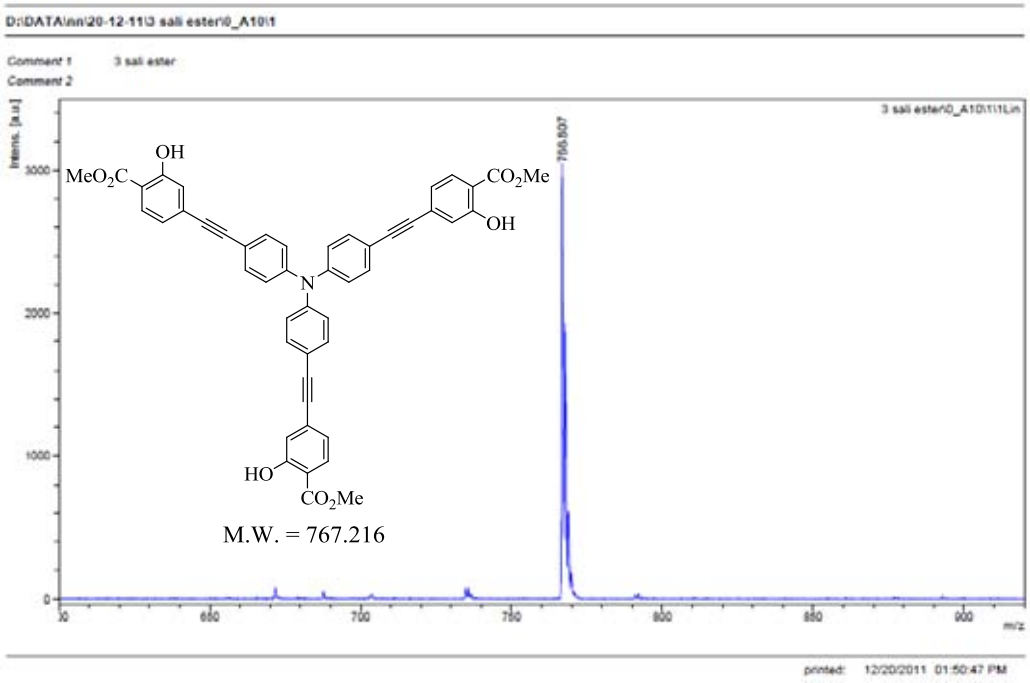

Figure B.6 MALDI-TOF of **13**.

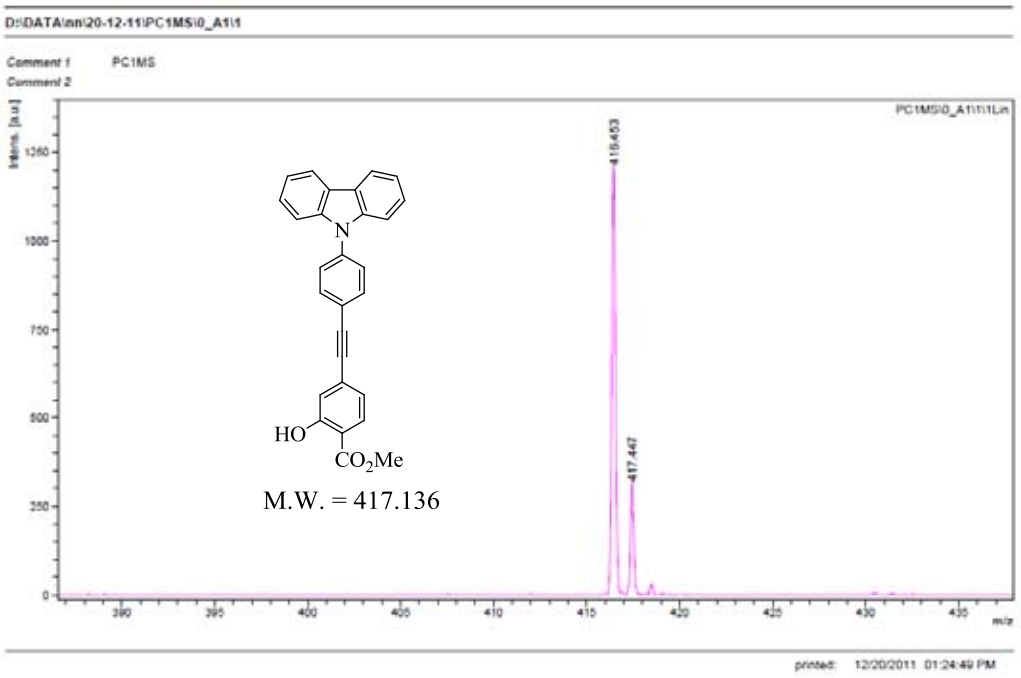

Figure B.7 MALDI-TOF of **14**.

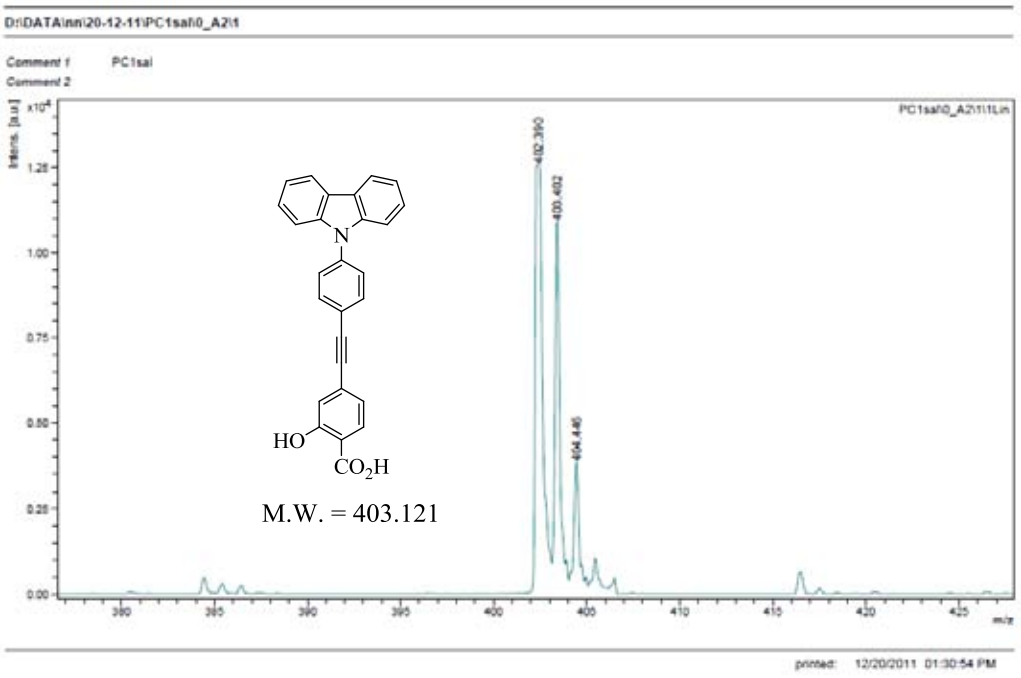

Figure B.8 MALDI-TOF of **5**.

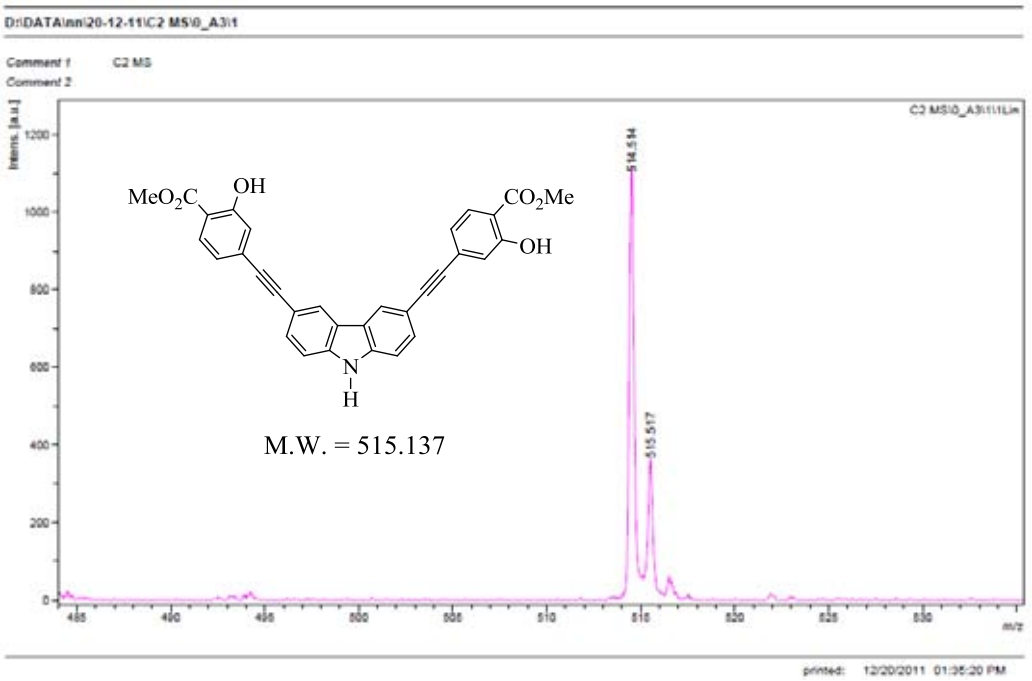

Figure B.9 MALDI-TOF of **15**.

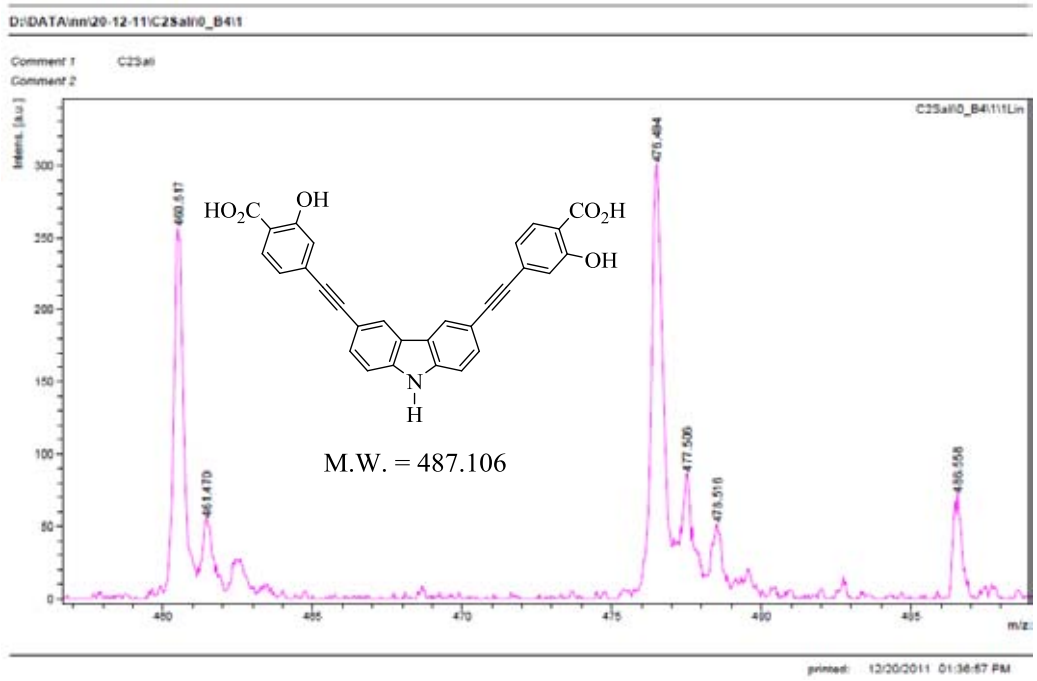

Figure B.10 MALDI-TOF of **6**.

VITEA

Mr. Pharkphoom Auttapornpitak was born on March 4, 1987 in Chonburi, Thailand. He got a Bachelor's Degree of Science in Chemistry from Srinakharinwirot University in 2008. In 2009, he started his a Master's Degree in Petrochemistry and Polymer Science program at Chulalongkorn University. During he had presented his research on "Water soluble fluorophores with *N*-Aryl carbazole core" in Pusan National University, Korea and National University of Singapore.

His address is 32 Moo 2, Khao-sok, Nong-Yai, Chonburi, Thailand 20190, Tel. 038-168528.